A FRACTURE MECHANICS APPROACH TO STATIC

AND FATIGUE FAILURE IN GLASS REINFORCED PLASTICS

by

ROBERT JAMES CANN

B.Sc., M.Sc.

Thesis submitted to the University of Nottingham
for the degree of Doctor of Philosophy

May 1977

CONTENTS

SUMMARY

The aim of this project was to examine the application of fracture mechanics to static and fatigue failure in GRP. The performance of two materials commonly used in shipbuilding was compared, and the stress intensity factor approach was chosen as being most useful in the design of GRP structures.

The literature survey showed that the conditions for its valid application to fracture toughness measurement were not established. Fracture toughness tests were carried out to examine the effect on critical stress intensity factor, K_c, of prolonged water immersion, specimen geometry and size. For the latter, a machine was designed and developed to apply static and pulsating loads to sheets of GRP up to one metre square. The material reinforced with woven roving fabric (WRF/PR) had a much higher fracture toughness than the material reinforced with chopped strand mat (CSM/PR), and was found to be virtually notch insensitive, implying that the K_c approach is not applicable. Large specimens of CSM/PR failed at very low stresses compared with small specimens. This material is notch sensitive and some of the conditions for the valid fracture toughness testing of notch sensitive GRP were established. The critical stress intensity factor of both materials was little affected by water immersion.

Fatigue crack propagation tests were carried out to establish crack growth laws and examine the effect on growth rate of prolonged water immersion. Growth laws were found that were applicable to dry

and wet CSM/PR, but water immersion greatly increased the rate of fatigue crack growth. The resistance to fatigue cracking of WRF/PR is superior to CSM/PR, because crack growth is blocked by rovings running normal to the crack, so that a growth law could not be found. Prolonged water immersion was found to destroy this blocking mechanism greatly reducing the resistance to fatigue crack growth, and a growth law could be determined. The material is still superior to CSM/PR in the wet condition.

The finite element method was used to determine the stress intensity factors of fracture toughness specimens, and compliance-crack length relations in fatigue crack propagation specimens.

ACKNOWLEDGEMENTS

Nomenclature

A	Constant in fatigue crack propagation law
a	Crack length or half-crack length
BEND	3 or 4 point bend type fracture toughness test specimen
C	Specimen compliance
CN	Centre notch type fracture toughness test specimen
CSM	Chopped strand mat reinforcement
DEN	Double edge notch type fracture toughness test specimens
E	Young's modulus
G	Strain energy release rate
GRP	Glass reinforced plastic(s)
J	Rice's J integral
K	Stress intensity factor
$\triangle K$	Stress intensity factor range, $K_{max} - K_{min}$
L	Length of specimen between grips
m	Constant in fatigue crack propagation law
N	Number of loading cycles in fatigue test
P	Load
PR	Polyester resin
r	Distance from crack tip
r_y	Irwin's correction factor
S_{11} $\left.\begin{array}{c}\\\\\\\\\end{array}\right\}$ S_{12} S_{22} S_{66}	Material compliances
SEN	Single edge notch type fracture toughness test specimen
T1 $\left.\begin{array}{c}\\\\\end{array}\right\}$ T2	Types of tensile specimen

t	Specimen thickness
UTS	Ultimate tensile strength
u,v	Displacements in the x, y directions respectively
W	Specimen width
WRF	Woven roving fabric reinforcement
x,y,z	Cartesian coordinates
σ_G	Gross stress applied to fracture toughness specimen
σ_N	Net stress on uncracked section
σ_{UTS}	Ultimate tensile stress
θ, r	Polar coordinates

Suffices

c	Critical value, value of failure
D	Dimensionless form
o, i	Initial value
I,II,III	Crack extension by modes I, II or III (see Fig. 2.1)

CHAPTER 1 INTRODUCTION

The savings in weight which can be achieved and the ease with which complicated shapes can be moulded makes GRP a useful substitute for steel and aluminium. To make it useable in highly stressed structures, much research has been carried out to establish static and fatigue failure criteria. The onset of debonding or resin cracking when used as a static failure criterion leads to uneconomic use of the material and is irrelevant to the type of failure by rapid crack propagation that has been experienced in some large structures. It has been shown (61), that in the presence of a stress concentrator, debonding and resin cracking occur at lower stresses in larger test specimens.

When either debonding or resin cracking is used as a criterion for fatigue failure, stress-log life curves extrapolate to zero stress at long lives. There is no proven fatigue limit as found in many steels.

A pilot study by Bishop (8) shows that fracture mechanics may provide a way of describing static and fatigue failure in some GRP. A considerable body of work on the application of the critical stress intensity factor approach in metals already exists, so that it is often possible to say what size of crack is tolerable in a structure at the design stage. It would be useful if this work could be applied to GRP. Comparatively little has been done in this direction, which provides the theme for the research described in this thesis. This work has been sponsored by the Ministry of Defence (Procurement Executive), and supervised by Dr. M. J. Owen, Department of Mechanical Engineering, University of Nottingham. Mr. J. England, Admiralty Materials Laboratory, has monitored the work for M.O.D.

The aim of this project is to explore the application of fracture mechanics, in particular the stress intensity factor method, to the description of static and fatigue failure in GRP, and to examine the difficulties encountered in previous attempts to do this. This leads to the division of the work into two main objectives:

1) To establish the requirements for a valid fracture toughness test on GRP, i.e. to obtain K_c values which are reasonably independent of specimen geometry, so that the failure of large specimens can be predicted from small ones.

2) To find a fatigue crack propagation law which is applicable to GRP beyond 20000 cycles.

The performance of two GRP materials in these respects was compared. The materials are described in detail in Appendix I. Because the sponsors are interested in using these materials in a marine environment, the effect of prolonged water immersion on their fracture toughness and fatigue crack growth was also examined.

To investigate the failure of large specimens, a testing machine had to be designed and developed, capable of applying static and pulsating loads to sheets of GRP up to 1 m square.

Use was made of the University of Nottingham's library of computer programs for the analysis of finite element problems, PAFEC, to examine the behaviour of the centre notch (CN) specimen used in fracture toughness and fatigue crack propagation tests.

CHAPTER 2   LITERATURE SURVEY

2.1   Introduction

The first part of the literature survey describes briefly four single parameter methods used to describe fracture toughness, their theoretical basis and practical application. There follows a discussion of results obtained from fracture toughness tests on various GRP, and the testing methods used. Comparison is difficult because of the variety of size and type of specimen, and reinforcing materials.

The second part of the survey describes several investigations into the damage caused in GRP by water, and the effect of this on tensile strength, stiffness, and fatigue resistance. Various types of water environment have been studied, but all have similar effects on GRP properties. No work has been found concerning its effects on fracture toughness or fatigue crack propagation.

The survey ends with a description of fatigue crack propagation laws and their application to GRP.

2.2   Single parameter methods of fracture toughness testing

Griffiths (1) suggested a thermodynamic approach to the problem of the strength of cracked bodies. The condition that a crack may extend is that the strain energy release, ΔU, due to a small amount of crack extension Δa, is equal to the energy needed to form a new surface corresponding to $\Delta a, \Delta \wedge$. The energy release rate equals the rate at which the energy is used up to form new surfaces when crack extension is just about to take place.

$$\frac{\partial U}{\partial a} = \frac{\partial \Lambda}{\partial a} \qquad\qquad 2.2.1$$

Irwin and Kies (2) showed that this applied to the failure of cracked steel plates provided initial crack growth is slow, so that the amount of strain energy used up in kinetic energy is small. It was shown that G, (the symbol G was adopted later for the strain energy release rate), is related to the compliance of the specimen, C, which is the displacement of its loading points per unit of load P:

$$G = \frac{P^2}{2t} \cdot \frac{dC}{da} \qquad\qquad 2.2.2$$

By measuring the compliance of specimens with different crack lengths, the relation between C and a can be found and hence dC/da. To determine the critical strain energy release rate, G_c, requires the load P_c and crack length a_c at failure.

Westergaard (3) showed that for a straight crack in an infinite plate the stress distribution is of the form:

$$\sigma_{ij} = \frac{\sigma\sqrt{\pi a}}{\sqrt{2r}} \ f_{ij}(\theta) \qquad\qquad 2.2.3$$

where σ is the uniform stress applied to the body normal to the crack, r is the distance from the crack tip, and $f_{ij}(\theta)$ are functions of θ. The quantity $\sigma\sqrt{\pi a}$ determines the magnitude of the stress field and is defined as K_I, the stress intensity factor for crack propagation

by the opening mode I, (see fig. 2.1). If the plate is subjected to uniform shear stress, τ , crack propagation is by mode II and the stress intensity factor is $K_{II} = \tau \sqrt{\pi a}$. These simple expressions for K have been modified to apply to cracked bodies of many different geometries, (4). In general

$$K = \sigma \sqrt{\pi a} \cdot Y \qquad\qquad 2.2.4$$

where Y is a geometrical correction term, usually a function of (a/W). Geometrical corrections are compared in fig. 2.2, expressed in the form $K/(\sigma \sqrt{W})$. The equivalence of K to G has been shown by Irwin (5). For an isotropic material:

$$G = K^2/E \qquad\qquad 2.2.5a$$

for an anisotropic material (12)

$$G = \left[\frac{S_{11}\, S_{22}}{2}\right]^{\frac{1}{2}} \left[\left(\frac{S_{22}}{S_{11}}\right)^{\frac{1}{2}} + \frac{2S_{12} + S_{66}}{2S_{11}}\right]^{\frac{1}{2}} K^2 \qquad 2.2.5b$$

where E is Young's modulus and the S_{ij} are material compliances.

Failure of a cracked body occurs when the intensity of the crack tip stress field, K, reaches a critical value K_c, at which catastrophic crack extension takes place. In steel (6) it was found that as specimen thickness increased, the adjacent lower stressed material prevented the more highly stressed material at the crack tip from contracting in the direction perpendicular to the plane of the specimen. K_c decreased with increasing specimen thickness until these conditions of plane strain were established then no further change with thickness took place. Irwin (7) accounted for crack tip yielding in ductile materials by adding a

length r_y to the original crack length, a, when calculating K_c:

$$r_y = \frac{1}{2\pi}\left[\frac{K}{\sigma y}\right]^2 \text{ for plane stress, } \frac{1}{6\pi}\left[\frac{K}{\sigma y}\right]^2 \text{ for plane strain}$$

2.2.6

where σy is the yield stress. Iterative computation has to be used to find K_c. The resulting size of r_y should be small compared with a. This correction has been applied to fracture toughness testing of GRP to allow for the damage that occurs at the crack tip in several different forms. The application of the K_c approach to GRP is new, but has predicted the failure of plates containing round holes and cracked beams, (8)(9).

Rice (10) found that the line integral:

$$J = \int_{\Gamma}(U_o \, dx_2 + \frac{n}{T} \frac{\partial u}{\partial x_1} \, ds)$$

2.2.7

where Γ is a path surrounding a crack tip, and has a constant value whichever path Γ is selected for the integral evaluation. U_o is the strain energy density, $\frac{n}{T}$ is the surface traction with respect to the outward normal $\underline{n}$; $\underline{u}$ is the displacement vector and ds is a segment of the curve Γ. Rice considered small scale yielding at the crack tip, and found that at distances large compared with the plastic zone size but still small compared with specimen size, the elastic singularity still defined the stress field. J is related to the rate of change of potential energy, V, and crack length:

$$J = \frac{-\partial V}{\partial a}$$

2.2.8

In a linearly elastic material, $V = -U$, so that $J = G$, and the strain energy release rate approach may be regarded as a special case of the J integral.

Begley and Landes (11) have described the use of the J integral in fracture toughness testing of high strength steels, using 3-point bend specimens. J was determined from the relationship 2.2.8, failure occurring when $J = J_c$. Light (12) used a 3-dimensional finite element model to find J by the energy method and by directly evaluating 2.2.7. In 3-point bend specimens they were equivalent up to general yield, but they diverge as yield is approached in tension specimens. To overcome this, a new parameter was proposed, Q, where if U_e and U_p are elastic and plastic strain energies

$$\delta U_e - \delta U_p = Q \, \delta a \qquad\qquad 2.2.9$$

which is similar to a generalised theory of fracture mechanics proposed by Andrews (13).

The strain energy density factor, S, (14) is a single parameter method of describing mixed mode fractures. Considering the strain energy dU per unit thickness in an element around the crack tip of volume t.dA:

$$\frac{dU}{da} = \frac{1}{r} (a_{11}K_I^2 + 2a_{12}K_I K_{II} + a_{22}K_{II}^2) + .. \qquad\qquad 2.2.10$$

where a_{ij} are functions of θ and the material's elastic constants. The magnitude of the singularity is:

$$S = a_{11}K_I^2 + 2a_{12}K_I K_{II} + a_{22}K_{II}^2 \qquad\qquad 2.2.11$$

Crack extension occurs when S reaches a critical value S_c and takes place in the direction θ in which $dS/d\theta = 0$. Wu (15) found this by plotting the strength field vector $\vec{\mathfrak{I}}$ of the material and the stress field vector $\vec{J}$ of the specimen around the crack tip. Where they coincide indicates the direction of crack extension and the magnitude of the stress field required for it to take place.

2.3 Fracture toughness measurement in GRP

In the work discussed below, which is displayed in table 2.1, K_c values are to be assumed calculated using the failure load of the specimen and the initial crack length unless otherwise stated. Corrected K_c values do not appear in table 2.1 since the methods of correction used vary so widely Dimensions of specimen types are shown in fig. 2.3.

Wu and Reuter (16) investigated the effect of crack length and orientation on K_c values obtained from centrally notched (CN) specimens of a unidirectional glass/epoxy composite. The crack was stained so that extension could be recorded by photographs taken at intervals during the loading. A critical speed above which crack extension was judged to have become unstable was used as a criterion for finding the load and crack length with which to calculate K_c. K_c calculated from the initial crack length and critical load varied from about 1.3 (shortest crack) to 1.8 MPa $m^{\frac{1}{2}}$ (longest crack). Using the observed critical crack lengths increased K_c by an average of 11% and cut down the variation slightly.

Sanford and Stonesifer (17) obtained similar results using small double edge notch (DEN) and single edge notch (SEN) tensile specimens of various epoxy resins reinforced with unidirectional glass fibres.

It was found that the effect on K_c and G_c of changing the resin system and curing process, both of which may affect bond strength, could be examined, but there was a difference between results obtained from the two specimen types. In all cases SEN K_c was higher than DEN K_c by about 19%. G_c was evaluated by the compliance method described in section 2.2. Alterations in resin system, curing schedule, fibre strength, and fibre diameter do not cause the same fractional changes in K_c and G_c.

Beaumont and Phillips (18) obtained K_c and G_c values for chopped fibre mat/polyester resin using 3-point bend (BEND) and DEN specimens. In BEND specimens, G_c was evaluated from the total strain energy (given by the area under the load displacement curve), divided by the fracture surface area. In DEN specimens it was converted from K_c using equation 2.2.5a. The BEND K_c and G_c values were fairly independent of crack length, the mean being 8.0 MPa $m^{\frac{1}{2}}$ and 15 kJm^{-2} respectively. The grooved DEN specimens gave K_c and G_c values that varied little from 6 MPa $m^{\frac{1}{2}}$ and 6 kJm^{-2}. As in the Sanford and Stonesifer work, specimens of different geometry give different values of fracture toughness.

The same authors (19) used BEND specimens to find G_c as before, and CN specimens to find K_c in unidirectional glass fibre/epoxy resin. The notches were perpendicular to the fibres and the specimens were found to be notch insensitive, failure occurring when the stress on the nett section reached the failure stress of the material.

McGarry et al (20) used DEN and CN specimens to measure K_c in several GRP materials. The results from crossplied unidirectional fibre/epoxy DEN specimens were substantially constant over the range of crack lengths tested, but K_c from DEN and CN specimens of balanced

weave fabric/polyester resin rose slightly with increasing crack length, the DEN values being slightly higher than the CN. In tests on chopped fibre mat/polyester resin DEN specimens, the presence of a damage zone was noted. Its radius was estimated to be 2.03 mm, added to the initial crack length, and K_c calculated using this new crack length. It is not known whether this zone corresponded to sub-critical crack growth. The correction does not eliminate variation in K_c with crack length.

Hamilton and Berg (21) compared K_c from DEN and CN specimens of unidirectional fibre/epoxy resin laid up $60^o/60^o/60^o$. The specimens used here were 254 mm wide and exhibited transverse buckling. DEN specimens twisted and CN specimens bulged around the crack. This causes crack propagation to take place by a mixture of modes I and III, and was used to explain the difference in K_c obtained from the two specimen types. By doubling the thickness and so reducing buckling, the average K_c value from CN specimens increased by 15% while that from the DEN specimens decreased by 10%. The difference in results from the two types was reduced from 44% to 4%.

Owen and Bishop (8) used the results of DEN fracture toughness tests to predict the failure of specimens of several GRP materials containing round holes. Irwin's correction, (equation 2.2.6), was used in the plane stress form to account for variation in K_c with width. In the absence of a yield stress, several values were tried until one close to the estimated resin cracking stress produced K_c values constant over the width range 75-150 mm. This process could not be extended to include unpublished values from a 600 mm wide specimen. DEN specimens of Tyglass Y221 fabric polyester resin had to be grooved to make the crack propagate across the warp direction fibres, otherwise it tended to run parallel with these fibres to the grips.

Owen and Rose (22) examined the effect on K_c of adding different quantities of flexible resin to reinforced and unreinforced polyester resin. CN specimens were used, and in the unreinforced resin they were able to observe sub-critical crack growth. The plane stress Irwin correction was used with σy equal to the 0.1% offset stress.

Holdsworth et al (23) outlined a compliance method for obtaining G_c that allowed for irrecoverable energy, which was similar to that used by Begley and Landes (11) for finding J. The area beneath the unloading line of a load-displacement plot taken from a CN specimen, U_r, varied linearly with the square of the maximum load, P^2, for P up to 95% of the failure load. If this is true, the unloading specimen compliance, $C' = 2U_r/P^2$ is constant to failure and there is no sub-critical crack growth. U_r was found by measuring the specimen unloading compliance C'.

The material tested was chopped strand mat/polyester resin. K_c was also found using CN specimens. It was calculated using Irwin's tangent formula and the polynomial formula of Isida (4). Irwin's correction was applied to both, putting σy equal to the resin cracking stress of the material. The iterative computation did not always converge in the Isida formula. Corrected K_c from both formulae were converted to G_c, and found to be in good agreement.

Holdsworth (24) also examined the effect of specimen size and geometry on K_c values in chopped strand mat/polyester resin, chopped strand mat/urethane resin and woven fabric/polyester resin. There is considerable scatter in results which tends to obscure the real variation of K_c with geometry. This is due to specimen glass content which varied between 25 and 34%. In CN and DEN specimens there was a region of crack

length between (a/W) = 0.15 and 0.25 where K_c was fairly constant. This region corresponded to a maximum or a minimum depending on specimen type. K_c tended to increase with specimen width in all types, but least in BEND specimens. There was little difference between uncorrected K_c calculated using Irwin's or Isida's formula (4), but whereas correction increased Irwin K_c by approximately 10%, corrected Isida K_c could not always be obtained, and were as much as 40% higher. Holdsworth et al (9) then used corrected K_c values found from 250 mm wide CN specimens and calculated using Irwin's formula, to predict fairly accurately the failure stress of specimens of the same width containing round hole, and box section beams containing holes or cracks.

Mandell et al (25) used an anisotropic hybrid finite element analysis to find the compliance of SEN specimens and found the geometrical correction term Y in equation 2.2.4 appropriate for the chopped strand mat/polyester resin material under investigation. The compliance was related to Y through equations 2.2.2 and 2.2.5b. The anisotropic finite element Y values agreed well with those calculated from experimental compliances, but was about 10% less than the isotropic analytical Y values, (4).

Gagar and Broutman (26) also used Irwin's correction, (2.2.6), to allow for the damage zone at the crack tip in SEN specimens of chopped strand mat/polyester resin, but with σy equal to 30% of the specimen failure stress. At this load debonding began at the crack tip. This procedure gave values of r_y that were in reasonable agreement with observed values. Microscopic examination of specimens loaded to various fractions of the failure load revealed debonding but no sub-critical

crack growth. Keeping specimens at these loads, cracks were observed
to grow steadily until instability occurred and the specimen broke, (27).
The increase in crack length to the point of instability was added to
the initial crack length and used to calculate K_c, which was found to
be independent of the applied load, and 69% higher than the uncorrected
K_c value in table 2.1. The effect of size and crack length on K_c found
using these methods of correction was not examined, but it was shown to
be independent of thickness.

SEN specimens were used by Barnby and Spencer (28)(29), to determine
K_{Ic} and K_{IIc} for various fibre and crack orientations. To allow for the
effect on Y in equation 2.2.4 of the anisotropy and inhomogeneity of
the unidirectional/epoxy resin under investigation, it was found by the
experimental compliance method outlined by Mandell et al (25). Agreement
between theoretical and experimental Y values is not as good as that
obtained on the same specimen type by Mandell et al (25) and Walters (56),
possibly because the compliance was measured over a shorter gauge length
than the length of the specimen. Critical load was given by the 5%
offset slope procedure described by Srawley and Brown (6). The effect
of size and crack length on values of K_{Ic} so obtained was not investigated,
but the presence of a damage zone at the crack tip parallel with the
fibres was noted.

2.4   Effect of water immersion on GRP

Fried et al (30) subjected filament wound epoxy resin laminates
to immersion in water at pressures of 0, 45.9, and 91.7 MPa for several
months and then examined the deterioration in compressive strength,

interlaminar shear strength and modulus. Strength properties decreased by about 10% over the first six months and then no further. This reduction was independent of the pressure at which the specimens had been immersed.

Wyatt and Ashbee (31) immersed very thin laminates of treated and untreated chopped E-glass fibres and polyester resin in water at 20 and 100°C, and observed the incidence of debonding by optical retardation. Untreated fibres debonded after 5 minutes immersion in boiling water and after 15 hours at 20°C. Where the fibres were treated with a coupling agent, no debonding occurred after ten months immersion at 20°C. At 100°C, resin swelling reverses the compressive shrinkage along the fibres that takes place during curing and the resulting nett tensile stress causes rapid debonding. Resin swelling at 20°C is insufficient to produce a tensile stress, but while treated fibres retain their bond strength, untreated ones are hydrophyllic.

In investigating the effect of moisture on glass-epoxy laminates, Vaughan and McPherson (32) found that keeping the pre-preg in an atmosphere at 95% relative humidity and 38°C, reduced the tensile strength of the laminate by about 10%. This was attributed to the effect of the moisture on the resin, as the coupling agent-glass interface was unaffected.

Pritchard and Taneja, (33) also found the tensile strength of chopped strand mat/polyester resin was reduced by 10% and the flexural modulus by 3% when immersed in a stream of hot water. Applying strain on the specimen being immersed increased the rate at which water was absorbed. The treatment caused gel coat cracks, debonding and resin cracks associated with debonded fibre bundles. Damage was worse near the exposed surfaces.

Blaga and Yamasaki (34)(35) examined the effect of weathering on chopped strand mat/polyester resin, both artificial and outdoor. They divided the damage process into two stages. The first was failure of the glass-resin interface which required stresses induced either by thermal cycling or moisture absorption as already described. The second stage was surface cracking due to radiation. The breakdown of the interface region was attributed to the chemical action of water and induced stresses. As the spray was on for only a short period of the cycle, the moisture contribution to the induced stresses is small.

The effect of steam and oil on the fracture toughness and fatigue strength of carbon fibre reinforced plastics (CFRP) was investigated by Beaumont and Harris (36). Specimens were immersed in steam for 48 h at $100^\circ C$ and in oil for 150 h at $100^\circ C$ before testing, and were kept in these environments while being tested. CFRP fail at lower strains than GRP so there is no resin cracking prior to failure. To examine environmental attack on the resin and resin/fibre interface and compare the performance of treated and untreated CFRP, bending or torsion specimens were used rather than tension specimens. Fracture toughness was measured using 3-point bend specimens with fractures going normal or parallel to the fibres. With the fracture normal to the fibres, treated and untreated CFRP were found to be unaffected by oil or steam, but in the parallel direction it was reduced by about 16% by both environments. Water at room temperature was found to have little effect on the fatigue life of untreated CFRP tested in tension or flexure, but steam had a more serious effect on specimens tested in torsion which depended on the failure criteria used. Fatigue crack propagation studies were carried out by measuring the density of cracks across the

specimen cross-section. After a given number of cycles, crack density was highest in the steam treated specimens.

Romans et al (37) subjected rings of filament wound S-glass strands in epoxy resin to repeated constant compressive displacement under distilled water to compare the performance of different resins in this environment. The specimen was said to have failed when the load fell by 20%. (Similar criteria were used in the torsion tests of Beaumont and Harris (36).) Glass content was found to have a profound influence on the fatigue life of the specimens.

2.5   Stress intensity approach to fatigue crack propagation

Paris (38), and Weertman (39) suggested that crack growth in metals is related to stress intensity factor through the relationship:

$$\frac{da}{dN} = A \triangle K^m \qquad\qquad 2.5.1$$

where a is the crack length, N is the number of cycles, $\triangle K$ is the stress intensity factor range, and A, m are constants. A critical analysis of crack propagation laws put forward by other workers led Paris and Erdogan (40) to conclude that they were not universally applicable, but that equation 2.5.1, with m = 4, was. It has since been applied to many metals and shown to be useful in predicting the safe life of cracked components.

Equation 2.5.1 still predicts a finite rate of crack growth as $\triangle K$ approaches K_c. Forman et al (41) overcame this difficulty by introducing K_c into the fatigue crack propagation equation:

$$\frac{da}{dN} = A \triangle K^m \left[(1 - R)K_c - \triangle K \right]^{-1} \qquad\qquad 2.5.2$$

where $R = K_{min}/K_{max}$. As $K_{max} \longrightarrow K_c$, da/dN $\longrightarrow \infty$. Walton et al (42) suggest that:

$$\frac{da}{dN} = A \triangle K \left[K_c \sigma_y \right]^{-2} \qquad\qquad 2.5.3$$

where σ_y is the yield stress, but found equation 2.5.1 valid up to 0.8 K_c.

To determine the constants A, m, from crack length-cycle data various numerical methods have been used. In polynomial curve fitting (43), polynomials of high order, though fitting the a,N data better, are likely to have inflexions that cause large variations in da/dN. This can be improved by using cubic spline fitting (44). Alternatively, the data smoothing techniques proposed by Munro (45) and Smith (46) can be used.

The fatigue crack growth equation has been shown to apply to polymers by Borduas et al (47) and Owen and Rose (22). Mukherjee and Burns (48) have applied a modified form to PMMA that accounts for changes in mean stress intensity factor.

Relatively few fatigue crack growth studies have been done on composite materials. Hertzberg et al (49) tried to start crack growth in unidirectional Boron fibre/epoxy resin and glass fibre/epoxy resin perpendicular to the fibres but found it to be unstable. This was attributed to the brittleness of the resin. Sih et al (50) examined the propagation of cracks parallel to the fibres of similar material. Beaumont and Harris (36) also found it impossible to establish stable

fatigue crack growth across the fibres of unidirectional material, (CFRP), even when the centre notch specimens were grooved along the crack. Thornton (51) found a form of equation 2.5.1 applicable to a random metal fibre/epoxy resin composite. Concentrations of fibres were found to hold up crack growth causing scatter in the results. Owen and Bishop (52) showed how the crack growth law could be applied to safe life design in polyester resin reinforced with chopped strand mat or woven fabric up to 20000 cycles. A compliance approach was applied to the problem of measuring crack length where damage obscures the crack tip. Harris et al (53) found that 2.5.1 adequately described fatigue crack growth in a unidirectional all metal composite, but at high fibre contents the crack tended to propagate along the fibres to the grips causing the specimen to split. Crack growth rate decreased with increasing fibre content.

2.6   Discussion and conclusions

The most useful fracture toughness testing parameter in predicting the failure of a cracked structure is the critical stress intensity factor, K_c. It is now possible to evaluate the stress intensity factor for a great number of different geometries either from established analytical formulae, or using finite element analysis with 2-dimensional anisotropic elements. The other methods would require the difficult determination of the change in strain energy, potential energy or compliance of the structure with crack length.

Comparison of the GRP fracture toughness values given in table 2.1 is difficult because of the wide variety of specimen types and test

methods used. In all materials, K_c and G_c vary with 1) specimen type, 2) specimen size, 3) crack length, and 4) glass content. Variation of K_c with crack length is also encountered in fracture toughness specimens of polymers (54).

Hamilton and Berg (21) showed that in crossplied unidirectional GRP, the difference in K_c from DEN and CN specimens was due to transverse buckling. In table 2.1 this difference is least where thick specimens have been tested so reducing this buckling. This does not apply to BEND specimens, whose K_c values differed widely from those given by tension specimens.

To evaluate K_c, values of a critical load, P_c, and critical crack length, a_c, at failure are needed for use with a stress intensity formula appropriate to the specimen geometry under test. In the work reviewed here, P_c was either the peak load indicated by a load displacement recording taken during the test, or given by the offset slope method (6). The crack length originally cut in the specimen, a_o, is often used for a_c, but many investigators added small increments to a_o to allow for crack tip damage or sub-critical crack growth. These increments were either found by observation or calculated from equation 2.2.6. Since GRP exhibit no yield stress, the following have been used in 2.2.6:

1) the stress to give a constant K_c value over a range of widths (8);

2) the 0.1% proof stress (22);

3) the resin cracking stress (24);

4) the stress at which debonding occurs at the crack tip (26).

The convergence of the iterative computation used to calculate K_c was not always obtained, (24). Owen and Bishop (8) and Holdsworth (9) used

corrected K_c values from DEN and CN specimens to successfully predict

the failure stresses of cracked GRP structures. Corrected K_c values

from both these types of specimen vary with crack length, so K_c was

chosen from the centre of a range of crack length where it is approximately

constant.

None of the correction methods used give K_c values that are any

more constant with crack length than uncorrected results. Many are used

without considering whether they reduce the effects of specimen geometry

variations on K_c, (22)(26)(27). Only the elaborate measurements of crack

length and velocity at failure by Wu and Reuter (16) gave a constant K_c

over a small range of short cracks. Such measurements are difficult in

GRP where damage obscures the position of the crack tip, (22). The size

and shape of the crack tip damage zone depended on the reinforcement

used and the strength of the bond between fibres and resin. In random

strand or fibre materials, it was close to and collinear with the original

crack. In woven fabric materials, it often extended over a large area

of the specimen, and in crossed unidirectional plied materials, several

cracks extend from the crack tip, following the directions of the fibres

in each ply. It is unlikely that any correction method would be suitable

for all GRP.

The most common material tested has been chopped strand mat in

polyester or epoxy resin. Allowing for differences in glass content

indicated by the ultimate tensile strength in the fourth column of table

2.1, there is little difference in K_c obtained from different types of

tension specimen. The difference between corrected results is greater.

For example, Owen and Bishop's (8) corrected K_c values are about 10%

greater than the uncorrected ones, Holdsworth's (24) increased by up to 40%, and Gagar and Broutman's stress rupture method increased K_c by 69%, (27).

Water absorbed by GRP attacks the fibre/resin interface causing debonding damage. The rate at which debonding occurs increases with temperature, and the damage is more extensive if the material is under tensile strain while under water. Prolonged immersion at room temperature causes a reduction in tensile strength and stiffness of about 10%. The effect of oil and steam on the fracture toughness of CFRP is noticeable only when the fracture is parallel with the fibres (36). When specimens are used whose strength depends on the properties of the resin and fibre/resin interface, the fatigue life of CFRP is considerably reduced by exposure to these environments. GRP is similarly affected by testing in water at room temperature. The resin cracking in GRP subjected to fatigue accelerates water absorption and damage (37). The reduction in fatigue life is proportionately much greater than the reduction in strength and stiffness.

The Paris fatigue crack propagation law has been shown to apply to GRP up to 20 000 cycles, (52). Resistance to crack growth in GRP is expected to depend on glass content, (53) and to be adversely affected by water absorption. It may be difficult to propagate cracks across the fibres of unidirectional materials with high fibre contents or brittle resin matrices.

CHAPTER 3

THE EFFECT OF GLASS CONTENT AND WATER ABSORPTION

ON MATERIAL PROPERTIES

3.1   Introduction

The two GRP materials investigated in this project, described in detail in Appendix I, are designated CSM/PR, (specimen numbers prefixed RC), and WRF/PR, (specimen numbers designated RCW). The ultimate tensile strength, (UTS), and material compliances, S_{11}, S_{12}, S_{22}, and S_{66} were determined. The material compliances are given by:

$$\begin{bmatrix} e_1 \\ e_2 \\ e_6 \end{bmatrix} = \begin{bmatrix} S_{11} & S_{12} & 0 \\ S_{12} & S_{22} & 0 \\ 0 & 0 & S_{66} \end{bmatrix} \cdot \begin{bmatrix} \sigma_1 \\ \sigma_2 \\ \sigma_6 \end{bmatrix} \qquad 3.1.1$$

Some specimens were subjected to prolonged water immersion under pressure before testing, to see how this treatment affected strength and compliance.

The objectives were firstly to expose any anisotropy in these materials; secondly, to see if their differences in fracture toughness and fatigue crack propagation resistance corresponded to their differences in UTS; thirdly, the material compliances are required for finite element predictions of stress intensity factor and specimen compliance. There was scatter in all the UTS and compliance results, partly due to variations in specimen glass content.

3.2   Specimens and methods

For measurement of UTS and material compliances, S_{11} and S_{22}, initially the tensile specimens shown in fig. 3.1a were used (T1).

The larger specimen recommended in BS 2782, part 3 1970 (see fig. 3.1b, designated T2) provides a more representative sample for materials like WRF/PR and superseded T1 for all tensile tests. Blanks for T1 specimens were cut from laminates using a diamond impregnated slitting wheel and shaped with a tungsten carbide tipped router. T2 specimens required no shaping, the ends were reinforced with material cut from the same laminate and bonded to the main part of the specimen with Araldite.

Plans showing how the laminates were divided up into specimens were made to record the position and direction of each one relative to the warp direction of the top ply. The lay up angles of each ply are also referred to the top ply warp direction.

To find the material compliances S_{12} and S_{66}, the central deflection of a square plate of the material subjected to a twisting moment was measured as suggested by Tsai (55). The deflection, W_o, is plotted against load P to obtain W_o/P in the expression:-

$$S_g = \frac{4h^3}{3l^2} \frac{W_o}{P} \qquad\qquad 3.2.1$$

then

$$S_G = S_{66} \text{ for } \theta = 0^o, 90^o$$

$$S_G = 2(S_{22} - S_{12}) \text{ for } \theta = +45^o \qquad\qquad 3.2.2$$

$$S_G = 2(S_{11} - S_{12}) \text{ for } \theta = -45^o$$

The loading arrangement and dimensions of the plate are shown in fig. 3.1c.

Tensile tests were carried out in a modified Type "E" Tensometer universal testing machine, extension being measured by a Hounsfield extensometer linked to the chart drive. After testing, the glass content

of all tensile and plate twist specimens was determined as follows. Approximately 10 gms of material was cut from the specimen, and placed in a weighed tray. In WRF/PR tensile specimens, there was severe resin shedding around the break so this material had to be taken from near the ends. Tray and specimen were weighed together and placed in a muffle furnace heated to 600°C. After 12 hours, all the resin had burnt away, the tray and contents were weighed and the glass content by weight of the specimen calculated.

3.3   UTS and material compliances of dry CSM/PR and WRF/PR

The variations in UTS and S_{11}, S_{22} values obtained from individual specimens were attributed to the following causes; 1) glass content, 2) anisotropy, 3) curing schedule, 4) variation in resin and glass properties. For the UTS and S_{11}, S_{22} values obtained from CSM/PR laminates RC1 and RC2, (3 ply 0°/90°/0°, curing schedule A), a linear variation with glass content was assumed, (fig. 3.2), and there can be seen to be no difference between 0° and 90° specimens large enough to indicate anisotropy. The UTS and $S_{11,22}$ values at 35% glass content are estimated from fig. 3.2 to be 118.1 MPa and 0.1094 GPa^{-1}. The onset of debonding and resin cracking was very difficult to detect. Debonding occurred at very low loads, and the resin cracking stress, (table 3.1), varies between specimens more than the UTS.

In the manufacture of subsequent laminates, the curing schedule was changed to B. UTS and $S_{11,22}$ values from CSM/PR laminates RC12. (3 ply 0°/90°/0°), RC17, (6 ply 0°/90°/0°/90°/0°/90°), RC18, (9 ply 0°/90°/0°/90°/0°/90°/0°/90°/0°) and RC28 (3 ply 0°/90°/0°) are shown plotted against glass content in fig. 3.3.

The RC28 specimens were type T2 for comparison with WRF/PR T2 specimens. There are no definite trends in fig. 3.3 that can be attributed to specimen type, specimen direction, or specimen thickness. Straight lines were fitted to the data in fig. 3.3 using the least squares method. The UTS and $S_{11,22}$ at 35% glass content were found to be 124.8 MPa and 0.1004 GPa^{-1}. The difference in these values for B cured material and the values quoted for A cured material is small compared with the scatter in the data in figs. 3.2 and 3.3. No effect on the UTS and material compliances $S_{11,22}$ due to change in curing schedule could be detected. This scatter arises because CSM is a random reinforcement, and it is possible for a large proportion of the specimen fibres to be so aligned to contribute little to its strength or stiffness. There may also be variation in the properties of the resin and glass. The narrow range over which glass content varies amplifies these effects.

The RC28 specimens were cut from a laminate measuring 915 mm square. Laminates of this size were to be made into large fracture toughness specimens, and the RC28 specimens were to determine the variation in glass content and possible anisotropy in such a specimen. The positions and glass contents of these specimens are shown in fig. 3.4. The coefficient of variation of the glass contents in fig. 3.4 is 6%.

No difference in the strength or compliance properties of WRF/PR specimens cut in the 0° and 90° directions could be detected using T1 or T2 specimens. This might have been expected from the imbalanced weave of the fabric reinforcement, (table A1). Using T2 specimens, cut from laminates RCW25, (3 ply $0^{o}/0^{o}/0^{o}$), RCW30, (6 ply $0^{o}/0^{o}/0^{o}/0^{o}/0^{o}/0^{o}$), and RCW29, (9 ply $0^{o}/0^{o}/0^{o}/0^{o}/0^{o}/0^{o}/0^{o}/0^{o}/0^{o}$), the UTS and $S_{11,12}$ values

in table 3.3 and fig. 3.5 were obtained. Straight lines were fitted to the data using the least squares method. There is less scatter due to the regular structure of the reinforcing material. The UTS and $S_{11,22}$ values at 65% glass content were found to be 385.2 MPa and 0.04037 GPa^{-1}.

For comparison with the reinforced materials, the UTS and S_{11} values for the polyester resin were determined using T1 specimens. There was considerable scatter in the results, the coefficient of variation of the UTS from 9 specimens being 28%. The mean values of UTS and S_{11} were found to be 8.2 MPa and 1.567 GPa^{-1}. Several of the specimens broke in more than one place.

Four plate twist specimens of CSM/PR were cut with $\theta = 0^{\circ}$, 0°, $+45^{\circ}$ and $+45^{\circ}$. The W_o/P and S_G values obtained showed variation which was more attributable to glass content than orientation, (fig. 3.6 and table 3.5). Eight plate twist specimens of WRF/PR were cut with 4 at $\theta = 0^{\circ}$ and 4 at $\theta = +45^{\circ}$. Fig. 3.7 shows large differences between the 0° and $+45^{\circ}$ specimens. Assuming a linear variation between S_G and glass content, (fig. 3.8 and 3.9), S_G at 35% (CSM/PR) and 65% (WRF/PR) glass contents, were found and S_{12}, S_{66} calculated using equations 3.2.2.

3.4 The effect of water immersion on UTS and material compliances

Tensile (T2), plate twist and fracture toughness specimens were immersed in tap water under a pressure of 6.9 MPa at ambient temperature for 16 weeks. This treatment is used by the Admiralty Materials Laboratory to simulate several years immersion at ordinary ambient pressure. The water absorbed during this treatment is expressed as the percentage increase in weight of the specimen. From table 3.6 the water

absorbed can be seen to depend on the material rather than the type or size of specimen except where the ends of the specimen have been reinforced, (marked R in table 3.6). Since all the water immersion specimens were cut from material of the same thickness, the proportion of the area of the unsealed, cut edges to the total surface area of the specimen varies. The nominal value of this for each specimen type and material is given in table 3.6. No effect on the amount of water absorbed by the specimens due to this could be found, so moulded and cut surfaces allow water to pass through at the same rate. The mean amount of water absorbed by CSM/PR specimens was 1.2% and by WRF/PR specimens 0.63% (excluding specimens with reinforced ends).

The same sort of damage caused by water absorption was found to be evenly distributed throughout all the different specimens. The plate twist specimens shown in plate 1 were typical. In both materials, the damage took the form of patches of debonded fibres. There was no surface or interior cracking of the resin.

The values of UTS and $S_{11,22}$ obtained from 4 CSM/PR and 4 WRF/PR T2 specimens, their glass contents, and amount of water absorbed is given in table 3.7. From table 3.7 it can be seen that the amount of water absorbed is independent of glass content. The mean glass content of each of these groups of specimens was used to estimate the UTS and $S_{11,22}$ values that would have been obtained had the specimens been tested dry. The same procedure was used to find the probable dry S_G value of water treated plate twist specimens, and hence S_{12} and S_{66}. The changes in UTS and material compliances due to water immersion are summarised in table 3.8 and are small compared with changes due to glass content.

3.5 Conclusions

The UTS and material compliances found for CSM/PR and WRF/PR and the effect of the water immersion treatment is summarised in table 3.8. Since the scatter in results is mostly due to variation in glass content, consistent UTS and material compliance values can be obtained by assuming a linear variation of properties with glass content and quoting values at a particular glass content. In CSM/PR, $S_{11} = S_{22}$ and there is negligible difference between S_G obtained from $0°$ and $+45°$ plate twist specimens, so the material is regarded as plane isotropic. In WRF/PR $S_{11} = S_{22}$ and different values of S_G were obtained from $0°$ and $+45°$ specimens, the material is orthotropic. No difference in UTS and material compliance due to the alteration in curing schedule could be detected.

The amount of water absorbed by specimens of CSM/PR and WRF/PR is not affected by size, geometry (unless the ends are reinforced), or glass content in the ranges used. This is borne out by the similarity of debonding damage throughout specimens of the same material. The effect on UTS and material compliances of the water immersion treatment is generally small compared with variations due to other causes. It is comparable with that found by Pritchard and Taneja (33) in another CSM/PR material, when subjected to prolonged immersion in a stream of hot water.

An exception to this can be seen from table 3.8 to be the large increase in the S_{12} of WRF/PR (169%) due to water absorption. This corresponds to the greater W_o/P values, (fig. 3.7), obtained from wet $0°$ plate twist specimens. There is, however, a loss of accuracy in the

use of equations 3.2.2 to determine S_{12}, which may have been diminished

further by the rather small length/thickness ratio of the plate twist

specimens. The S_{12}, S_{66} values obtained here are adequate for use

in the finite element analysis, described in the next chapter.

CHAPTER 4

DETERMINATION OF STRESS INTENSITY FACTOR

AND COMPLIANCE USING THE FINITE ELEMENT METHOD

4.1 Introduction

It has been shown that stress intensity factor values obtained from finite element models of GRP fracture toughness specimens agree well with those from analytical solutions, (25)(56)(61) provided the crack is orientated parallel to one of the principal planes of the material. The length/width ratio, (L/W), of the models used has always been 2 or greater. In the next chapter, fracture toughness tests are described which use 915 mm wide centre notch, (CN), specimens with L/W reduced to 0.82 to save material. The grips are closer to the crack and the constraints they apply may have an appreciable effect on the stress intensity at the crack tip, particularly of a long crack. A finite element model of a CN specimen was set up for solution by the University of Nottingham PAFEC system, (Program for Automatic Finite Element Calculations) to assess the effect of a) crack length, b) end restraints, and c) length/width ratio on stress intensity factor values.

In the fatigue crack propagation tests described in Chapter 5, the crack length is found by measuring the compliance of the specimen under test. The compliance of a specimen is the inverse of its stiffness, the displacement being measured at gauge points on the centreline of the specimen, an equal distance above and below the crack. This compliance is then compared with values obtained from a calibration specimen in which the crack length has been altered with a jewellers saw and measured with a travelling microscope. Changes in specimen compliance due to

crack length are small compared with differences that may exist between the compliance of the test and calibration specimens due to glass content. Holdsworth (23) had to use a correction factor to ensure that the compliance of specimens whose glass content is not the same as that of the calibration specimen fitted the calibration curve. The finite element model of the CN specimen was used to determine the compliance calibration curve of the fatigue crack propagation specimens used in this project. Expressing the specimen compliance in dimensionless form provides a theoretical justification for Holdsworth's procedure, by showing that in this form the compliance is independent of glass content provided that displacement is measured close to the crack.

4.2   The finite element model

The finite element model is that used by Walters (56) to determine the stress intensity factor in single edge notch specimens of varying crack length, (fig. 4.1). It uses a relatively small number of 8-noded isoparametric anisotropic elements, compared with the large numbers of triangular or rectangular elements used in previous investigations. The elements become smaller as they approach the line of the crack, and around the tip of the crack blocks of the smallest elements are nested which can be moved along the bottom edge of the model to alter the crack length. By altering the boundary constraints of the model to those shown in fig. 4.1 a quarter of the CN type specimen can be modelled, which is sufficient, as CSM/PR is isotropic, and in WRF/PR specimens the crack lies in one of the principal planes of the material. By identifying the appropriate node as the crack tip, the mid-side

nodes adjacent to the tip are automatically moved closer to it by a quarter of the element side's length, in order to model better the $r^{-\frac{1}{2}}$ strain singularity.

Various methods can be used to obtain the stress intensity factor, K, from the finite element solution to a cracked structure. The simplest, as suggested by Chan et al (57), uses the displacements of the nodes along the crack in conjunction with the Westergaard (3) equations for the displacements u and v near the crack tip:

$$u = \frac{K_I \cdot r^{\frac{1}{2}}}{G \cdot (2\pi)^{\frac{1}{2}}} \cos \frac{\theta}{2} \left[\frac{1-V}{1+V} + \sin^2 \frac{\theta}{2} \right] \qquad 4.2.1$$

$$v = \frac{K_I \cdot r^{\frac{1}{2}}}{G \cdot (2\pi)^{\frac{1}{2}}} \sin \frac{\theta}{2} \left[\frac{2}{1-V} - \cos^2 \frac{\theta}{2} \right] \qquad 4.2.2$$

for plane stress, where r, θ are polar coordinates with their origin at the crack tip, the line $\theta = \pi$ being the crack. G is the shear modulus, and V is Poisson's ratio. K_I is K in mode I, (see fig. 2.1). Setting $\theta = \pi$ in equation 4.2.2 gives:

$$K_I^* = \frac{EV}{4} \left[\frac{2\pi}{r} \right]^{\frac{1}{2}} \qquad 4.2.3$$

·where K_I^* now refers to a local value of K at distance r from the tip along the crack, and E is Young's modulus. Plotting K_I^* against r there is a region where the relationship is linear which can be extrapolated back to r = 0 to obtain K at the crack tip. Bishop (61), extended this method to anisotropic materials, and Walters (56) set up a sub-routine (SINTFAC) to apply this method in conjunction with PAFEC, taking v from the nodal displacements along the crack. For an anisotropic material, (orthotropic):

$$K_I^* = \frac{v}{S_{22}} \left[\frac{\pi}{2r} \right]^{\frac{1}{2}} \cdot \frac{\beta_1 \beta_2}{\beta_1 + \beta_2} \qquad 4.2.4$$

where

$$\beta_1, \beta_2 = \left[\frac{S_{12}}{S_{11}} + \frac{S_{66}}{2S_{11}} \pm \left[\frac{S_{12}^2}{S_{11}^2} + \frac{S_{12}S_{66}}{S_{11}^2} + \frac{S_{66}^2}{4S_{11}^2} - \frac{S_{22}}{S_{11}} \right]^{\frac{1}{2}} \right]^{\frac{1}{2}} \qquad 4.2.5$$

and S_{11}, S_{12}, S_{22}, S_{66} are the material compliances.
For comparison with the analytic formula used for K, (equation 5.2.2), K^*/K where K^* is determined from the finite element model and K from the formula was plotted against r/W.

Specimen compliance was found from the load applied to the model and the displacement of a point on it corresponding to the position of gauge points on actual specimens.

4.3   Effect of specimen geometry and end constraints on K

K^*/K is shown plotted against r/W for specimens of the two materials with various crack lengths, end restraints and length/width ratios in fig. 4.2 and 4.3. The relationship is not linear up to r = 0 due to the inability of the elements to cope with the singularity at the crack tip. Further refinement of the mesh near the crack tip by nesting blocks of elements in the elements immediately adjacent to it had no effect on K^*/K. The extrapolated values of K^*/K at r = 0 for the various conditions are summarised in table 4.1. The crack lengths examined were a/W = 0.05 and 0.30, and the length/width ratios 0.75 and 2.00.

Initially, a uniform load was applied along the top edge of the model with no constraints, and there was some variation in displacement. All the loaded nodes were then constrained to have equal displacement.

A further restraint was added by specifying no lateral displacement of the loaded nodes. Both had a negligible effect on models with L/W = 2. When these restraints, which are meant to represent those applied to specimens by testing machine grips, were removed from models with a_o/W = 0.3 and L/W = 0.75, K^*/K at r = 0 was found to increase by about 48% in both materials. These do not appear in fig. 4.2 or 4.3 because there was no linear region which could be extrapolated to r = 0.

Agreement between the finite element and analytic solutions for K is closest in models with the shortest crack length and having the isotropic compliances of CSM/PR. In both materials the finite element solution is up to 8% higher at the longer crack length with L/W = 2, but reducing the specimen length actually improves the agreement in CSM/PR models. In WRF/PR models with the longer crack the finite element solution is less than the analytic by 8.5%. Even the largest of these differences is small compared with variations in K_c values due to other causes.

4.4 The compliance of CN specimens

Irwin (58) has given the following expression for the compliance, C, of an isotropic CN specimen:

$$C_D = \frac{Ct}{S_{11}} = \frac{2}{\pi} \cosh^{-1}\left[\frac{\text{ch}\frac{\pi y}{W}}{\cos\frac{\pi a}{W}}\right] - \left(1 - \frac{S_{12}}{S_{11}}\right)\frac{y}{W}\left[1 + \left[\frac{\sin\frac{\pi a}{W}}{\text{sh}\frac{\pi y}{W}}\right]^2\right]^{-\frac{1}{2}}$$

$$- \frac{S_{12}}{S_{11}}\frac{y}{W} \qquad\qquad\qquad 4.4.1$$

where S_{11}, S_{12} are the isotropic material compliances for which $S_{66} = 2(S_{11} - S_{12})$. The distance from the crack to the gauge points

above and below it is y, (fig. 2.1) and t is the specimen thickness. The specimen compliance is expressed in a dimensionless form, C_D. Examining the terms in equation 4.4.1, C_D should be constant if S_{11}/S_{22} is constant.

The compliances of CSM/PR and WRF/PR and a third material not used in this project but with $S_{11} \neq S_{22}$, (the compliances of this material were taken from Bishop (61)), were used to obtain specimen compliances from the finite element model, and were then increased by 50% and a second solution obtained with the compliances all increased in proportion. This was an attempt to model an increase in material compliance due to a drop in glass content. The C_D values obtained are given in table 4.2. C_D from CSM/PR and WRF/PR is only slightly affected by the change, but in the third material C_D rises by 32%. The approach seems inappropriate for anisotropic materials where $S_{11} \neq S_{22}$.

Close examination of the material compliance/glass content relations set out in Chapter 2 shows that the assumption that S_{12} increases in proportion to S_{11} as glass content changes is not justified. However, in equation 4.4.1 C_D is still independent of S_{12}/S_{11} provided y/W is small. The second and third term of the expression become small compared with the first term which contains no S_{12} term.

The compliance C_D of 100 mm wide and 915 mm wide CN specimens used in fatigue crack propagation tests, both with gauge point distance y = 4 mm, was estimated from finite element models with CSM/PR and WRF/PR material compliances. The crack length was varied by moving the nested blocks of small elements near the crack from block to block and altering the constraints along the model's bottom edge accordingly. C_D against (a/W)

is shown in fig. 4.4 with equation 4.4.1 for comparison. The isotropic compliances of CSM/PR were used in the equation with y = 4 mm and W = 100 mm.

In CSM/PR agreement between 100 mm, 915 mm and equation 4.4.1 is good at small crack lengths. 915 mm specimens of WRF/PR and CSM/PR agree closer at all crack lengths than the 100 mm specimens because y/W is smaller. The finite element C_D was compared with C_D values obtained from calibration specimens of the two materials, the crack length being increased with a jewellers saw and measured with a travelling microscope. The agreement is good considering that S_{11} was estimated from the glass content of the specimens using the relations in fig. 3.3 and 3.5. The C_D measurements from 915 mm specimens are higher than the finite element prediction because part of the crack opening displacement was due to a small amount of transverse buckling taking place around the transducer mountings near the centre of the crack, which could not be eliminated.

In the finite element analysis of specimen compliance, it was found that end restraints had little effect on specimens with L/W = 2. Walters (56) found good agreement between K values obtained directly from the finite element model using the K^*/K method described here, and those obtained from the specimen compliance using the relation between K and strain energy release rate, G. From equations 2.2.2 and 2.2.5b:

$$\left[\frac{K}{\sigma_G\sqrt{W}}\right]^2 = \frac{1}{2}\left[\frac{S_{22}}{2S_{11}}\right]^{-\frac{1}{2}}\left[\left[\frac{S_{22}}{S_{11}}\right]^{\frac{1}{2}} + \frac{2S_{12}+S_{66}}{2S_{11}}\right]^{-\frac{1}{2}} \cdot \frac{dC_D}{da_D} \qquad 4.4.2$$

or for an isotropic material:

$$\left[\frac{K}{\sigma_G \sqrt{W}} \right]^2 = \frac{1}{2} \frac{dC_D}{da_D}$$

where $C_D = Ct/S_{11}$ and $a_D = (a/W)$. However, in the compliance $-(a/W)$

relations obtained from the CN model, there were slight inflections

in polynomials, (of order 4) that were fitted to the curves for 100 mm

models, which would lead to large errors in estimating $dC_D/d(a/W)$, though

adequate for finding (a/W). This method was also used by Mandell et

al (25).

4.5 Conclusions

The analytical expression for K used to calculate K_c in all CN

specimens, (equation 2.2.2) is adequate for those with L/W = 0.82.

Agreement between finite and analytical values of K is best at short

crack lengths. The discrepancy between K_c evaluated by the two methods

at long crack lengths would be small compared with changes in K_c due to

crack length and specimen size.

Specimen compliance expressed in the dimensionless form C_D provides

a means of estimating crack length that is independent of glass content

provided the gauge length over which the compliance is measured is

small, (see section 6.2 for the application of this method).

CHAPTER 5

THE K_c APPROACH TO FRACTURE TOUGHNESS MEASUREMENT

IN CSM/PR AND WRF/PR

5.1 Introduction

In section 2.3 it was shown that measuring the fracture toughness

of GRP using the critical stress intensity factor (K_c) approach produced

candidate values for K_c which varied with a) specimen type, b) specimen

size, and c) crack length. The aims of this part of the project were

firstly to determine the effect on the K_c values of CSM/PR and WRF/PR

of changes in specimen size and geometry and the extent to which small

specimens can be used to predict the failure of very large cracked

specimens, representing the size of real structures. If K_c varies with

crack length, in constant $\triangle K$ range fatigue crack propagation tests, the

ratio between $\triangle K$ and K_c will also vary and may affect the crack growth

rate.

Secondly, to compare the fracture toughness of the two GRP materials

in the dry state and after the water immersion treatment described in

section 3.4.

Most fracture toughness testing standards, (6) are concerned with

ductile metals. In ductile specimens plastic yielding begins at the

crack tip, and slip occurs at 45° to the crack plane in thin specimens.

In thick specimens, conditions of plane strain exist across the crack

front, except near the ends. Near the ends of the crack front the

material is close to free surfaces and able to contract. Away from the

ends, the plane strain conditions arise because the material adjacent

to the crack front is at a much lower stress than the material closest
to the crack front and prevents it from contracting.

This restraint causes tensile stresses across the crack front.
In GRP the inter-ply strength is low and would not sustain plane strain
conditions. The conditions in the whole specimen are plane stress,
and the layers behave as if separated. There should therefore be no
difference between K_c values obtained from specimens of few or very
many plies. In shipbuilding, GRP is used in thicknesses up to 50 plies.
Considerable savings in material and time would be made if K_c values
could be obtained from thin specimens that would be applicable to thicker
material.

5.2 Specimens and methods

For measuring the fracture toughness of CSM/PR material double
edge notch, (DEN), and centre notch, (CN), specimens were used. These
specimens are shown in fig. 2.1. For WRF/PR, only CN specimens were
used. Specimens were cut from laminates using a diamond impregnated
slitting wheel. Notches were made using a 1 mm thick jewellers saw,
a 1.5 mm hole being made in the middle of CN specimens for this purpose.

Specimens up to 150 mm wide were tested in a modified Type "E"
Tensometer or Instron 1195 machine both with autographic load-
displacement recording facilities. In the former the testing speed
was 0.0212 mm/sec and in the latter, 0.0167 mm/sec. At this low speed,
such a small difference has a negligible effect on results. The capacity
of these machines being only 100 kN, a 500 kN Denison machine had to be
used to test specimens of WRF/PR greater than 3 plies thick and 50 mm
wide, or containing very small cracks.

For testing sheets of GRP up to 1000 mm wide, a testing machine had to be specially designed and constructed. It was designed to apply a static load up to 1000 kN and a pulsating load up to 500 kN. A sketch of the testing frame is shown in fig. 5.1; plate 2 shows the layout of the testing facility. The frame is made of two pairs of 610 x 229 (24" x 9") universal beams (A in fig. 5.1), the upper pair being supported on two pairs of 203 x 203 (8" x 8") universal columns (B). The upper pair of beams support a hydraulic loading cylinder (C) which applies the load to the specimen grips (D). The lower grip is raised and lowered electrically by a mechanism housed in the lower pair of beams (E). The frame is free standing at supports (F). The strain energy stored in the frame must be small compared with that stored in the specimen, so that the energy required to form new crack surfaces comes from the specimen rather than the loading frame. The frame must therefore be stiff, and the volume of material used in its construction kept as low as possible. To reduce friction no seals were used between the loading cylinder and piston; by using a long, plain piston friction is cut down and a long leakage path created which controls losses. To avoid having a gland in the base of the loading cylinder, a yoke and two connecting rods (R and S in fig. 5.1) are used to transmit the load from the piston to the upper grips.

A diagram of the hydraulic system for supplying pressure to the loading cylinder is shown in fig. 5.2. It is possible to supply the loading cylinder with pulsating pressure, steady pressure, or both. The dynamic supply is provided by a twin-cylinder pulsating pump (G) which has already been used successfully for other work (59). Two

opposed pistons (H) are made to reciprocate by rotating eccentrics, (I). As they move outward these pistons cut off the oil supply ports (J) compressing the oil now trapped in the system, forcing the piston in the loading cylinder upwards. By altering the position of the supply ports along the cylinder, the volume of oil trapped in the system by each stroke is changed, and hence the delivery pressure varied. The position of the supply ports is altered by an electric motor, which can be operated manually or by an automatic control system. A radial-piston pump (K) supplies static pressure, which can be varied by bleeding back to the open reservoir through a control/safety valve (L). By opening or closing valves P or Q static or dynamic pressure can be applied to the loading cylinder.

Load measurement was by a 4-arm strain-gauge bridge attached to the centre of the yoke R in fig. 5.1. The bridge power supply was stabilized at 10V dc, and the output was fed via an·amplifier to the Y side of an X-Y plotter.

In tests on small DEN specimens of CSM/PR, the opening of the crack was measured by a clip gauge bearing on steel blocks fixed to the specimen above and below the crack. The output of the clip gauge strain gauges was fed to the chart drive of the Type "E" Tensometer. In later tests on CN specimens, the machine crosshead movement was used in place of the clip gauge output. The measurement of specimen compliance using the finite element method described in the previous chapter provides a relation between the displacement at the centre of the crack and the ends of the specimen, and has shown that for long cracks, the compliance measured at these two places is the same.

On the specially built machine, displacement measurements were made using LVDT or linear resistance transducers, the output being fed to the X side of the X-Y plotter. Initially, 2 X-Y plotters were used to monitor the displacement of the upper grips and the central opening of the crack. The load/displacement plots using these outputs gave the same failure load, so only the crack opening was monitored in subsequent tests.

Various off-set slope methods have been used to find the failure load in fracture toughness tests. The simplest and most consistent was found to be the peak load indicated by the load displacement recording. The amount of crack growth occurring prior to the peak load being reached was very small compared with the sawn crack length, so this initial crack length was used to calculate K_c. For DEN specimens, the formula (4) was used:

$$K_c = \sigma_{CG} \sqrt{W} \left[\tan \frac{\pi a_o}{W} + 0.1 \sin \frac{2\pi a_o}{W} \right]^{\frac{1}{2}} \qquad 5.2.1$$

and for CN specimens, the polynomial formula (6) was used:

$$K_c = \sigma_{CG} \sqrt{W} \left[\frac{a_o}{W} \right]^{\frac{1}{2}} \cdot \left[1.77 + 0.454 \left(\frac{a_o}{W} \right) - 1.02 \left(\frac{a_o}{W} \right)^2 + 5.4 \left(\frac{a_o}{W} \right)^3 \right] \qquad 5.2.2$$

where σ_{CG} is the gross stress applied to the ends of the specimen at failure, a_o is the initial crack length, and W is the specimen width.

5.3   The effect on K_c of specimen size, thickness and water absorption

Geometrically similar specimens were used to compare the effects of specimen size, thickness and water absorption on the fracture toughness of CSM/PR and WRF/PR. The half-crack length/width ratio, (a_o/W), was

kept as close to 0.1667 as possible on all specimens. For DEN specimens the length/width ratio, (L/W), was 2.67, and 2.00 for CN specimens. DEN specimens were made in widths 75, 100, and 150 mm and CN specimens 50, 100, and 150 mm. Thickness variation was achieved by cutting specimens from laminates of 3, 6, and 9 plies, the lay of both materials being as described in section 3.3.

K_c values obtained from DEN specimens of 3 ply CSM/PR, (table 5.1), using the peak recorded load and the initial crack length in equation 5.2.1 were found to vary with width and glass content. The glass content of each specimen was determined by burning the resin off about 10 gm of the material cut from the specimen after testing. (See section 3.2 for details of this procedure.) Assuming a linear variation of K_c with glass content, (fig. 5.3), it was possible to estimate that K_c at 35% glass content from the 150 mm specimens was 21.9% higher than the 75 mm value, (see summary of K_c values, table 5.4). The glass contents of the 100 mm specimens were all around 31%, but their K_c does not differ greatly from that of the 150 mm specimens at this glass content. The specimens were found to twist axially about 1° during testing.

The K_c values obtained from 3, 6, and 9 ply CN specimens of CSM/PR (table 5.2) were also plotted against specimen glass content (fig. 5.4) which shows no variation definitely attributable to thickness. Assuming a linear relation, the least squares method was used to determine K_c at 35% glass content for each width and thickness, (see table 5.4). Three ply specimens of CSM/PR were subjected to the water immersion treatment described in section 3.4 and, using the above procedure, their K_c values at 35% glass content were determined, (see fig. 5.5 and table 5.3).

The K_c values from 50, 100, and 150 mm wide specimens were found to be reduced by 15%, 5%, and 8% respectively.

Three, 6 and 9 ply CN specimens of WRF/PR were tested and their glass contents determined to find K_c at 65%. The glass content of WRF/PR did not vary as widely as CSM/PR, so that it was impossible to detect a quantifiable dependence on glass content, (fig. 5.6 and table 5.5). Where it was inappropriate to estimate K_c at 65%, the mean values only are given in table 5.7. To prevent grip failures the ends of 100 and 150 mm wide specimens were reinforced with strips of GRP material bonded on with Araldite. Nine ply 100 mm specimens had to be tested in a 500 kN Denison machine using wedge grips.

Plates 3 and 4 show 50 mm wide 3, 6, and 9 ply CN specimens of CSM/PR and WRF/PR. In the CSM/PR specimens, the fracture damage is confined to a narrow region, collinear with the original crack which broadens towards the edges, no strand protruding from the surface is greater than about 8 mm long. In the WRF/PR specimens, the fracture damage at the edges reaches the grips, and rovings up to 50 mm long are protruding from the surface. In both materials, there is no change in damage zone size with thickness. Plate 5 shows 150 mm wide CN specimens of 3 ply CSM/PR and WRF/PR. The CSM/PR damage zone is confined to a narrow region along the fracture surface, but the damage in the WRF/PR specimen extends nearly to the grips on one edge. In WRF/PR specimens, the crack does not travel across the specimen, but one or other of the uncracked ligaments gives way suddenly and completely.

K_c values obtained from dry and wet WRF/PR specimens are summarized in table 5.7. Variation in thickness does not have an appreciable effect

on K_c. The water immersion treatment reduces the K_c of 50, 100, and

150 mm wide CN specimens of 3 ply WRF/PR by 11%, 14%, and 15% respectively.

Fig. 5.8 summarizes the K_c values obtained from the different

widths of specimen used, 3, 6, and 9 ply results being combined. The

effect of water immersion on K_c is small compared with the increases

in K_c with width, and of the same order as the difference in K_c obtained

from DEN and CN specimens. The difference in K_c values obtained from

DEN and CN specimens could be due to the change in curing schedule,

(Appendix I), but it is more likely to be due to geometry, (24). The

fracture toughness of WRF/PR measured by the critical stress intensity

factor method is about 4 times that of CSM/PR, but shows a much greater

increase with specimen size.

5.4   The effect on K_c of varying (a_o/W)

Assuming a constant value of K_c with (a_o/W), equation 5.2.2 implies

that $\sigma_{CG} \longrightarrow \infty$ as $(a_o/W) \longrightarrow 0$, and a finite value as $(a_o/W) \longrightarrow 0.5$.

Taking into account the upper bound put on σ_{CG} by the material UTS,

K_c cannot be expected to remain constant as $(a_o/W) \longrightarrow 0$, or when there

is a very small uncracked ligament, as $(a_o/W) \longrightarrow 0.5$.

100 mm wide CN specimens of CSM/PR and WRF/PR, each containing

notches of different length, were used to determine K_c as (a_o/W) varied

from 0 to 0.4. CSM/PR specimens with $(a_o/W) < 0.03$ had to be reinforced

at the ends to prevent grip failures. For the same reason the ends of

all WRF/PR specimens had to be reinforced and specimens with $(a_o/W) < 0.05$

had to be tested in the Denison machine using wedge grips. The glass

content of each specimen was determined after testing.

The K_c values obtained from CSM/PR specimens, σ_{CG}, the gross stress applied along each end of the specimen at failure, σ_{CN}, the nett stress on the uncracked ligaments at failure, are given in table 5.9 and shown plotted against (a_o/W) in fig. 5.9. In previous sections, linear relationships have been assumed between UTS and glass content, and K_c and glass content. If these are of the type:

$$\sigma_{UTS} = A_1(GC) + B_1 \qquad K_c = A_2(GC) + B_2 \qquad 5.4.1$$

where GC is the glass content, and A_1, B_1, A_2, B_2 are constants, it can be shown that:

$$\frac{K_c}{\sigma_{UTS}} = \frac{A_2}{A_1} \left(1 - \frac{B_1}{\sigma_{UTS}}\right) + \frac{B_2}{\sigma_{UTS}} \qquad 5.4.2$$

Thus provided $\sigma_{UTS} \gg B_1$, B_2, K_c/σ_{UTS} should be roughly constant and independent of glass content. From the glass content of 150 mm wide CN specimens of CSM/PR, the specimen UTS was estimated using the relation shown in fig. 3.3, and the dimensionless group $K_{DC} = K_c/(\sigma_{UTS}\sqrt{W})$ evaluated. Table 5.8 shows this quantity to be sunstantially cònstant. Accordingly, the K_c and failure stresses of the 100 mm wide CN specimens .given in table 5.9 were expressed in the forms:

$$\sigma_{DCG} = (\sigma_{CG}/\sigma_{UTS}) \qquad \sigma_{DCN} = (\sigma_{CN}/\sigma_{UTS})$$

$$K_{DC} = K_c/(\sigma_{UTS}\sqrt{W}) \qquad 5.4.3$$

where σ_{UTS} was found from the specimen glass content. These quantities are plotted against (a_o/W) in fig. 5.10. Comparing this figure with

fig. 5.9, it can be seen that some of the scatter associated with glass content variation has been removed. In both figures it can be seen that there is a narrow range between $(a_o/W) = 0.15$ and 0.3 where K_c is reasonably constant with crack length. Outside this range, K_c falls by up to 30%. A plate without a notch broke at an applied stress equal to the material UTS given in table 3.8.

The K_c values obtained from WRF/PR specimens are shown in fig. 5.11, (see table 5.10), and in the dimensionless forms, (equations 5.4.3), in fig. 5.12. Fig. 5.12 shows that the range of glass content variation in the WRF/PR specimens is so small that the use of the dimensionless expressions has no effect on the scatter in K_c, σ_{CG}, and σ_{CN}.

WRF/PR specimens tested in the Instron 1195 and Denison machines are shown in plate 6. Typically, the specimens with short cracks failed by tensile roving breakage on one side, then a vertical crack propagated to the grips on the other. Bolted grips were used on the specimen in plate 6a, and the specimens in plate 6b and c with shorter cracks were tested in the Denison using wedge grips. In plate 6c, $(a_o/W) = 0.02$ and the failure occurred away from the crack, near the grips. This failure is similar to that observed in an unnotched 100 mm wide plate, which failed at an applied stress roughly equal to the nett section failure stress of the cracked specimens. This nett section stress can be seen from fig. 5.11 to be independent of crack length. If unnotched plates fail at the same stress, the specimens are apparently insensitive to the introduction of cracks.

Finite element analysis of a WRF/PR plate using the model described in section 4.2 with the nested elements removed, and one edge restrained

to simulate gripping, showed a concentration of tensile stress at the edge of the plate where it enters the grips of 2.7 times the applied stress. The restraint applied by the grips is not perfect, so this figure is an upper bound. It accounts for the failure of the unnotched plate at 0.6 of the material UTS, and it is clearly a more severe stress concentration than the small crack in plate 6c.

As crack length increases, the area of critical stress concentration is transferred to the region ahead of the crack. Analysis of an unnotched CSM/PR plate shows the stress concentration to be 2.4, but it does not appear to have the same effect, the material being more sensitive to sawn cracks and resin cracks. Crack length having no effect on σ_{CN} in WRF/PR specimens, K_c rises to a maximum at $(a_o/W) = 0.19$ and falls away sharply as $(a_o/W) \longrightarrow 0$ or 0.5.

In the tests on CSM/PR specimens, the change in compliance shown on load/displacement recordings was the same as that found on a specimen with no notch, and is due to non-linearity in the material compliances rather than sub-critical crack growth. This supports Holdsworth's view that there is no sub-critical crack growth in CSM/PR. In the WRF/PR specimens there was a large amount of specimen extension and crack opening during loading but no growth collinear with the original crack.

5.5   The failure of large specimens of CSM/PR and WRF/PR

The 1000 kN testing machine described in section 5.2 was used to test several large CN specimens of CSM/PR and WRF/PR. To reduce the amount of material used in the specimens their length/width ratio was reduced to 0.82, their width being 915 mm and crack lengths various.

All 915 mm specimens except RC35/CN1000 and RCW31/CN1000 were reinforced at the ends to prevent grip failures. It has been shown that K_c is independent of thickness so the material used was only 3 layers thick, but transverse buckling must be prevented if the results are to be applicable to thicker specimens. In the first test, on a CSM/PR specimen with $(a_o/W) = 0.219$, the restraints used to prevent buckling were inadequate, and the test was repeated. The second specimen was sandwiched between a thick wooden plank and a thick Perspex block, both 219 mm wide extending across the middle of the specimen, (see fig. 5.1). The K_c values found in these first two tests are given in table 5.11, (RC35/CN1000 and RC36/CN1000). The improved buckling restraints increase K_c by 33.6%. Hamilton and Berg (21), showed that reducing transverse buckling by increasing thickness also increased the K_c values obtained from CN specimens of GRP.

K_c, σ_{CG}, and σ_{CN} obtained from all tests on 915 mm CSM/PR specimens except the first are shown plotted against (a_o/W) in fig. 5.13 which suggests that there may be a larger range of (a_o/W) over which K_c is constant. In RC37/CN1000, where $(a_o/W) = 0.006$, the failure did not originate at the central sawn crack but in the resin rich edge of the specimen where several cracks appeared early in the test, (see plates 7a and b). The failure stress of this specimen is about half the material UTS as found from T2 specimens, 66.8 MPa. Testing these specimens with smaller cracks would probably result in similar failures. The presence of very small cracks or resin rich regions in which cracks develop at low stresses results in substantial reductions in failure stress of large CSM/PR specimens. The load/displacement recordings were linear up to failure, showing that there was no sub-critical crack growth.

Two 915 mm wide specimens of WRF/PR were tested, (table 5.11).
In RCW31/CN1000 with $(a_o/W) = 0.220$, there was about 30 mm of collinear
crack growth after the peak load had been reached and then the crack
propagated down to the grips on each, the uncracked ligament sections
pulling away from the bolts. The failure of the second specimen is
shown in plate 7c. On reaching the peak load, the crack propagated
horizontally to the edge on the right hand side and then down to the
grips on the other side as in the previous specimen.

Comparing K_c values obtained from 100 mm and 915 mm CN specimens
of the two materials, with $(a_o/W) = 0.055$ and 0.22, those from WRF/PR
show the greatest changes with crack length and width. For both crack
lengths, in CSM/PR K_c from 915 mm specimens is 50% higher, but in WRF/PR
it is 230% higher. Large specimens of CSM/PR fail at stresses less than
half the material UTS, but large specimens of WRF/PR fail at approximately
the same stresses as the smaller specimens.

Fig. 5.14a shows K_c plotted against $\sqrt{W}$ for CSM/PR specimens
with $(a_o/W) = 0.1667$ using the results obtained in section 5.3, and
estimating K_c from fig. 5.13. Also included are K_c values found by
Holdsworth (24) and Bishop (61) which are given in table 2.1. For the
materials in fig. 5.14a, K_c appears to vary linearly with $\sqrt{W}$. Fig. 5.14b
shows that WRF/PR K_c varies linearly with W.

The trial of various yield stresses in Irwin's correction,
(equation 2.2.6), by Owen and Bishop (8) to find a K_c value that is
independent of width implies that since K_c is constant, r_y is also
constant. The method is therefore equivalent to adding equal increments
of crack length to the initial crack length of the different sized specimens
and seeing which one produces K_c that are independent of width. This

procedure was applied to the results obtained for 50, 100, 150, and 915 mm CN specimens of CSM/PR, and the K_c values obtained are given in table 5.12. There appear to be increments which make any 2 out of 4 roughly equal, but none make all K_c values equal.

5.6 Conclusions

The effect of specimen type on K_c values obtained from CSM/PR specimens is smaller than variations caused by size and crack length. Hamilton and Berg (21), showed the effect may be reduced by testing thicker specimens.

K_c does not change with specimen thickness so it is unlikely that either material is capable of supporting plane strain conditions.

The effect of damage caused by the water immersion treatment reduces K_c by roughly 10% in each material which is small compared with variations due to other causes.

WRF/PR shows a much greater increase in K_c with size than CSM/PR. 915 mm specimens of WRF/PR fail at the same stresses as 100 mm ones. The smaller increase in K_c with size in CSM/PR specimens means that 915 mm specimens fail at much lower stresses than 100 mm ones with the same crack length.

The failure stress of 100 mm CN specimens of CSM/PR is sensitive to small cracks and there is a narrow range of crack length over which K_c is fairly constant. The failure stress of 100 mm WRF/PR specimens is insensitive to increases in crack length.

K_c values from 100 mm wide CN specimens of CSM/PR could be used to provide a lower bound for the prediction of failure in bigger specimens and structures of this material, but the K_c approach is not

appropriate for WRF/PR. K_c values from small specimens would give very conservative failure predictions in large structures, the material being less sensitive to cracks than CSM/PR. The relationships suggested in fig. 5.14 could be used to obtain a closer approximation in CSM/PR.

The use of Irwin's correction does not eliminate changes in K_c with specimen size.

CHAPTER 6   FATIGUE CRACK GROWTH IN CSM/PR AND WRF/PR

6.1   Introduction

The published work discussed in section 2.5 shows that the fatigue crack propagation law,

$$\frac{da}{dN} = A \triangle K^m \qquad\qquad 6.1.1$$

that is found to apply to many metals, may also apply to some GRP. The first objective of this part of the project was to determine fatigue crack propagation laws for the two materials under investigation for periods greater than 20000 cycles.

The effect of damage due to prolonged water immersion on the strength, stiffness, and fracture toughness of CSM/PR and WRF/PR has been shown to be small. Other workers, (section 2.4), have shown that water has a more serious effect on fatigue strength, so it is likely to affect fatigue crack growth rate. The second objective is therefore to find out how crack growth is affected by water immersion treatment described in section 3.4.

6.2   Test methods

CN specimens were used for all fatigue crack propagation tests as shown in fig. 2.1. The 35 kN hydraulic pulsator testing machines have been described by Owen (60). Load measurement is by strain gauged load cells powered by a stabilised voltage supply. The output is fed via an amplifier to a digital voltmeter. The amplifier gain can be adjusted so that the DVM reads in kN. For dynamic measurement, the

bridge output is fed directly to an oscilloscope set to a high gain.

On beginning a test, the oscilloscope trace is set to a zero position,

the load cell is unbalanced so that an amount equal to minus the desired

load appears on the DVM. Dynamic load is then applied until the peak

of the load trace touches the zero position on the oscilloscope screen.

A tension-tension load cycle was applied to the specimens. The

load required to give a desired K_{max} value was calculated from equation

5.2.2, and 10% of this applied statically to the specimen as a base load

to prevent it going into compression. The cycle shape is such that

the minimum tensile load in it is small compared with the maximum load

and so can be regarded as nominally zero-tension. $K_{max} = \triangle K$, the stress

intensity factor range.

Measurement of crack length was by the compliance method.

Specimen compliance was measured using an X-Y plotter. The load cell

output was fed to the Y side, and the displacement of 2 steel blocks

fixed above and below the centre of the crack recorded by an LVDT

transducer, (fig. 6.1), fed to the X side. The specimen was loaded to

about 3 kN and unloaded 3 times, and the loading and unloading slopes

measured from the plotter recording.

At the beginning of a test the sawn crack was measured with a

travelling microscope and a value of the dimensionless compliance C_D

corresponding to the crack length found from the appropriate finite

element compliance-crack length relation, (fig. 4.4). The initial

compliance was then measured, and the value of C_D assigned to the mean

of the slopes on the plotter. This is allowable because C_D is constant

at a particular crack length regardless of specimen glass content, and

gives a constant by which all plotter slopes taken from a specimen during a test can be converted to C_D values. Note that this method does not require the plotter gains to be calibrated in Newtons and millimetres, but merely to be constant throughout a test. Crack length is expressed in the dimensionless form, $(a/W) = a_D$.

The test method chosen was to cycle several specimens each at a constant value of $\triangle K$. This requires the load to be reduced according to equation 5.2.2 as the crack length increases. If the crack growth law, 6.1.1, holds, then a_D should vary linearly with N and a constant value of da_D/dN be obtained from each specimen. Plotting $\log \triangle K$ against $\log da_D/dN$ linearises equation 6.1.1 so that the constants A and m may be obtained easily:-

$$\log(da/dN) = m \log \triangle K + \log A \qquad\qquad 6.2.1$$

The alternative is to cycle at constant load. To find A, m the numerical methods described in section 2.5 have to be used on the a_D, N curve to obtain da_D/dN. Only one specimen need be tested to find A and m but if there is scatter in the a_D, N curve da_D/dN may be grossly in error. There being only a limited amount of time and material available, this method was used on the 915 mm wide specimen.

Having measured the initial compliance, a specimen would be cycled for about 200-500 cycles at the initial load. The load was then removed and the compliance again measured. A computer program containing equation 5.2.2 and the polynomials fitted to the compliance-crack curves for the appropriate material and specimen, was used to calculate the increase in crack length and the new load to keep $\triangle K$ constant. Longer

periods of cycling followed by load adjustment were repeated until either the specimen broke or a large number of a_D, N results had been obtained. The cycling frequency on the Owen machines was 1.67 Hz, and on the large machine 3.00 Hz. The ends of WRF/PR specimens loaded greater than 23 kN had to be reinforced to prevent grip failures. Water immersed specimens were tested in a water jacket to prevent drying out under test.

6.3   Fatigue crack propagation in dry and wet CSM/PR

Fatigue crack propagation tests were carried out on 100 mm wide CN specimens of CSM/PR with $(a_o/W) = 0.1667$. Stable crack growth took place in a narrow band of $\triangle K$ values below K_c, and was collinear with the original crack, (plate 8). The crack length found by the compliance method corresponded reasonably well with the length of crack growth in the specimen.

It was found that the glass content of the specimens greatly affected the rate of crack growth. Curves of a_D versus cycles from specimens tested at various $\triangle K$ ranges are shown in fig. 6.2. In two specimens subjected to different $\triangle K$ ranges, ($\triangle K = 8.0$ MPa $m^{\frac{1}{2}}$ ○ and $\triangle K = 9.5$ MPa $m^{\frac{1}{2}}$ ■), crack growth occurs at the same rate. In the specimen subjected to $\triangle K = 7.75$ MPa $m^{\frac{1}{2}}$ ● for more than 2 million cycles, the rate of crack growth was very low. A higher propagation rate was observed in the specimen tested at $\triangle K = 7.5$ MPa $m^{\frac{1}{2}}$ □, which failed at 397640 cycles, (see table 6.1). $\triangle K$ can be expressed in the dimensionless form $\triangle K_D = \triangle K/(\sigma_{UTS}\sqrt{W})$, which was described in section 5.4, where σ_{UTS} is the local UTS of the material found from the glass content. From table 6.1, the $\triangle K_D$ values of the specimens tested at 8.0 and 9.0 MPa $m^{\frac{1}{2}}$ are approximately the same, and $\triangle K_D$ of the 7.5 MPa $m^{\frac{1}{2}}$ specimen

is higher than that of the 7.75 MPa $m^{\frac{1}{2}}$ specimen, which accounts for the observed rates of crack growth.

The curves in fig. 6.2 exhibit three phases of crack growth. An initial short phase of rapid crack growth, a longer period of steady crack growth at a roughly constant rate, and a final phase of rapid propagation as failure takes place. Usually in the later stages of a test, growth continued on one side of the specimen in preference to the other. The width of material remaining on this side was thus less than indicated by the mean length found from the compliance measurements. Premature failure of the specimen occurred, an example of which in fig. 6.2 is $\Delta K = 8.25$ MPa $m^{\frac{1}{2}} \nabla$.

The rate of crack growth, da_D/dN, in the central phase was determined by using the least squares method to fit a straight line through the points in this region. They are the thin dashed lines in fig. 6.2. A logarithmic graph of da_D/dN against K_D is shown in fig. 6.3. The constants A and m were determined from the least squares fit of equation 6.2.1 to the points in the figure giving:

$$\frac{da_D}{dN} = 3.37 \times 10^7 \, \Delta K_D^{20.33} \qquad\qquad 6.3.1$$

or, the following may be expected from dry CSM/PR with a glass content of 35%:

$$\frac{da}{dN} = 1.19 \times 10^{-26} \, \Delta K^{20.33} \qquad\qquad 6.3.2$$

where a is in metres and ΔK in MPa $m^{\frac{1}{2}}$.

In fig. 6.2, it can be seen that the central phase of the a_D, N curves of specimens tested at ΔK values close to K_c tends to be curved

rather than straight. It has been shown in section 5.4 that K_c falls as a_D increases beyond 0.2. Therefore as the crack in a cycled specimen lengthens beyond $a_D = 0.2$, the K_c value of the specimen gradually approaches the $\triangle K$ range at which the specimen is being tested. It might be expected therefore that da_D/dN increases with a_D rather than remaining constant. The crack propagation law due to Forman et al (41) equation 2.5.2, was devised to allow for the effect of K_c on crack propagation rate. If $K_{min} \approx 0$, it becomes:

$$\frac{da}{dN} = \frac{A \triangle K^m}{(K_c - \triangle K)} \qquad\qquad 6.3.3$$

Clearly if K_c is constant with crack length, cycling at constant $\triangle K$ would still cause growth at constant da/dN, but if as a increases, $K_c \longrightarrow \triangle K$, then $da/dN \longrightarrow \infty$. A quadratic polynomial was fitted to the K_{Dc} versus a_D data for 100 mm wide CN specimens of CSM/PR given in fig. 5.10 of the form:

$$K_{Dc} = B_o + B_1 a_D + B_2 a_D^2 \qquad\qquad 6.3.4$$

Substituting into 6.3.3 gives:

$$\frac{da_D}{dN} = \frac{A \triangle K_D^m}{B_o + B_1 a_D + B_2 a_D^2 - \triangle K_D} \qquad\qquad 6.3.5$$

Integrating along the a_D, N curves in fig. 6.2 where $\triangle K$ is constant with a_D gives, (see Appendix II):

$$N - N_i = k \left[\left[B_o - \triangle K_D \right] \cdot (a_D - a_{Di}) + \frac{B_1}{2} (a_D^2 - a_{Di}^2) + \frac{B_2}{3} (a_D^3 - a_{Di}^3) \right] \qquad 6.3.6$$

where a_{Di}, N_i are initial values at the beginning of the region of steady crack growth, and :

$$k = 1/(A \triangle K^m) \qquad\qquad 6.3.7$$

To fit equation 6.3.6 to the points in fig. 6.2 the least squares method was used to find a value of k which made the sum of the squares of the residuals a minimum, (see Appendix II). The solid lines in fig. 6.2 were determined in this way. The fit is reasonable except where premature failure occurs. Equation 6.3.7 can be expressed:

$$-\log k = m \log \triangle K_D + \log A \qquad\qquad 6.3.8$$

so that A and m can be found by plotting -log k against log $\triangle K_D$. Fig. 6.4 gives values for A and m as follows, (least squares fit):

$$\frac{da_D}{dN} = \frac{2.31 \times 10^3 \, \triangle K_D^{15.97}}{(K_{Dc} - \triangle K_D)} \qquad\qquad 6.3.9$$

or, at 35% glass content:

$$\frac{da}{dN} = \frac{2.94 \times 10^{-26} \, \triangle K^{15.97}}{(K_c - \triangle K)} \qquad\qquad 6.3.10$$

Three specimens of CSM/PR were subjected to the water immersion treatment described in section 3.4 and cycled at various constant $\triangle K$ values. Comparing dry and wet specimens in table 6.1 tested at similar $\triangle K$ values, growth takes place at a rate at least three orders of magnitude higher in the wet specimens. As tests were conducted at low $\triangle K$ compared with K_c, there is no discernable increase in da_D/dN with a_D

until just before failure, (see fig. 6.5). Equation 6.1.1 was applied as before, and fig. 6.6 gives values of A and m as follows:

$$\frac{da_D}{dN} = 1.32 \times 10^5 \, \Delta K_D^{12.86} \qquad\qquad 6.3.11$$

or, at 35% glass content:

$$\frac{da}{dN} = 3.92 \times 10^{-17} \, \Delta K^{12.86} \qquad\qquad 6.3.12$$

Comparing equations 6.3.12 with 6.3.2, the constant A appears to correspond to the large increase in da/dN due to water damage, (table 6.1), while the lower index, m, in the wet version indicates how close to K_c the values of ΔK are, at which observable rates of crack growth are taking place. Fatigued wet and dry CSM/PR specimens are shown in plate 8.

6.4 Fatigue crack propagation in dry and wet WRF/PR

Fatigue crack propagation tests were carried out on 100 mm wide CN specimens of WRF/PR with $(a_o/W) = 0.1667$. Fracture toughness tests on this material have shown that even large specimens are notch insensitive, unlike CSM/PR. In the last section, stable crack growth in CN specimens of CSM/PR was described which was collinear with the original crack, and occurred over a narrow range of ΔK_D values. The behaviour of WRF/PR specimens was completely different, although the apparent crack growth took place over roughly the same range of ΔK_D values.

Although an increase in compliance was recorded as the specimens were cycled, it did not correspond to observable, collinear crack growth. The load was reduced to keep ΔK constant as crack length apparently increased. The curves of (a/W) against cycles (N) for the values of ΔK_D

tested are shown in fig. 6.7, and can be divided into 4 phases as shown
in the inset. Phase 1 corresponds to the rapid growth of vertical
shear cracks at each end of the initial crack and normal to it. This
occurs over the first few hundred loading cycles, blunting the initial
crack and blocking horizontal crack growth. The compliance measurements
indicate a large increase in horizontal crack growth which will henceforth
be called "apparent crack growth".

In phase 2 the vertical shear cracks grow steadily accompanied
by increasing cross-over damage in the uncracked ligaments, (see plates
9a and b). The change in specimen compliance in this phase is due to
lengthening of the vertical cracks, which increases the length of the
ligaments whose compliance is really being measured, (see fig. 6.8).
In phase 3 the rate of apparent crack growth decreases abruptly. The
vertical cracks have stopped growing, probably because the load which
is steadily being reduced is no longer large enough to propagate them.
Apparent crack growth in this phase is caused by increasing cross-over
damage in the ligaments and resin shedding around the horizontal rovings
bridging the vertical cracks. Cross-over damage becomes concentrated
at the tip of one of the vertical cracks.

In the final phase, the fibres bridging the vertical crack give
way and there is a large increase in specimen compliance. Load is
transferred to the damaged section of the ligaments adjacent to the
tips of the vertical cracks. Horizontal crack propagation then takes
place across this region, continuing steadily until the ligament gives
way, (plate 9c). The mechanism of this failure is shown schematically
in fig. 6.8.

Damaged sections were cut from specimens which had failed in this way, and from specimens where the load was too low for the final phase to occur, even after long periods of cycling. The resin was burnt from the samples in a muffle furnace to examine the damage to the rovings. The failed final phase sections showed breakage of the rovings bridging the vertical cracks, and that the horizontal failure comprised breakage of individual rovings up to 10 mm away from the mean line of the failure, so that the section was still held together by friction. In the phase 3 sections, some of the rovings bridging the vertical cracks had broken, and there was some breakage of vertical strands.

To see whether specimen size affected this behaviour, a 915 mm CN specimen with an initial total crack length of 100 mm was subjected to cycling at a constant load of 125 kN in the testing machine described in section 5.2. The test was carried out at constant load because the crack growth rate in fig. 6.7 appears to be independent of $\triangle K$, (table 6.2). The same vertical cracks occurred at each end of the central crack, increasing in length as cycling progressed. The graph of apparent (a/W) with cycles is shown in fig. 6.9.

The fatigue crack propagation behaviour of this material is changed by the water immersion treatment. There is initially a sharp rise in compliance due to the growth of vertical cracks at the crack tips, but their length is much shorter than the vertical cracks in the dry specimens, and they appear ineffective in preventing horizontal crack propagation. However, for a given $\triangle K$ range, the apparent initial crack growth in the wet specimens is larger, so that some horizontal crack growth may be taking place, (see plate 9d). There is no growth of vertical cracks,

the specimen passes directly from phase 1 to the final phase. Examination of the glass in failed sections shows a horizontal failure similar to that occurring in the dry specimens but closer to the line of the original crack. Increases in specimen compliance with cycling is due to horizontal crack growth, which takes the form of progressive cross-over damage and vertical roving breakage.

The damage caused by prolonged water immersion eliminates the crack blunting mechanism in WRF/PR, rendering it sensitive to the presence of cracks. Fatigue life of cracked specimens is reduced accordingly. The curves of (a_D) against cycles, (fig. 6.10), for the wet specimens can be seen to be unlike those for the dry ones, (fig. 6.7). Comparing specimens subjected to the same $\triangle K$ range, ($\triangle K = 22$ MPa $m^{\frac{1}{2}}$, $\triangle K_D \approx 0.17$), the dry specimen was still intact after 4904000 cycles, while the wet one broke after 271680 cycles. In the dry specimens, the period taken up by phase 2, vertical crack growth, increases with $\triangle K$, but the growth rate is about the same (see table 6.2). In phase 3, the growth rate is also roughly independent of $\triangle K$, but it lasts for a shorter period as $\triangle K$ increases. In the wet specimens, the growth rate is constant with cycles and increases with $\triangle K$ as in CSM/PR specimens. At $\triangle K = 22$MPa $m^{\frac{1}{2}}$, the rate of apparent phase 2 crack growth in the dry specimens is 2.15×10^{-7}, while the rate of crack growth in the wet specimens is 4.1×10^{-7}. The latter is more serious because it corresponds more closely to horizontal crack growth.

Fig. 6.11 shows that for the wet specimens a linear relationship exists between $\log(da_D/dN)$ and $\log(\triangle K_D)$, so that equation 6.1.1 seems appropriate. From fig. 6.11 values of A and m may be found giving:

$$\frac{da_D}{dN} = 0.00794 \, \Delta K_D^{5.6} \qquad\qquad 6.4.1$$

or, at 65% glass content:

$$\frac{da}{dN} = 1.66 \times 10^{-15} \, \Delta K^{5.6} \qquad\qquad 6.4.2$$

As in wet CSM/PR, the values of ΔK at which these specimens were tested is too low to be affected by the variation in K_c with crack length.

Comparing this work with that of other investigators, the type of vertical crack propagation found in dry WRF/PR occurs in unidirectional composites, (49)(53). Owen and Bishop (52) subjected CN specimens of a woven fabric/polyester resin to constant ΔK range cycling (from 3.5 to 15.9 MPa $m^{\frac{1}{2}}$, $K_c = 21$ MPa $m^{\frac{1}{2}}$) and found that although a large damage zone formed ahead of the crack comprising vertical cracks and cross-over damage, horizontal crack growth did take place and equation 6.1.1 was applicable. The woven fabric (Tyglass Y449) is much finer than the ECK25 used in WRF/PR, which would be little affected by cycling at $\Delta K = 15.9$ MPa $m^{\frac{1}{2}}$. The glass content of the Owen and Bishop material was 57% compared with 66% in WRF/PR, insufficient to account for their difference in crack growth resistance.

6.5   Conclusions

The rate of fatigue crack propagation in CSM/PR is dependent on glass content.

Equation 6.1.1 is valid for CSM/PR up to two million cycles, but equation 6.3.3 is a better description of crack growth at ΔK values

close to K_c. At lower ΔK, they are equivalent.

The resistance to fatigue crack propagation of WRF/PR is superior to CSM/PR and is due to crack blunting which blocks horizontal crack growth. The application of growth laws is inappropriate.

For marine applications, the most important finding is the severe reduction in fatigue crack growth resistance caused by prolonged water immersion. Although the resistance of WRF/PR is still greater than CSM/PR, its crack blunting mechanism is destroyed, and the growth law becomes applicable.

CHAPTER 7

CONCLUSIONS AND SUGGESTIONS FOR FUTURE WORK

The static and fatigue properties of both GRP materials tested in this project are dependant on glass content. This is most serious in CSM/PR, because even when prepared under laboratory conditions, the glass content of a large laminate can vary up to $\pm10\%$ of the mean. In commercial laminates, there is likely to be a larger variation. It is easier to produce WRF/PR laminates with the same glass content, (see Appendix I), and variation within the laminate is less.

Of the two materials, the tensile strength and fracture toughness of WRF/PR is superior, failure stress being virtually insensitive to the presence of cracks of specimen size. The K_c approach is not appropriate for this material. Tests on the largest specimens of CSM/PR show that it is possible for failures by rapid crack propagation to occur in large structures made of notch sensitive GRP material. Resin rich regions act as crack initiation sites for these failures and the K_c method can be used to estimate the failure of larger cracked specimens of notch sensitive material. Some of the requirements for valid fracture toughness testing of GRP using the critical stress intensity factor approach have been established from the literature survey, and the results given in Chapter 5. They are as follows:

1) Allowance should be made for variations in specimen glass content, and K_c should be quoted at a particular glass content.

2) The specimen should either be thick enough for transverse buckling to be negligable, or supports should be used to prevent it. K_c should then be independant of specimen thickness, and among tension specimens, variations due to geometry should be reduced.

3) The material under test should be notch sensitive. The greater the

notch sensitivity, the more applicable the K_c approach.

4) The specimen should be as big as is practicable, since the load/displacement recordings of large specimens show the least deviation from linearity.

A K_c that is entirely independant of crack length or width of specimen has not been found, but the work of Holdsworth (24) and Bishop (61) shows that K_c from specimens with (a_o/W) not tending to 0 or 0.5 can be used to predict the failure of structures of comparable size.

The Paris fatigue crack propagation law describes low rates of crack growth in CSM/PR adequately up to 2 million cycles. Higher rates of growth are better described by using Forman's law and allowing for the variation in K_c with crack length. WRF/PR is much more resistant to fatigue cracking than CSM/PR, because the progress of the cracks is blocked by rovings normal to the crack. The growth laws do not provide an adequate description of this behaviour.

Perhaps the most important results obtained regarding the use of GRP in shipbuilding are those concerning the effect of prolonged water immersion on CSM/PR and WRF/PR. The effect on tensile strength, stiffness and fracture toughness is small in proportion to the greater reduction in resistance to fatigue crack propagation. In CSM/PR the rate of crack growth at a given $\triangle K$ value is increased by at least three orders of magnitude. In WRF/PR, the fatigue crack blocking mechanism is destroyed, so that the Paris crack growth law becomes applicable, but the material is still superior to CSM/PR.

Future investigations could be directed at finding a resin or glass treatment which makes the glass-resin interface less susceptible to attack by water. Flexible resins which crack at higher strains may be more resistant to fatigue crack growth in hostile environments.

More tests should be conducted on large specimens to examine fully the effect of specimen size and crack length on fracture toughness and fatigue crack propagation. A control system based on a diode function generator to keep $\triangle K$ constant as the crack length increases was designed and a prototype built, intended for use with the machine described in section 5.2. Its development would greatly shorten fatigue crack propagation test programs which when carried out by the methods described in section 6.2 are extremely time consuming.

References

1. Griffith, A. A.   "The Phenomenon of Rupture and Flow in Solids", Phil. Trans. Roy. Soc. (London), vol. 221, 1920, p.163.

2. Irwin, G. R. and Kies, J. A.   "Critical Energy Rate Analysis of Fracture Strength", Welding J. Research Supplement, vol. 33, 1954, p.193.

3. Westergaard, H.M.   "Bearing pressures and cracks", A.S.M.E. J. Appl. Mechanics, 1939, p.49.

4. Paris, P. C. and Sih, G. C.   "Stress Analysis of Cracks", ASTM, STP 381, Philadelphia, 1965, p.30.

5. Irwin, G. R.   "Analysis of Stresses and Strains near the end of a Crack Traversing a Plate", Trans. A.S.M.E., J. Appl. Mechanics, vol.24, 1957, p.361.

6. Brown, W. F. and Srawley, E.   "Plane Strain Crack Toughness Testing of High Strength Metallic Materials", A.S.T.M. STP 410, 1966

7. Irwin, G. R.   "Plastic Zone Near a Crack and Fracture Toughness", 7th Sagamore Ordnance Materials Research Conference, 1960.

8. Owen, M. J. and Bishop, P. T.   "Critical Stress Intensity Factors Applied to Glass Reinforced Polyester Resin", J. Composite Materials, vol. 7, 1973, p.146.

9. Holdsworth, A. W., Owen, M. J. and Morris, S.   "Macroscopic Fracture Mechanics of Glass Reinforced Polyester Resin Laminates", J. Composite Materials, vol. 8 1974, p.117

10. Rice, J. R.   "A Path Independent Integral and the Approximate Analysis of Strain Concentration by Notches and Cracks", Trans. A.S.M.E. J. Appl. Mechanics, 1966, p.379.

11. Begley, J. A. and Landes, J. D.   "The J Integral as a Fracture Criterion", A.S.T.M. STP 514, Philadelphia 1972, p.1.

12. Light, M.S.   "A Numerical Investigation into Post-yield Fracture". Univ. of Wales, Ph.D Thesis, 1975.

13. Andrews, E. H.   "A Generalized Theory of Fracture Mechanics", J. Materials Science, vol. 9, 1974, p.887.

14. Sih, G. C.   "Strain Energy Density Factor Applied to Mixed Mode Crack Problems", Int. J. Fracture, vol. 10, 1974, p.305.

15. Wu, E. M.   "Failure Criteria to Fracture Mode Analysis of Composite Materials", 39th Meeting AGARD, Structures and Materials Panel, Munich, 1974.

16. Wu, E. M. and Reuter, R. C.
Application of Fracture Mechanics to Orthotropic Plates" University of Illinois, Department of Theoretical and Applied Mechanics, Report No. AD-613 576, 1963

17. Sandford, R. J. and Stonesifer, R.
"Fracture Toughness Measurements in Unidirectional Glass Reinforced Plastics", J. Composite Materials, vol. 5, 1971, p.241.

18. Beaumont, P. W. R. & Phillips, D. C.
"The Fracture Energy of a Glass-fibre Composite", J. Materials Science, vol. 7, 1972, p.682.

19. Beaumont, P. W. R. & Phillips, D. C.
"Tensile Strength of Notched Composites", J. Composite Materials, vol. 6, 1972, p.32.

20. McGarry, F. and Mandell, J. F.
"Fracture Toughness studies of Fibre Reinforced Plastic Laminates", Faraday Special Discussions of the Chemical Society, No. 2, 1972.

21. Hamilton, R. and Berg, C.
"Fracture Mechanics of Fibre Glass Laminates", Fibre Science and Technology, vol. 6, 1973, p.55.

22. Owen, M. J. and Rose, R. G.
"The Fracture Toughness and Crack Propagation Properties of Polyester Resin Casts and Laminates", J. Phys. D: Appl. Phys., vol. 6, 1973, p.42.

23. Holdsworth, A., Morris, S. and Owen, M. J.
"An Energy Approach to the Determination of Fracture Toughness of GRP", J. Phys. D: Appl. Phys., vol. 7, 1974, p.2036.

24. Holdsworth, A. W.
"Fracture Toughness of Glass Reinforced Plastics" Nottingham University Ph.D. Thesis, 1973.

25. Mandell, J. F., McGarry, F. J., Wang, S. S. and Im, J.
"Stress Intensity Factors for Anisotropic Fracture Test Specimens of Several Geometries", J. Composite Materials, vol. 8, 1974, p.106.

26. Gagar, S., and Broutman, L. J.
"The Development of a Damage Zone at the Tip of a Crack in Glass Fibre Reinforced Polyester Resin", Int. J. Fracture, vol. 10, 1974, p.606.

27. Gagar, S., and Broutman, L. J.
"Effect of Crack Tip Damage on Fracture of Random Fibre Composites", Materials Science and Engineering, vol. 21, 1975, p.177.

28. Barnby, J. T. and Spencer, B.
"Crack Propagation and Compliance Calibration in Fibre Reinforced Polymers", J. Materials Science, vol. 11, 1976, p.78.

29. Spencer, B., and Barnby, J. T.
"The Effects of Notch and Fibre Angles on Crack Propagation in Fibre Reinforced Polymers", J. Materials Science, vol. 11, 1976, p.83.

30. Fried, N., Kaminetsby, J. and Silverglect, M.
"The Effect of Deep Submergence Operational Conditions on Filament Wound Plastics", 21st Annual Technical Conference, Society of Plastics Industries, Reinforced Plastics Division, 1966.

31. Wyatt, R. C. and Ashbee, K. H. G.
"Deloading of Carbon Fibre/Polyester Resin Composites Exposed to Water: Comparison with 'E' Glass Composites", Fibre Science and Technology, vol. 2, 1969-70, p.29.

32. Vaughn, D. J. and McPherson, E. L.
"Effects of Adverse Environmental Conditions on the Resin Glass Interface of Epoxy Composites", Composites, vol. 4, 1973, p.131.

33. Pritchard, G. and Taneja, N.
"Water Damage in Polyester/Glass Laminates; I : An Apparatus for the Study of Water Damage in Uniaxially stressed Materials, II : Microscopic Evidence", Composites, vol. 4, 1973, p.181 and p.199.

34. Blaga, A. and Yamasahi, R.
"Mechanism of Breakdown in the Interface Region of Glass Reinforced Polyester by Artificial Weathering", J. Materials Science, vol. 8, 1973, p.654.

35. Blaga, A. and Yamasaki, R.
"Mechanism of Surface Microcracking of the Matrix in Glass Reinforced Polyester by Artificial Weathering", J. Materials Science, vol. 8, 1973, p.1331.

36. Beaumont, P.W.R. and Harris, B.
"The Effect of Environment on Fatigue and Crack Propagation in Carbon Fibre Reinforced Epoxy Resin", International Conference on Carbon Fibres, their Components and Applications, Plastics Institute, London, 1971, paper 49.

37. Romans, J. B., Sands, A. G. and Cowling, J. E.
"Fatigue Behaviour of Glass Filament Wound Epoxy Composites in Water", Industrial and Engineering Chemistry, Product Research and Development, vol. 11, 1972, p.261.

38. Paris, P. C.
"A Note on the Variables Affecting the Rate of Crack Growth due to Cyclic Loading", Boeing Co. Document No. D-17867, Addendum N, 1957.

39. Weertman, J.
"Rate of Growth of Fatigue Cracks Calculated from the Theory of Infinitesimal Dislocations Distributed on a Plane", Int. J. Fracture Mechanics, vol. 2, 1966, p.460.

40. Paris, P. C. and Erdogan, F.
"A Critical Analysis of Crack Propagation Laws", J. Basic Engineering, vol. 85, 1963, p.528.

41. Forman R. G., Kearny, V. E. and Engle, P. M.
"Numerical Analysis of Crack Propagation in Cyclic Loaded Structures", J. Basic Engineering vol. 89, 1967, p.459.

42. Walton, D. and Ellison, E. G.
"Fatigue Crack Initiation and Propagation", International Metallurgical Reviews vol. 17, 1972, p.100.

43. Davies, K. B. and Feddersen, C. E.
"Evaluation of Fatigue Crack Growth Rates by Polynomial Curve Fitting", Int. J. Fracture, vol. 9, 1973, p.116.

44. McCartney, L. N. and Cooper, P.
"Computerised Processing of Fatigue Crack Propagation Data", National Physical Laboratory Report, Mathematical Applications, 1972.

45. Munro, H. G.
"The Determination of Fatigue Crack Growth Rates by a Data Smoothing Technique", Int. J. Fracture, vol. 9, 1973, p.366.

46. Smith, R. A.
"The Determination of Fatigue Crack Growth Rates from Experimental Data", Int. J. Fracture, vol. 9, 1973, p.352.

47. Borduas, H. F., Culver, L. E., and Burno, D. J.
"Fracture Mechanics Analysis of Fatigue Crack Propagation in PMMA", J. Strain Analysis, vol. 3, 1968, p.193.

48. Mukherjee, B. and Burns, D. J.
"Effect of Frequency, Mean Range of Stress Intensity Factors on Fatigue Crack Growth in PMMA", Experimental Mechanics, vol. 11, 1971, p.433.

49. Hertzberg, R. W. Manson, J. A. and Nordberg, H.
"Fatigue Crack Propagation in Resin-fibre Composites", Ohio State University, Report No. AD-700 434, 1963.

50. Sih, G. C. Hilton, P. D. and Wei, R. P.
"Exploratory Development of Fracture Mechanics in Composite Systems", Report No. AD-709 214, 1970.

51. Thornton, P. A.
"Fatigue Crack Propagation in a Discontinuous Composite", J. of Composite Materials, Vol. 6, 1972, p.147.

52. Owen M. J. and Bishop, P. T.
"Crack Growth Relationships for Glass Reinforced Plastics and their Application to Design", J. Phys. D : Appl. Phys., vol. 7, 1974, p.1214.

53. Harris, B., Anleara, A. O. and McGuire, M.A.
"Fatigue Crack Propagation in Metal Matrix/ Metal Fibre Composites", J. Phys. D : Appl. Phys., vol. 9, 1976, p.365.

54. Marshall, G. P., Culver, L. E., and Williams, J. G.
"Crack and Braze Propagation in Polymers: a Fracture Mechanics Approach", Plastics and Polymers, vol 37, 1969, p.75.

55. Tsai, S. W.
"Experimental Determination of the Elastic Behaviour of Orthotropic Plates", J. Engineering for Industry, vol. 87, 1965, p.315.

56. Walters, J. V.   "Finite Element Analysis of Fibre Reinforced Plastic Limbs", Univ. of Nottingham Ph.D. Thesis, 1975.

57. Chau, S. K., Tuba, I. S. and Wilson, W. K.   "On the Finite Element Method in Linear Fracture Mechanics", Engineering Fracture Mechanics, vol. 2, 1970, p.1.

58. Irwin, G. R.   "Fracture Testing of High-strength Sheet Materials Under Conditions Appropriate for Stress Analysis", NRL Report No. 5486, 1960.

59. Dudley, B. R. and Pope, J. A.   "State and Fatigue Testing Machine for Rotor Discs", J. Mechanical Engineering Science, vol. 3, 1961, p.241.

60. Owen, M. J.   "A New Fatigue Testing Machine for Reinforced Plastics", Trans. and J. Plastics Institute, vol. 35, 1967, p.353.

61. Bishop, P. T.   "Failure of Reinforced Plastics caused by Stress Concentrations", Univ. of Nottingham, Ph.D. Thesis, 1973.

TABLE 2.1 : SURVEY OF GRP FRACTURE TOUGHNESS RESULTS

NOMENCLATURE

REF	No. in list of references	S_{11}	Minimum normal material compliance
CN	Centre notch specimens	t	Specimen thickness
DEN	Double edge notch specimens	a	Crack length (half crack length in CN specimens)
SEN	Single edge notch specimens	W	Specimen width
BEND	3 or 4 point bend specimens	K_c	Uncorrected critical stress intensity factor (Mode I)
U.T.S.	Ultimate tensile strength	G_c	Critical strain energy release rate
CSM	Chopped strand mat	G	Suffix in thickness column indicates grooved specimens

K_c are uncorrected values, calculated by the author where not given in the reference.
Corrected values are discussed in the text, (section 2.3).

reinforce- ment	matrix	U.T.S. M.Pa	S_{11} GPa^{-1}	CN					DEN					SEN					BEND				
				t mm	a mm	W mm	K_c MPa m$^{\frac{1}{2}}$	G_c kJm^{-2}	t mm	a mm	W mm	K_c MPa m$^{\frac{1}{2}}$	G_c kJm^{-2}	t mm	a mm	W mm	K_c MPa m$^{\frac{1}{2}}$	G_c kJm^{-2}	t mm	a mm	W mm	K_c MPa m$^{\frac{1}{2}}$	G_c kJm^{-2}
unidirect- ional	Epoxy			1.27	6.73	152	1.84																
				1.27	19.30	152	1.69																
				1.27	3.05	152	1.42																
				1.27	19.43	152	1.73																
				1.27	18.80	152	1.84																
				1.27	18.92	152	1.67																
				1.27	6.86	152	1.55																
				1.27	6.86	152	1.63																
				1.27	14.61	152	1.84																
				1.27	12.95	152	1.80																
				1.27	12.70	152	1.71																
				1.27	12.70	152	1.81																
				1.27	2.92	152	1.56																
				1.27	2.92	152	1.30																
				1.27	4.19	152	1.51																
				1.27	3.18	152	1.50																
				1.27	6.35	152	1.61																
				1.27	6.73	152	1.65																
				1.27	6.86	152	1.53																
				1.27	12.70	152	1.76																
				1.27	12.75	152	1.63																
				1.27	12.45	152	1.83																

TABLE 2.1 continued

REF	Author	reinforcement	matrix	U.T.S. (M.Pa)	S_{11} (GPa^{-1})	CN t (mm)	CN a (mm)	CN W (mm)	CN K_c (MPa m^{½})	CN G_c (kJm^{-2})	DEN t (mm)	DEN a (mm)	DEN W (mm)	DEN K_c (MPa m^{½})	DEN G_c (kJm^{-2})	SEN t (mm)	SEN a (mm)	SEN W (mm)	SEN K_c (MPa m^{½})	SEN G_c (kJm^{-2})	BEND t (mm)	BEND a (mm)	BEND W (mm)	BEND K_c (MPa m^{½})	BEND G_c (kJm^{-2})
17	SANDFORD & STONESIFER	unidirectional S-HTS	EPON 826/CL								2.54		76.2	1.187	0.1751	2.54		38.1	1.396	0.1576					
		E-HTS	ERL 2256/0820								2.54		76.2	1.439	0.2277	2.54		38.1	1.670	0.2102					
		E-HTS	EPON 826/CL								2.54		76.2	1.209	0.1926	2.54		38.1	1.472	0.2802					
		E-HTS	ERL 2256/0820								2.54		76.2	0.9340	0.0525	2.54		38.1	1.132	0.0525					
		S-HTS	EPON 826/CL (B-staged)								2.54		76.2	0.2967	0.0525	2.54		38.1	0.3516	0.0876					
		S-HTS	EPON 826/MABA								2.54		76.2	1.374	0.5429	2.54		38.1	1.626	0.4904					
18	BEAUMONT & PHILLIPS	Random chopped E-glass fibres. G refers to grooved specimens	Polyester		0.1587						G 1.5	1.25	25.0	6.93	7.62						1.5	1.05	10.00	10.1	16.2
											G 1.5	2.50	25.0	9.68	14.86						1.5	3.05	10.00	9.4	14.0
											G 1.5	3.75	25.0	10.27	16.74						1.5	4.80	10.00	10.0	16.0
											G 1.5	5.00	25.0	9.35	13.86						3.5	1.30	10.00	9.9	15.4
											3.5	1.25	25.0	4.39	3.06						3.5	2.90	10.00	9.9	15.6
											3.5	2.50	25.0	6.04	5.80						3.5	4.85	10.00	9.4	14.0
											3.5	3.75	25.0	6.58	6.88						1.5	1.00	10.00	8.1	10.4
											3.5	5.00	25.0	6.41	6.52						1.5	0.30	10.00	7.9	10.0
											3.5	6.25	25.0	5.59	4.96						1.5	4.80	10.00	9.1	14.0
											1.5	4.38	25.0	5.99	5.70						3.5	1.30	10.00	7.8	9.8
											1.5	3.95	25.0	8.15	10.55						3.5	0.29	10.00	7.9	10.0
																					3.5	4.80	10.00	7.1	8.0
19	BEAUMONT & PHILLIPS	S-glass unidirectional	Scotchply Epoxy	145.0	0.0117	G 1.0	8.2	25.4	95.3															143.00	242.00
						G 1.0	9.0	25.4	96.0																
						G 1.0	9.9	25.4	76.5																
						G 1.0	10.5	25.4	51.0																
20	MCGARRY & MANDELL	Scotchply 1002 unidirectional 0°/0°/0°/90° / 90°	Epoxy		0.0433							2.4	25.4	25.10											
												2.4	25.4	28.93											
												2.54	25.4	27.95											
												2.29	31.7	26.63											
												5.08	31.7	21.92											
												5.08	31.7	27.40											
												5.08	31.7	28.93											
												7.62	31.7	25.65											
												7.62	31.7	26.52											
												7.62	31.7	23.78											
												7.87	31.7	27.07											

TABLE 2.1 continued

RFF	reinforce-ment	matrix	U.T.S. $M.Pa$	S_{11} GPa^{-1}	CN t mm	a mm	w mm	K_c $MPa\,m^{\frac{1}{2}}$	G_c kJm^{-2}	DEN t mm	a mm	w mm	K_c $MPa\,m^{\frac{1}{2}}$	G_c kJm^{-2}	SEN t mm	a mm	w mm	K_c $MPa\,m^{\frac{1}{2}}$	G_c kJm^{-2}	BEND t mm	a mm	w mm	K_c $MPa\,m^{\frac{1}{2}}$	G_c kJm^{-2}
20 MCGARRY & MANDELL	Scotchply 1002 unidirect-ional 90°/0°/0°/ 0°/90°	Epoxy		0.0363							6.35	38.1	50.20											
											6.73	38.1	43.29											
											9.52	38.1	44.17											
											9.52	38.1	42.63											
											9.93	38.1	43.29											
											10.67	38.1	49.89											
											5.08	50.8	41.32											
											6.35	50.8	39.68											
											9.14	50.8	46.80											
	1 ply 181-style balanced weave fabric	Epoxy and polyester			0.25	0.25	38.1	8.4		0.25	1.04	38.1	18.4											
					0.25	0.64	38.1	11.2		0.25	1.78	38.1	18.2											
					0.25	1.04	38.1	12.9		0.25	2.52	38.1	18.2											
					0.25	1.02	38.1	14.0		0.25	2.54	38.1	19.8											
					0.25	1.27	38.1	14.8		0.25	2.54	38.1	17.3											
					0.25	1.70	38.1	16.4		0.25	3.56	38.1	16.0											
					0.25	2.29	38.1	15.8		0.25	5.72	38.1	18.4											
					0.25	3.30	38.1	17.8		0.25	6.35	38.1	19.3											
					0.25	4.98	38.1	18.2		0.25	6.35	38.1	20.6											
					0.25	6.20	38.1	17.8																
	Random chopped fibres 6-plies	Polyester								1.78	2.29	25.4	6.96											
										1.78	2.79	25.4	8.06											
										1.78	3.56	25.4	8.42											
										1.78	3.30	25.4	7.52											
										1.78	3.56	25.4	8.48											
										1.78	5.33	25.4	8.35											
										1.78	4.57	25.4	9.51											
										1.78	5.01	25.4	9.27											
21	Unidirect-ional 60°/60°/60°	Epoxy			0.889	25.4	25.4	13.63		0.889	101.6	25.4	19.57											
					1.651	25.4	25.4	15.72		1.651	121.6	25.4	16.48											
8	A Supramat E-glass CSM 3-plies	Polyester	137.0	0.101						3.2	12.50	75.0	10.47											
										3.2	16.67	100.0	11.08											
										3.2	25.00	150.0	11.80											
										3.54	109.00	600.00	15.65											

– HAMILTON & BERG

B – OWEN & BISHOP

TABLE 2.1 continued

RFF	reinforcement	matrix	U.T.S. M.Pa	S_{11} GPa^{-1}	CN t mm	CN a mm	CN w mm	CN K_c MPa m$^{1/2}$	CN G_c kJm^{-2}	DEN t mm	DEN a mm	DEN w mm	DEN K_c MPa m$^{1/2}$	DEN G_c kJm^{-2}	SEN t mm	SEN a mm	SEN w mm	SEN K_c MPa m$^{1/2}$	SEN G_c kJm^{-2}	BEND t mm	BEND a mm	BEND w mm	BEND K_c MPa m$^{1/2}$	BEND G_c kJm^{-2}
8 OWEN & BISHOP	Tyglass Y221 E-glass A1100 Silane finish 9-plies B - 0°	Polyester	402.0	0.0354						2.79 2.79 2.79	12.50 16.67 25.00	75.0 100.0 150.0	42.44 42.44 47.27											
	B - 90°		52.4	0.0894						2.79 2.79 2.79 3.09	12.50 16.67 25.00 100.00	75.0 100.0 150.0 600.0	4.73 4.73 4.73 6.31											
	C Tyglass Y449 E-glass A1100 Silane finish 7-plies	Polyester	229.0	0.0487						3.09 3.09 3.09	12.50 16.67 25.00	75.0 100.0 150.0	19.60 20.98 22.70											
22 OWEN & ROSE	None CSM FGE 2000 E-glass 1 ply	Polyester	52.9 52.9 78.9	0.2597 0.2597	1.25 8.00 1.25	12.7 12.7 12.7	76.2 76.2 76.2	0.825 0.699 9.61																
23	Tyglass Y227 E-glass 1 ply	Polyester	255.4		1.25	12.7	76.2	13.63																
	CSM Supremat 6-plies	Polyester	85.0	0.1205	5.8 5.8 5.8 5.8	10.0 15.0 20.0 25.0	100.0 100.0 100.0 100.0		20.65 19.61 17.79 17.20															
25	M(CSM) + R(WRF 779-style) as M/R/M/R/M	Polyester		0.0545											5.49	various	114.3	19.30						

23 - HOLDSWORTH, MORRIS, & OWEN
25 - MANDELL ET AL

TABLE 2.1 continued

reinforcement	matrix	U.T.S. M.Pa	S_{11} GPa⁻¹	test	t mm	a mm	w mm	K_c MPa m^½	G_c kJm⁻²	REF
CSM	Polyester	85.0	0.1205	CN	5.8	10.0	100.0	8.81		24 HOLDSWORTH
				CN	5.8	15.0	100.0	9.43		
				CN	5.8	20.0	100.0	9.78		
				CN	5.8	25.0	100.0	8.91		
				CN	5.8	15.0	100.0	9.43		
				CN	5.8	22.5	150.0	8.98		
				CN	5.8	30.0	200.0	8.60		
				CN	5.8	37.5	250.0	9.16		
				CN	5.8	90.0	600.0	10.66		
				DEN	5.8	10.0	100.0	8.39		
				DEN	5.8	15.0	100.0	8.12		
				DEN	5.8	20.0	100.0	8.86		
				DEN	5.8	25.0	100.0	9.98		
				DEN	5.8	15.0	100.0	8.12		
				DEN	5.8	37.5	250.0	10.04		
				BEND	6.0	30.0	150.0	5.64		
				BEND	6.0	40.0	200.0	6.63		
				BEND	6.0	50.0	250.0	6.64		
CSM	Urethane	67.7	0.0599	BEND	6.0	30.0	150.0	5.63		24 HOLDSWORTH
				BEND	6.0	40.0	200.0	6.21		
				BEND	6.0	50.0	250.0	6.24		
Tyglass Y449	Polyester	202.3	0.1880	CN	3.6	10.0	100.0	17.14		24 HOLDSWORTH
				CN	3.6	15.0	100.0	17.72		
				CN	3.6	20.0	100.0	17.29		
				CN	3.6	25.0	100.0	16.91		
				CN	3.6	15.0	100.0	17.72		
				CN	3.6	22.5	150.0	19.86		
				CN	3.6	30.0	200.0	20.33		
				CN	3.6	37.5	250.0	21.58		
				DEN	3.6	10.0	100.0	16.10		
				DEN	3.6	15.0	100.0	17.90		
				DEN	3.6	20.0	100.0	18.88		
				DEN	3.6	25.0	100.0	17.88		
				DEN	3.6	15.0	100.0	17.90		
				DEN	3.6	37.5	250.0	23.14		
				BEND	3.6	30.0	150.0	13.99		
				BEND	3.6	40.0	200.0	15.14		
				BEND	3.6	50.0	250.0	17.76		
CSM 3 plies	Epoxy	160		SEN	3.18	5.08	25.4	13.42		26
unidirectional	Epoxy	1295		SEN	3.10	12.7	25.4	14.4		28

26 - GAGAR & BROUTHAN
28 - BARNBY & SPENCER

Table 3.1 Tensile and Compliance Tests, CSM/PR

Specimen No. and Direction	Resin Cracking Stress MPa	Ultimate Tensile Stress MPa	Glass Content by weight %	S_{11} GPa^{-1}	S_{22} GPa^{-1}
RC1/T1/1 0°	74.3	95.70	31.47		
RC1/T1/2	75.9	120.42	34.57		
RC2/T1/5	52.2	103.36	33.62		
RC2/T1/7	50.8	106.43	33.80		
RC2/T1/8	47.4	111.61	34.11		
Mean value	60.1	107.50	33.51		
Highest value	75.9	120.42	34.57		
Lowest value	47.4	95.70	31.47		
RC1/T1/11 90°	41.4	104.30	33.70		
RC1/T1/12	48.0	96.95	32.93		
RC2/T1/6	40.1	96.57	32.90		
RC2/T1/10	38.6	106.54	33.47		
Mean value	42.0	101.09	33.25		
Highest value	48.0	106.54	33.70		
Lowest value	38.6	96.57	32.90		
RC1/T1/14 0°			34.12	0.1060	
RC2/T1/13			36.46	0.1000	
RC2/T1/14			37.18	0.0987	
Mean value			35.92	0.1016	
Highest value			37.18	0.1060	
Lowest value			34.12	0.0987	
RC1/T1/15 90°			33.77		0.1169
RC1/T1/16			32.48		0.1247
RC2/T1/11			33.99		0.1141
RC2/T1/12			33.48		0.1159
Mean value			33.43		0.1179
Highest value			33.99		0.1247
Lowest value			32.48		0.1141

Table 3.2 Tensile and Compliance Tests, CSM/PR

Specimen No. and Direction	Ultimate Tensile Strength MPa	Glass Content by Weight %	S_{11} GPa^{-1}	S_{22} GPa^{-1}
3-layer				
RC12/T1/1 0°	106.18	32.89	0.1118	
RC12/T1/2	130.48	35.94	0.0959	
RC12/T1/5	121.33	38.27	0.0970	
RC12/T1/6	117.27	35.03	0.1067	
Mean value	118.82	35.53	0.1029	
Highest value	130.48	38.27	0.1118	
Lowest value	106.18	32.89	0.0959	
RC12/T1/3 90°	118.28	34.80		0.1062
RC12/T1/4	124.08	32.44		0.1155
RC12/T1/7	125.91	34.24		0.1072
RC12/T1/8	129.28	39.54		0.0953
Mean value	124.39	35.26		0.1061
Highest value	129.28	39.54		0.1155
Lowest value	118.28	32.44		0.0953
Mean of all RC12/T1 Specimens	121.60	35.94	0.1045	0.1045
Highest value	130.48	38.27	0.1155	0.1155
Lowest value	118.28	32.44	0.0953	0.0953
Coefficient of Variation %	6.45	6.97	0.728	0.728
6-layer				
RC17/T1/1 90°	131.01	37.68		0.08766
RC17/T1/2 0°	141.33	37.64	0.1073	
RC17/T1/3 0°	127.47	35.82	0.1110	
9-layer				
RC18/T1/1 90°	141.14	36.09		0.08671
RC18/T1/2 0°	136.23	36.64	0.1025	
RC18/T1/3 0°	135.57	36.09	0.1076	

Table 3.2 Tensile and Compliance Tests, CSM/PR (continued)

Specimen No. and Direction	Ultimate Tensile Stress MPa	Glass Content by weight %	S_{11} GPa^{-1}	S_{22} GPa^{-1}
3-layer				
RC28/T2/13 0°	118.90	34.49	0.09047	
RC28/T2/14	122.84	37.20	0.09408	
RC28/T2/15	133.43	34.88	0.10268	
RC28/T2/16	126.63	36.03	0.09580	
RC28/T2/17	125.77	37.82	0.10074	
Mean value	125.51	36.08	0.09675	
Highest value	133.43	37.82	0.10268	
Lowest value	118.90	34.49	0.09047	
Coefficient of variation%	4.27	3.98	5.13	
RC28/T2/1 90°	102.21	34.21		0.09618
RC28/T2/2	122.25	33.13		0.08448
RC28/T2/3	124.64	36.76		0.08487
RC28/T2/4	120.68	31.53		0.11623
RC28/T2/5	137.69	35.39		0.10958
RC28/T2/6	139.72	36.92		0.09863
RC28/T2/7	137.80	37.06		0.08495
RC28/T2/8	144.17	37.62		0.09180
RC28/T2/9	125.92	34.54		0.08959
RC28/T2/10	117.95	32.96		0.09482
RC28/T2/11	114.68	32.04		0.10778
RC28/T2/12	102.89	32.21		0.10895
Mean value	124.22	34.53		0.09732
Highest value	144.17	37.62		0.11623
Lowest value	102.21	31.53		0.08448
Coefficient of variation %	11.11	6.32		11.28
Mean value of all RC28 specimens	124.60	34.99	0.09716	9716
Highest value	144.17	37.62	0.11623	0.11623
Lowest value	102.21	31.53	0.08448	0.08448
Coefficient of variation %	9.44	5.95	9.71	9.71

Table 3.3: Tensile and Compliance Tests, WRF/PR

Specimen No. and Direction	Ultimate Tensile Stress MPa	Glass Content by weight %	S_{11} GPa^{-1}	S_{22} GPa^{-1}
3-Layer				
RCW25/T2/7 0°	246.16	53.59	0.05227	
RCW25/T2/8	248.05	52.60	0.05068	
RCW25/T2/9	231.60	50.00	0.05564	
RCW25/T2/10	233.03	50.45	0.05567	
RCW25/T2/11	246.05	51.14	0.05027	
RCW25/T2/12	248.76	51.68	0.05099	
Mean value	242.27	51.58	0.05259	
Highest value	248.76	53.59	0.05567	
Lowest value	231.60	50.00	0.5027	
Coefficient of variation %	3.22	2.61	4.70	
RCW25/T2/1 90°	238.13	49.83		0.06144
RCW25/T2/2	247.12	50.79		0.05575
RCW25/T2/3	253.61	51.79		0.05460
RCW25/T2/4	232.59	49.06		0.05994
RCW25/T2/5	252.01	50.94		0.05011
RCW25/T2/6	234.25	50.03		0.04865
Mean value	242.95	50.41		0.05509
Highest value	253.61	51.79		0.06144
Lowest value	232.59	49.06		0.04865
Coefficient of variation %	3.77	1.91		9.27
Mean value of all RCW25 specimens	242.61	50.99	0.05384	0.05384
Highest value	253.61	53.59	0.06144	0.06144
Lowest value	231.60	49.06	0.04865	0.04865
Coefficient of variation %	3.34	2.49	7.50	7.50
6-Layer				
RCW30/T2/1 0°	362.85	62.71	0.03858	
RCW30/T2/2 90°	319.72	64.92		0.04379
RCW30/T2/3 0°	421.21	66.69	0.04060	
RCW30/T2/4 0°	432.52	67.44	0.03790	

Table 3.3: Tensile and Compliance Tests, WRF/PR (continued)

Specimen No. and Direction	Ultimate Tensile Stress MPa	Glass Content by weight %	S_{11} GPa^{-1}	S_{22} GPa^{-1}
RCW29/T2/1 0°	351.49	69.98	0.03315	
RCW29/T2/2 90°	402.25	69.23		0.03594
RCW29/T2/3 0°	446.88	70.13	0.03315	
RCW29/T2/4 0°	415.46	69.57	0.03551	

Table 3.4 : Tensile and Compliance Tests on Polyester Resin

Specimen No.	Ultimate tensile stress MPa	S_{11} GPa^{-1}
RCR1/T1/1	4.12	1.586
RCR1/T1/2	9.36	1.547
RCR1/T1/3	4.97	1.575
RCR1/T1/4	7.66	1.529
RCR1/T1/5	10.03	1.599
RCR1/T1/6	9.00	-
RCR1/T1/7	10.98	-
RCR1/T1/8	8.18	-
RCR1/T1/9	9.43	-
Mean value	8.19	1.567
Highest value	10.98	1.599
Lowest value	4.12	1.529
Coefficient of Variation %	28.0	1.8

Table 3.5: S_G values from plate twist tests

Specimen No., Direction, and Material	Glass Content by weight %	S_G GPa^{-1}
PT5 0° CSM/PR	31.41	0.3208
PT6 45° Dry	36.96	0.2583
PT7 0°	35.58	0.2796
PT8 45°	34.15	0.2857
PT9 45° WRF/PR	62.55	0.1212
PT10 45° Dry	60.38	0.1253
PT11 0°	56.85	0.2775
PT12 0°	55.76	0.2883
PT13 0°	64.81	0.2146
PT14 0°	63.17	0.2456
PT15 45°	64.32	0.0990
PT16 45°	63.95	0.1092
PT17 0° CSM/PR	36.88	0.2670
PT18 45° Wet	37.71	0.2550
PT19 0°	37.97	0.2408
PT20 45°	36.33	0.2830
PT21 45° WRF/PR	67.68	0.0987
PT22 45° Wet	69.22	0.1130
PT23 45°	68.06	0.0982
PT24 45°	68.19	0.0963
PT25 0°	67.81	0.2409
PT26 0°	68.38	0.2404
PT27 0°	67.45	0.2353
PT28 0°	68.09	0.2351

Table 3.6: Water absorption by CSM/PR and WRF/PR specimens

Material	Specimen Type	Nominal total surface area mm^2	% cut edge area of total area	Increase in weight due to water absorption %
CSM/PR Nominal thickness 3.2 mm	Plate twist	6162	10.87	1.15
	T2	14924	22.94	0.82 R
	CN50	17451	8.31	1.28
	CN100	55121	5.66	1.27
	CN150	118709	3.97	1.19
WRF/PR Nominal thickness 2.0 mm	Plate twist	5911	7.09	0.69
	T2	13640	15.69	0.51 R
	CN50	16907	5.36	0.55
	CN100	53573	2.94	0.65
	CN150	121230	5.96	0.62

Specimens marked R had reinforced ends

Table 3.7: Tensile and compliance tests, wet CSM/PR and WRF/PR

Specimen No. and direction	Ultimate Tensile Strength MPa	Glass Content by weight %	Water Intake by weight %	S_{11} GPa^{-1}	S_{22} GPa^{-1}
RC46/T1/1 0°	137.09	38.15	0.802	0.1060	
RC46/T1/2 0°	137.17	38.41	0.808	0.1010	
RC46/T1/3 0°	134.12	39.67	0.859	0.1034	
RC46/T1/4 0°	136.54	40.66	0.819	0.0942	
Mean value	136.23	39.22	0.822	0.1012	
Highest value	137.17	40.66	0.859	0.1060	
Lowest value	134.12	38.15	0.802	0.0942	
RCW45/T1/1 0°	379.37	69.81	0.460	0.03471	
RCW45/T1/2 0°	349.74	70.05	0.483	0.03459	
RCW45/T1/3 0°	339.02	68.71	0.530	0.03851	
RCW45/T1/4 0°	333.68	67.18	0.547	0.03981	
Mean value	350.45	68.94	0.505	0.03691	
Highest value	379.37	70.05	0.547	0.03981	
Lowest value	333.68	67.18	0.460	0.03459	

Table 3.8: Summary of ultimate tensile stress and material compliances

Property	Units	CSM/PR at glass content 35%	% change due to water absorption	WRF/PR at glass content 65%	% change due to water absorption
UTS	MPa	124.8	-2.5	385.2	-17.5
S_{11}	GPa^{-1}	0.1004	+10.4	0.04037	+2.1
S_{22}	GPa^{-1}	0.1004	+10.4	0.04037	+2.1
S_{12}	GPa^{-1}	- 0.0399	-6.9	- 0.00823	+169.2
S_{66}	GPa^{-1}	0.2805	+2.5	0.2240	+16.3

Table 4.1:   Summary of k*/k values and key to figs. 4.2 and 4.3

a/w = a_D	L/W	Material	End Constraint	K*/K at r/N = 0
0.05 □	0.75	CSM/PR	Constrained*	1.035
0.05 ■	0.75	WRF/PR	Constrained	1.018
0.05 ○	2.00	CSM/PR	Free	1.000
0.05 ●	2.00	WRF/PR	Free	0.998
0.30 □	0.75	CSM/PR	Constrained	0.997
0.30 ■	0.75	WRF/PR	Constrained	0.915
0.30 △	2.00	CSM/PR	Constrained	1.079
0.30 ▲	2.00	WRF/PR	Constrained	1.047
0.30 ○	2.00	CSM/PR	Free	1.075
0.30 ●	2.00	WRF/PR	Free	1.054

*   "Constrained" implies:-

1) All nodes at loaded end of specimen are displaced the same amount in the direction of load, y.

2) No displacement in x direction by nodes at loaded end of specimen.

Table 4.2: Specimen Compliances Estimated for Various Materials using the Finite Element Method

Material	t/W	L_2/W	S_{12} GPa^{-1}	S_{12} GPa^{-1}	S_{22} GPa^{-1}	S_{66} GPa^{-1}	$\frac{S_{12}}{S_{11}}$	$\frac{S_{22}}{S_{11}}$	$\frac{S_{66}}{S_{11}}$	C mN^{-1}	$C_D = \frac{Ct}{S_{11}}$
CSM/PR	0.03175	2.0	0.1045	-0.0326	0.1045	0.295	-0.3120	1.0	2.823	0.2143×10^{-7}	0.6511
CSM/PR	0.03175	2.0	0.1500	-0.0468	0.1500	0.423	-0.3120	1.0	2.823	0.3064	0.6486
WRF/PR	0.0241	2.0	0.04573	-0.01952	0.04573	0.2576	-0.4269	1.0	5.533	0.1548	0.8158
WRF/PR	0.0241	2.0	0.06860	-0.02928	0.06860	0.3864	-0.4269	1.0	5.633	0.2320	0.8152
Y221/PR	0.03175	2.0	0.0354	-0.0118	0.0894	0.209	-0.3333	2.525	5.904	0.1622	1.4546
Y221/PR	0.03175	2.0	0.0531	-0.0177	0.1341	0.314	-0.3333	2.525	5.909	0.3199	1.9138

Table 5.1: Fracture toughness tests, DEN specimens, CSM/PR

Specimen No.	Crack length/width ratio a/w	Glass content by weight %	Gross stress at failure MPa	Net stress at failure MPa	K_c MPa $m^{\frac{1}{2}}$
Nominal width 75 mm, 3-Layer					
RC1/DEN75/8	0.1942	32.99	31.70	51.83	7.73
RC1/DEN75/9	0.1713	35.06	37.31	56.75	8.47
RC1/DEN75/13	0.1705	33.15	33.79	51.27	7.65
Nominal width 100 mm, 3-Layer					
RC2/DEN100/3	0.1687	31.76	35.95	54.25	9.34
RC1/DEN100/5	0.1632	31.58	38.36	56.95	9.78
RC1/DEN100/6	0.1700	31.34	30.97	46.92	8.08
RC1/DEN100/7	0.1700	30.94	33.80	51.21	8.82
Nominal width 150 mm, 3-Layer					
RC1/DEN150/4	0.1701	34.78	32.26	48.89	10.30
RC2/DEN150/1	0.1687	30.55	26.65	40.22	8.46
RC2/DEN150/2	0.1742	34.25	28.96	44.45	9.37

Table 5.2: Fracture toughness tests, CN specimens, CSM/PR

Specimen No.	Half-crack length/ width ratio a/w	Glass content by weight %	Gross stress at failure MPa	Net stress at failure MPa	K_c Isida MPa $m^{\frac{1}{2}}$
Nominal width 50 mm, 3-Layer					
RC13/CN50/1	0.1688	33.18	55.15	83.27	9.65
RC13/CN50/2	0.1664	34.22	56.41	84.54	9.77
RC13/CN50/3	0.1703	38.01	59.81	90.70	10.30
RC13/CN50/4	0.1684	41.16	65.68	99.03	11.46
Nominal width 50 mm, 6-Layer					
RC14/CN50/1	0.1761	39.18	62.65	96.71	11.24
RC14/CN50/2	0.1672	35.45	56.32	84.61	9.79
RC14/CN50/3	0.1694	35.47	57.74	87.33	10.12
RC14/CN50/4	0.1739	35.36	56.77	87.06	10.11
RC17/CN50/1	0.1643	36.47	57.72	85.96	9.93
Nominal width 50 mm, 9-Layer					
RC15/CN50/1	0.1633	36.86	60.92	90.46	10.43
RC15/CN50/2	0.1671	36.30	59.35	89.14	10.31
RC15/CN50/3	0.1636	36.61	60.23	89.51	10.33
RC15/CN50/4	0.1725	36.74	56.98	86.97	10.09
RC18/CN50/1	0.1691	37.81	57.97	87.59	10.15

Table 5.2 continued: Fracture toughness tests, CN specimens, CSM/PR

Specimen No.	Half-crack length/width ratio a/w	Glass content by weight %	Gross stress at failure MPa	Net stress at failure MPa	K_c Isida MPa m$^{\frac{1}{2}}$
Nominal width 100 mm, 3-Layer					
RC13/CN100/5	0.1680	36.45	43.57	65.63	10.73
RC27/CN100/1	0.1684	33.56	40.33	60.81	9.94
RC27/CN100/2	0.1679	38.87	46.67	70.27	11.48
RC27/CN100/8	0.1712	35.99	46.05	70.03	11.46
Nominal width 100 mm, 6-Layer					
RC14/CN100/5	0.1693	36.41	44.24	66.90	10.96
RC17/CN100/1	0.1655	36.12	44.46	66.64	10.92
RC17/CN100/2	0.1664	35.20	44.23	66.30	10.87
RC17/CN100/3	0.1657	35.88	43.55	65.13	10.67
RC17/CN100/4	0.1684	36.28	44.56	67.18	11.02
Nominal width 100 mm, 9-Layer					
RC15/CN100/5	0.1652	35.62	45.05	67.26	11.00
RC18/CN100/1	0.1710	37.73	45.90	69.75	11.47
RC18/CN100/2	0.1662	35.34	43.84	65.67	10.77
RC18/CN100/3	0.1657	35.27	43.71	65.38	10.72
RC18/CN100/4	0.1669	36.08	43.95	65.97	10.83

Table 5.2 continued: Fracture toughness tests, CN specimens, CSM/PR

Specimen No.	Half-crack length/width ratio a/w	Glass content by weight %	Gross stress at failure MPa	Net stress at failure MPa	K_c Isida MPa m$^{\frac{1}{2}}$
Nominal width 150 mm, 3-Layer					
RC13/CN150/6	0.1667	34.23	37.94	56.92	11.40
RC13/CN150/7	0.1699	34.50	38.18	57.84	11.61
RC24/CN150/5	0.1688	36.07	38.20	57.68	11.56
Nominal width 150 mm, 6-Layer					
RC14/CN150/6	0.1722	37.19	39.52	60.28	12.11
RC14/CN150/7	0.1703	35.26	37.48	56.84	11.41
RC17/CN150/1	0.1695	36.64	38.77	58.64	11.74
RC21/CN150/1	0.1654	34.46	38.36	57.31	11.45
RC21/CN150/2	0.1669	36.48	38.99	58.53	11.71
RC21/CN150/3	0.1669	35.27	37.60	56.45	11.30
Nominal width 150 mm, 9-Layer					
RC15/CN150/6	0.1694	37.41	40.86	61.79	12.38
RC15/CN150/7	0.1679	35.65	38.63	58.16	11.64
RC18/CN150/1	0.1686	34.27	36.05	54.38	10.90
RC20/CN150/1	0.1687	39.99	43.35	65.41	13.11
RC20/CN150/2	0.1677	37.33	40.22	60.52	12.11
RC20/CN150/3	0.1674	38.06	41.88	61.75	12.36

Table 5.3 : Fracture toughness tests, CN specimens, wet CSM/PR

Specimen No.	Half-crack Length/Width Ratio a/W	Glass Content by weight %	Gross Stress at Failure MNm⁻²	Net Stress at Failure MNm⁻²	K_c Isida MPa m$^{\frac{1}{2}}$
Nominal Width 50 mm, 3-layer					
RC19/CN50/1	0.1654	35.88	52.65	78.68	9.10
RC22/CN50/1	0.1659	32.76	45.76	68.47	7.91
RC22/CN50/2	0.1657	31.11	44.42	66.43	7.68
RC22/CN50/3	0.1661	36.77	52.49	78.61	9.08
RC22/CN50/4	0.1692	37.73	53.63	81.05	9.38
Nominal Width 100 mm, 3-layer					
RC19/CN100/1	0.1658	31.50	37.85	56.63	9.28
RC19/CN100/2	0.1661	34.68	40.93	61.30	10.05
RC19/CN100/4	0.1650	37.16	44.16	65.79	10.77
RC22/CN100/5	0.1660	34.21	40.37	60.44	9.86
RC22/CN100/9	0.1689	35.07	39.03	58.95	9.65
Nominal Width 150 mm, 3-layer					
RC19/CN150/1	0.1682	36.86	37.06	55.86	11.18
RC22/CN150/6	0.1676	33.23	32.23	48.49	9.69
RC22/CN150/7	0.1671	30.50	30.52	45.83	9.18
RC24/CN150/1	0.1673	32.32	32.53	48.89	9.79
RC24/CN150/4	0.1669	35.02	36.05	54.12	10.83

Table 5.4:   Summary of Mean K_c Values and K_c Values at 35%
Glass Content, CSM/PR

Nominal Width mm	Number of Layers	Number of Specimens	Mean K_c MPa $m^{\frac{1}{2}}$	35% Glass Content MPa $m^{\frac{1}{2}}$
DEN 75 Dry	3	3	7.95	8.36
100	3	4	9.01	-
150	3	3	9.37	10.19
CN 50 Dry	3	4	10.35	9.97
100	3	4	10.90	10.57
150	3	3	11.52	11.53
CN 50 Wet	3	5	8.63	8.67
100	3	5	9.92	10.04
150	3	5	10.14	10.60
CN 50 Dry	6	5	10.24	9.79
100	6	5	10.89	10.77
150	6	6	11.62	11.40
CN 50 Dry	9	5	10.26	10.26
100	9	5	10.96	10.67
150	9	6	12.08	11.23
CN 50 Dry	3,6,9	14	10.27	9.89
100	3,6,9	14	10.92	10.63
150	3,6,9	15	11.78	11.41

Table 5.5 : Fracture toughness tests, CN specimens, WRF/PR

Specimen No.	Half-crack Length/Width Ratio a/W	Glass Content by weight %	Gross Stress at Failure MPa	Net Stress at Failure MPa	K_c Isida MPa m$^{\frac{1}{2}}$
Nominal Width 50 mm, 3-Layer					
RCW33/CN50/18	0.1751	63.81	204.34	314.44	36.50
RCW33/CN50/19	0.1661	63.54	198.72	297.61	34.39
RCW33/CN50/20	0.1643	66.92	215.43	320.86	37.01
RCW33/CN50/21	0.1641	66.23	207.55	309.01	35.66
Nominal Width 50 mm, 6-Layer					
RCW30/CN50/5	0.1689	64.46	139.51	210.66	24.39
RCW30/CN50/6	0.1657	64.84	157.07	234.91	27.17
RCW30/CN50/7	0.1659	66.45	194.74	291.42	33.69
Nominal Width 50 mm, 9-Layer					
RCW29/CN50/5	0.1640	68.17	151.29	226.75	26.30
RCW29/CN50/6	0.1666	70.04	170.71	256.01	29.73
RCW29/CN50/7	0.1647	69.89	220.99	329.60	38.16
Nominal Width 100 mm, 3-Layer					
RCW33/CN100/10	0.1652	68.85	196.93	294.07	47.98
RCW33/CN100/11	0.1661	65.47	177.62	265.98	43.45
RCW33/CN100/12	0.1682	67.62	200.50	302.14	49.43
RCW33/CN100/13	0.1684	64.69	176.90	266.79	43.65

Table 5.5 continued : Fracture toughness tests, CN specimens, WRF/PR

Specimen No.	Half-crack Length/Width Ratio a/W	Glass Content by weight %	Gross Stress at Failure MPa	Net Stress at Failure MPa	K_c Isida MPa m$^{\frac{1}{2}}$
Nominal Width 100 mm, 6-Layer					
RCW30/CN100/9	0.1667	64.34	163.97	245.95	40.30
RCW30/CN100/10	0.1658	63.12	160.86	240.68	39.44
Nominal Width 100 mm, 9-Layer					
RCW29/CN100/8	0.1679	68.02	176.33	265.46	43.41
RCW29/CN100/9	0.1679	70.49	188.02	283.05	46.29
RCW29/CN100/10	0.1688	70.81	191.42	288.93	47.28
Nominal Width 150 mm, 3-Layer					
RCW33/CN150/7	0.1661	65.25	171.80	257.24	51.54
RCW33/CN150/8	0.1668	67.01	179.73	269.67	54.09
RCW39/CN150/1	0.1668	67.71	194.08	291.28	58.39
RCW39/CN150/2	0.1658	67.06	190.82	285.48	57.20

Table 5.6 : Fracture toughness tests, CN specimens, wet WRF/PR

Specimen No.	Half-crack length/width ratio a/W	Glass content by weight %	Water intake by weight %	Gross stress at failure MPa	Nett stress at failure MPa	K_c MPa $m^{\frac{1}{2}}$
Nominal Width 50 mm, 3-layer						
RCW33/CN50/22	0.1639	66.85	0.551	182.00	270.76	31.24
RCW33/CN50/23	0.1627	68.40	0.568	183.12	271.45	31.29
RCW33/CN50/24	0.1673	67.89	0.544	184.75	277.65	32.11
RCW33/CN50/25	0.1656	68.40	0.550	189.20	282.92	32.69
Nominal Width 100 mm, 3-layer						
RCW33/CN100/14	0.1661	66.39	1.065	155.09	232.23	37.92
RCW33/CN100/15	0.1661	66.74	0.857	164.51	246.32	40.22
RCW33/CN100/16	0.1717	64.50	0.928	148.10	225.56	36.95
RCW33/CN100/17	0.1701	64.47	0.868	154.56	234.25	38.36
Nominal Width 150 mm, 3-layer						
RCW33/CN150/1	0.1683	65.39	0.600	145.08	218.67	43.92
RCW33/CN150/2	0.1713	66.40	0.612	141.85	215.74	43.36
RCW33/CN150/3	0.1662	64.75	0.651	144.02	215.72	43.25
RCW33/CN150/4	0.1676	66.49	0.595	144.34	217.14	43.56

Table 5.7: Summary of Mean K_c Values and K_c Values at 65% Glass Content, WRF/PR

Nominal Width mm	Number of Layers	Number of Specimens	Mean K_c MPa $m^{\frac{1}{2}}$	65% Glass Content K_c MPa $m^{\frac{1}{2}}$
CN 50 Dry	3	4	35.89	35.84
100	3	4	46.13	43.83
150	3	4	55.31	50.63
CN 50 Wet	3	4	31.83	-
100	3	4	38.36	-
150	3	4	43.52	-
CN 50 Dry	6	3	28.42	-
100	6	2	39.87	-
50	9	3	31.40	-
CN 100 Dry	9	3	45.66	-
50	3,6,9	10	32.3	-
100	3,6,9	9	44.58	42.59

Table 5.8 : K_c and K_{DC} for 150 mm wide CN specimens of CSM/PR

Specimen No.	Glass Content by weight %	Local UTS MPa	K_c MPa m$^{\frac{1}{2}}$	K_{DC}
RC13/CN150/6	34.23	122.10	11.40	0.2409
RC13/CN150/7	34.50	123.06	11.61	0.2434
RC14/CN150/6	37.19	132.58	12.11	0.2357
RC14/CN150/7	35.26	125.75	11.41	0.2342
RC15/CN150/6	37.41	133.36	12.38	0.2399
RC15/CN150/7	35.65	127.13	11.64	0.2366
RC24/CN150/5	36.07	128.62	11.56	0.2321
RC18/CN150/1	34.27	122.24	10.90	0.2301
RC20/CN150/1	39.99	142.49	13.11	0.2376
RC20/CN150/2	37.33	133.08	12.11	0.2351
RC20/CN150/3	38.06	135.66	12.36	0.2353
RC17/CN150/1	36.64	130.64	11.74	0.2323
RC21/CN150/1	34.46	122.92	11.45	0.2407
RC21/CN150/2	36.48	130.07	11.71	0.2326
RC21/CN150/3	35.27	125.79	11.30	0.2320
Mean value	36.19		11.79	0.2359
Highest value	39.99		13.11	0.2434
Lowest value	34.23		10.90	0.2301
Coefficient of Variation %	4.52		4.64	1.66

Table 5.9 : Fracture toughness tests, CN specimens, 3-layer CSM/PR

Specimen No.	Half-crack Length/Width Ratio a/W	Glass Content by weight %	Gross Stress at Failure MPa	Net Stress at Failure MPa	K_c Isida MPa m$^{\frac{1}{2}}$
RC27/CN100/3	0.05341	37.71	72.40	81.06	9.50
RC27/CN100/4	0.1011	36.44	56.93	71.35	10.47
RC27/CN100/5	0.1308	33.95	48.96	66.31	10.40
RC27/CN100/6	0.1119	34.11	51.41	66.24	10.01
RC27/CN100/9	0.08327	37.01	62.40	74.87	10.34
RC27/CN100/10	0.06041	35.43	65.88	74.93	9.22
RC27/CN100/11	0.09177	33.50	53.59	65.64	9.36
RC27/CN100/12	0.2056	35.42	39.57	67.21	11.08
RC26/CN100/1	0.04902	32.24	68.50	75.95	8.63
RC26/CN100/2	0.03911	33.41	72.37	78.51	8.11
RC26/CN100/3	0.02932	32.14	81.58	86.66	7.89
RC26/CN100/5	0.03464	35.05	77.46	83.22	8.15
RC28/CN100/27	0.02078	36.69	100.25	104.58	8.14
RC28/CN100/28	0.03595	37.52	90.96	98.00	9.76
RC28/CN100/30	0.03039	36.57	96.50	102.75	9.50
RC28/CN100/34	0.06004	33.11	67.63	76.86	9.45
RC28/CN100/35	0.1850	33.50	40.30	63.98	10.55

Table 5.9 continued : Fracture toughness tests, CN specimens, 3-layer CSM/PR

Specimen No.	Half-crack Length/ Width Ratio a/W	Glass Content by weight %	Gross Stress at Failure MPa	Net Stress at Failure MPa	K_c Isida MPa m$^{\frac{1}{2}}$
RC28/CN100/19	0.1993	34.46	41.94	69.73	11.53
RC28/CN100/22	0.1756	35.22	46.58	71.80	11.76
RC28/CN100/24	0.2238	32.42	36.12	65.40	10.73
RC28/CN100/31	0.1495	32.37	45.33	64.67	10.43
RC28/CN100/36	0.2982	31.56	25.47	63.11	9.41
RC38/CN100/4	0.4001	37.63	14.27	71.46	7.02
RC38/CN100/5	0.3511	35.97	22.56	75.75	9.68
RC38/CN100/6	0.2507	33.76	32.34	64.86	10.41
RC38/CN100/7	0.2776	36.04	31.03	69.77	10.80
RC38/CN100/8	0.3258	35.08	23.84	68.40	9.52
RC46/CN100/8	0.0000	35.76	126.12	126.12	0.00

Table 5.10 : Fracture toughness tests, CN specimens, 3-layer WRF/PR

Specimen No.	Half-crack length/ width ratio. a/W	Glass Content by Weight %	Gross Stress at Failure MPa	Nett Stress at Failure MPa	K_c MPa m$^{\frac{1}{2}}$
RCW36/CN100/16G	0.02111	66.82	237.95	248.44	19.46
RCW36/CN100/17	0.05147	64.98	233.82	260.65	30.12
RCW36/CN100/18	0.1020	66.67	213.32	268.01	39.46
RCW36/CN100/19	0.2012	67.10	162.47	271.85	44.85
RCW36/CN100/22	0.2522	67.74	133.26	268.83	43.06
RCW36/CN100/23	0.3001	64.19	95.62	239.17	35.50
RCW36/CN100/24	0.3483	66.61	79.56	262.21	33.84
RCW36/CN100/25	0.4015	64.60	51.27	260.33	25.33
RCW39/CN100/5D1	0.05051	64.13	242.68	269.95	30.98
RCW39/CN100/6D1	0.02961	64.41	264.80	281.46	25.71
RCW39/CN100/7D1	0.02037	62.89	256.49	267.38	20.62
RCW39/CN100/8D1	0.03948	61.07	233.63	253.66	26.28
RCW44/CN100/1D2	0.0000	67.15	244.08	244.08	0.00
RCW44/CN100/2D2	0.02011	67.50	213.83	222.80	17.06
RCW44/CN100/3D2	0.04989	67.10	218.58	242.81	27.73

G indicates grip failure

D1 indicates tested in Denison, L/W = 1.36

D2 indicates tested in Denison, L/W = 2.00

Table 5.11 : Fracture toughness tests on 915 mm wide CN specimens, CSM/PR and WRF/PR

Specimen No.	Half-crack length/ width ratio a/W	Gross stress at failure MPa	Nett stress at failure MPa	Kc MPa m$^{\frac{1}{2}}$
RC35/CN1000	0.2187	18.67	33.18	16.49
RC34/CN1000	0.05519	34.36	38.60	13.88
RC33/CN1000	0.01093	54.11	55.32	9.60
RC34/CN1000	0.006011	66.82	67.63	16.24 (see text)
RCW40/CN1000	0.05459	232.91	261.46	93.68
RCW31/CN1000	0.21990	183.25	327.12	161.98

Table 5.12: Corrected K_c values, CSM/PR

Increment r_y mm	K_c W = 50 mm	K_c W = 100 mm	K_c W = 150 mm	K_c W = 915 mm
0	9.89	10.63	11.41	16.02
2	11.34	11.41	11.97	16.15
4	12.83	12.19	12.52	16.27
6	14.42	12.98	13.08	16.40
8	16.15	13.79	13.65	16.53
10	18.07	14.63	14.22	16.66
12	20.23	15.50	14.80	16.79
14	22.66	16.41	15.40	16.91
16	25.41	17.36	16.01	17.04

Table 6.1: Fatigue crack propagation tests, CSM/PR

Specimen No.	ΔK MPa m$^{\frac{1}{2}}$	Glass content by weight %	ΔK_D	da_D/dN	Cycles to failure N_c
RC42/CN100/2 Dry	7.75	39.48	0.174	0.719×10^{-8}	2373000 S
RC42/CN100/7	7.50	34.93	0.190	0.206×10^{-6}	397640
RC28/CN100/33	8.25	34.95	0.209	0.421×10^{-6}	205630
RC28/CN100/32	9.00	34.92	0.228	0.740×10^{-6}	190530
RC38/CN100/12	8.00	32.09	0.221	0.234×10^{-5}	37790
RC28/CN100/25	9.50	37.15	0.227	0.257×10^{-5}	56300
RC38/CN100/2	8.50	31.21	0.241	0.195×10^{-4}	8500
RC24/CN100/3 Wet	5.00	35.22	0.126	0.301×10^{-6}	614050
RC24/CN100/8	6.50	33.89	0.170	0.249×10^{-4}	6770
RC24/CN100/2	8.25	35.44	0.207	0.160×10^{-3}	1890

S indicates test stopped without failure occurring.

Table 6.2: Fatigue crack propagation tests, WRF/PR, dry

Specimen No.	ΔK MPa $m^{\frac{1}{2}}$	Glass content by weight %	ΔK_D	da_D/dN phase 2	da_D/dN phase 3	Cycles to failure N_c
RCW36/CN100/21	22	67.68	0.168	0.215×10^{-6}	0.195×10^{-8}	4 904 000 S
RCW36/CN100/12	24	67.66	0.184	0.148×10^{-6}	0.126×10^{-8}	4 268 179 S
RCW36/CN100/3	26	64.71	0.215	0.155×10^{-6}	0.274×10^{-8}	2 287 000 S
RCW45/CN100/7	30	66.95	0.234	0.101×10^{-6}	0.278×10^{-8}	2 503 260
RCW39/CN100/12	34	65.52	0.275	0.112×10^{-6}	0.221×10^{-8}	1 493 400
Mean value				0.146×10^{-6}	0.219×10^{-8}	

S indicates test stopped without failure occurring.

Table 6.3: Fatigue crack propagation tests, WRF/PR, wet

Specimen No.	ΔK MPa m$^{\frac{1}{2}}$	Glass Content by Weight %	ΔK_5	da_p/dN	Cycles to Failure Nc
RCW36/CN100/8	14	55.46	0.114	0.402×10^{-7}	1970 000 S
RCW36/CN100/11	18	65.96	0.144	0.166×10^{-6}	494 500
RCW36/CN100/9	22	66.88	0.172	0.410×10^{-6}	271 680

S indicates test stopped without failure occurring

APPENDIX I: MATERIALS AND LAMINATE MAKING

The two GRP materials which have been used in this project both had a matrix of polyester resin. In CSM/PR, the reinforcement was chopped strand mat, and in WRF/PR it was woven roving fabric. A full description of resin, reinforcements, catalyst, and accelerator is given in Table A1.

The first two laminates, RC1 and RC2 were made with 1% catalyst and 0.5% accelerator. They took about 48 h to gel, and were then kept at 80°C for 3 h. This process (schedule A), is similar to that adopted by other workers, (24) (61). To cut down the gel time, 2% catalyst with 1% accelerator was used in all subsequent laminates. The curing schedule was also changed to one more appropriate for shipbuilding materials. On completing laying up, the laminate was left for 72 h at room temperature, and then kept at 40°C for a further 72 h, (schedule B).

All laminates were laid up by hand on glass plates covered with a sheet of Melinex release film. In CSM/PR, the desired glass content was 35% by weight, and to achieve this it was necessary to weigh the reinforcement and calculate the amount of resin needed in each ply. Spacers were placed on each side of the laminate, fastened at the corners, to prevent the mat spreading when rolled, and to maintain the desired thickness. These were sprayed with mould release agent. The resin was spread evenly over each layer and rolled with split washer rollers to ensure proper wetting out. When the last layer had been wetted out, the spacers were unfastened, moved away from the edges of the laminate, and scraped clean of fibres and resin. Surplus resin was then deposited across the middle of the laminate, a sheet of Melinex placed over it and rolled slowly with a 100 mm diameter solid roller to remove air which becomes entrained in the surplus resin. A glass plate

was then placed on top of the Melinex, held down by weights distributed evenly over its surface.

Spacers were unnecessary for WRF/PR laminates which did not spread on rolling. The glass content could be kept at about 65% simply by rolling out the excess resin, and the thickness of laminates with the same number of plies was consistent.

In the making of large laminates, 1 m square, the bottom glass plate was supported by pads attached to a rigid framework to keep the laminate flat. To minimise handling the glass plates, the framework was mounted on a trolley and could be slid into the oven on rollers.

The thickness of 3, 6 and 9 layer CSM/PR at 35% glass content, was 3.2, 6.4 and 9.6 mm respectively. In WRF/PR at 65% the thickness of 3, 6 and 9 layer material was 2.1, 4.2 and 6.3 mm respectively.

Table A1: Description of materials

Abbreviation	Trade name	Description
CSM	Fibreglass Supremat	Chopped strand mat, E-glass, 450 gm/m^2
WRF	Turner Bros. ECK25	Woven roving fabric, E-glass, 830 gm/m^2, 197 ends/m warp, 158 ends/m weft
PR	B.P. Cellobond A2785CV	Polyester resin, isophthalic type containing:- Isophthalic acid Maleic anhydride 1:2 Propylene glycol dissolved in styrene with added aerosil thixotrope and used with:- Catalyst : Methyl ethyl ketone peroxide SD2 Accelerator : 0.5% cobalt in styrene, NL48/ST

APPENDIX II: INTEGRATION OF THE FORMAN CRACK GROWTH EQUATION

The rate of fatigue crack propagation is given by:

$$\frac{da}{dN} = \frac{A \triangle K^m}{(K_c - \triangle K)} \qquad \text{A2.1}$$

where A, m are constants. This can be expressed in the dimensionless form:

$$\frac{da_D}{dN} = \frac{A \triangle K_D^m}{(K_{Dc} - \triangle K_D)} \qquad \text{A2.2}$$

in which $a_D = (a/W)$, $\triangle K_D = (\triangle K / \sigma_{UTS} \sqrt{W})$, and, for 100 mm wide CN specimens of CSM/PR:

$$K_{DC} = B_o + B_1 a_D + B_2 a_D^2 \qquad \text{A2.3}$$

where $B_o = 0.188$, $B_1 = 0.938$, and $B_2 = -2.333$. Substituting A2.3 into A2.2 gives:

$$\frac{da_D}{dN} = \frac{A \triangle K_D^m}{([B_o - \triangle K_D] + B_1 a_D + B_2 a_D^2)} \qquad \text{A2.4}$$

If $\triangle K_D$ is kept constant with increasing a_D integration gives:

$$N - N_i = \frac{1}{A \triangle K^m} \int_{a_{Di}}^{a_D} ([B_o - \triangle K_D] + B_1 a_D + B_2 a_D^2) da_D$$

where a_{Di}, N_i are values of a_D, N at the start of the integration.

$$N - N_i = k \left[(B_o - \triangle K_D)(a_D - a_{Di}) + \frac{B_1}{2}(a_D^2 - a_{Di}^2) + \frac{B_2}{3}(a_D^3 - a_{Di}^3) \right] \qquad \text{A2.5}$$

where

$$k = 1/A \triangle K^m \qquad \text{A2.6}$$

For each a_D, N curve in Fig. 6.2, a value of k can be found which gives the best fit of equation A2.5. The sum of the squares of residuals, R, is S, and there are n points:
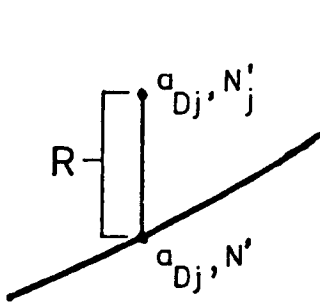
$$j = n$$
$$\sum_{j = i} (N'_j - N')^2 = S \qquad \text{A2.7}$$

where $N'_j = N_j - N_i$. The criterion for a best fit is that S should be a minimum with respect to k:

$$\frac{dS}{dk} = 0 \qquad \text{A2.8}$$

$$S = \sum^n \left(N'_j - k \left[(B_o - \Delta K_D)(a_D - a_{Di}) + \frac{B_1}{2} (a_D^2 - a_{Di}^2) + \frac{B_2}{3} (a_D^3 - a_{Di}^3) \right] \right)^2$$

$$\frac{dS}{dk} = \sum^n \left(-2 N'_j \left[(B_o - \Delta K_D)(a_D - a_{Di}) + \frac{B_1}{2} (a_D^2 - a_{Di}^2) \right. \right.$$
$$\left. + \frac{B_2}{3} (a_D^3 - a_{Di}^3) \right] + 2k \left[(B_o - \Delta K_D)(a_D - a_{Di}) + \frac{B_1}{2} (a_D^2 - a_{Di}^2) \right.$$
$$\left. \left. + \frac{B_2}{3} (a_D^3 - a_{Di}^3) \right]^2 \right) = 0 \qquad \text{or:}$$

$$j = n \qquad j = n$$
$$\sum_{j = i} N'_j = k \sum_{j = i} \left[(B_o - \Delta K_D)(a_D - a_{Di}) + \frac{B_1}{2} (a_D^2 - a_{Di}^2) + \frac{B_2}{3} (a_D^3 - a_{Di}^3) \right]$$

A2.

Thus k can be determined from a_D, N data and hence A and m from the logarithmic form of equation A2.6

FIG. 2.1 Crack Extension Modes

Mode I

Mode II

Mode III
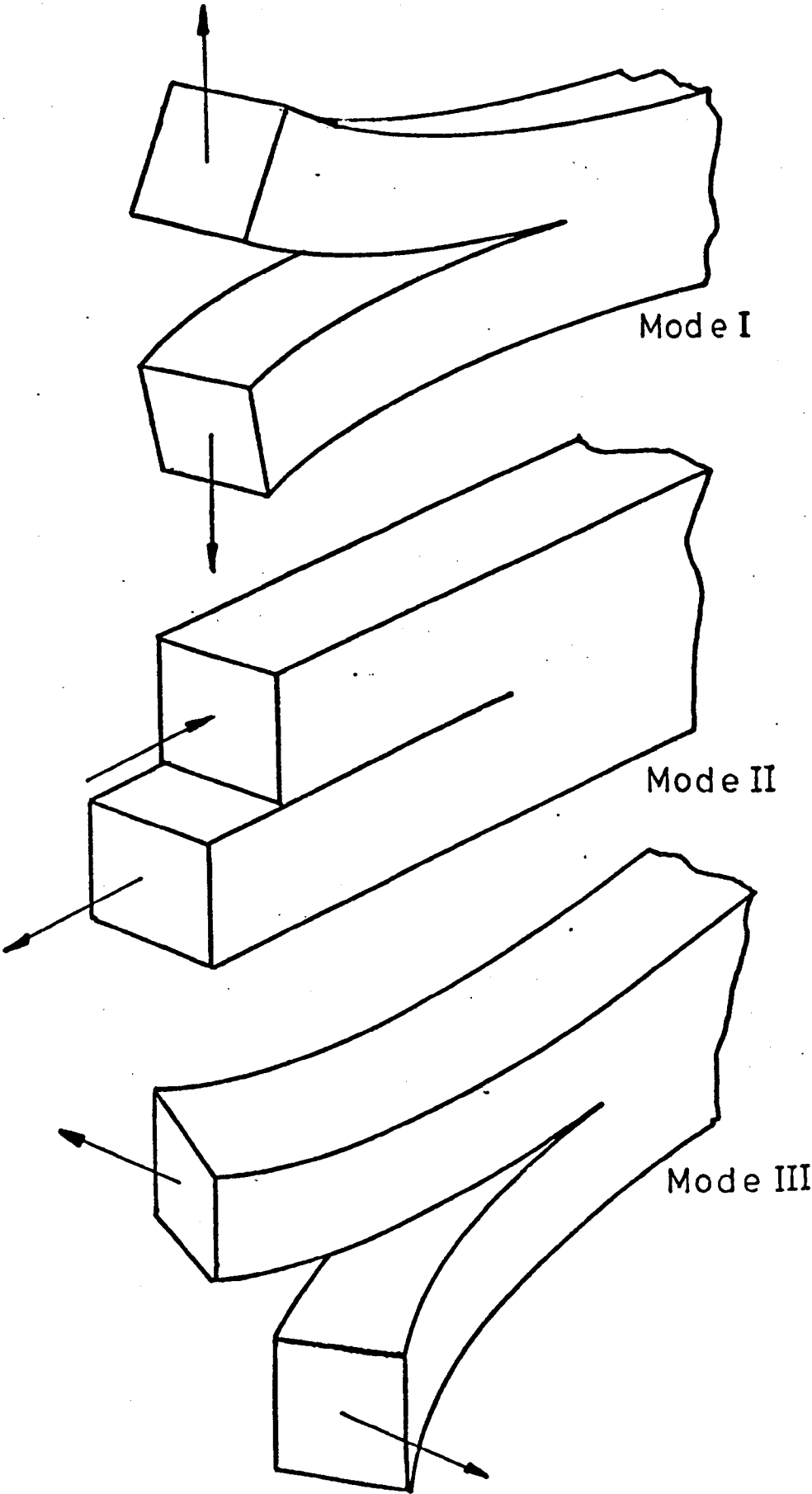
FIG.2.2 Dimensionless Stress Intensity Factor Versus Crack Length/Width Ratio (r)

DEN $(\tan\pi r + 0.1\sin\pi r)^{1/2}$ } Irwin

CN $(\tan\pi r)^{1/2}$

CN $r^{1/2}(1.77 + 0.454r - 1.02r^2 + 5.4r^3)$ Isida

INFINITE PLATE $(\pi r)^{1/2}$, Griffith

$\dfrac{K}{\sigma_N \sqrt{W}}$

a/W = r
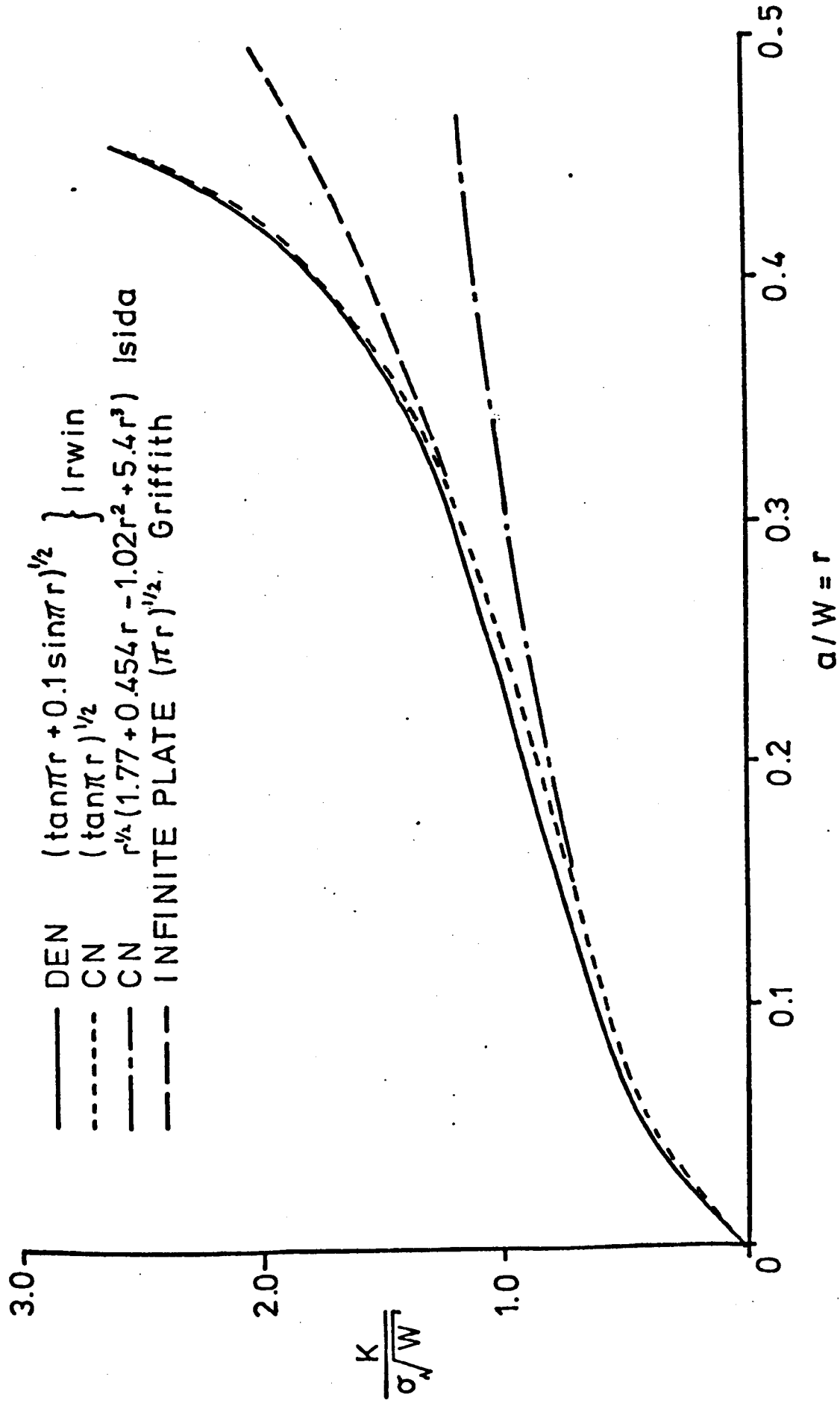
FIG.2.3 Types of Fracture Mechanics Specimen
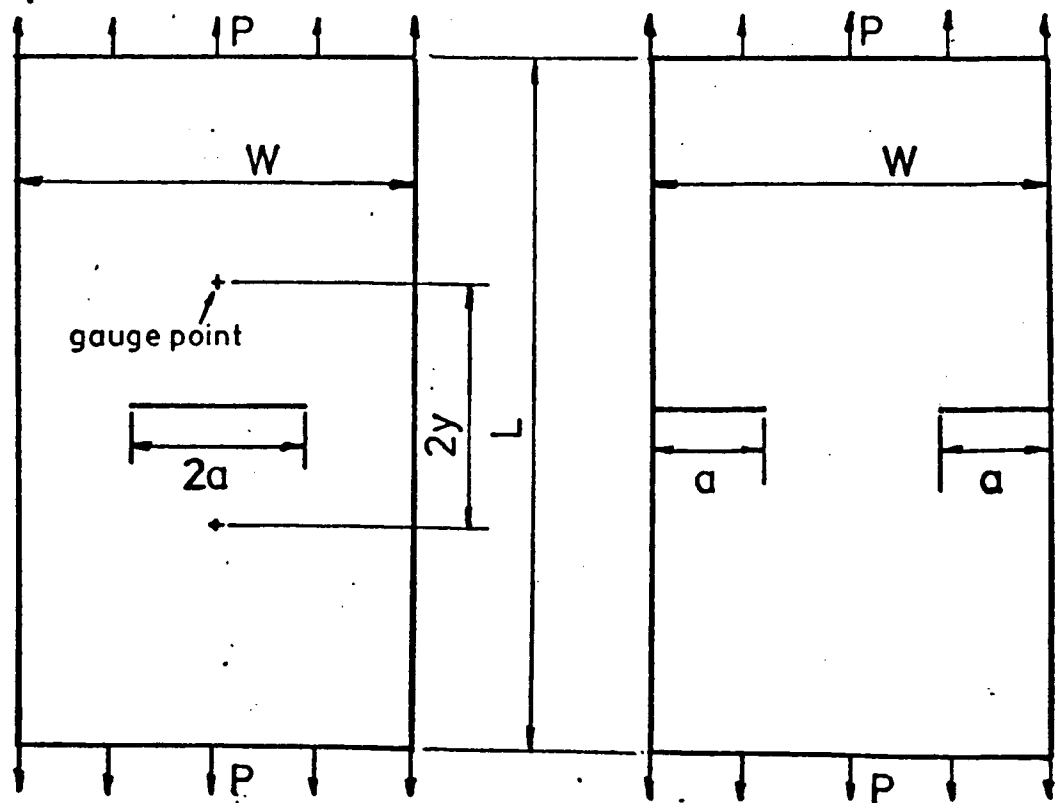
2.3a. Centre-notch CN

2.3b. Double-edge-notch DEN
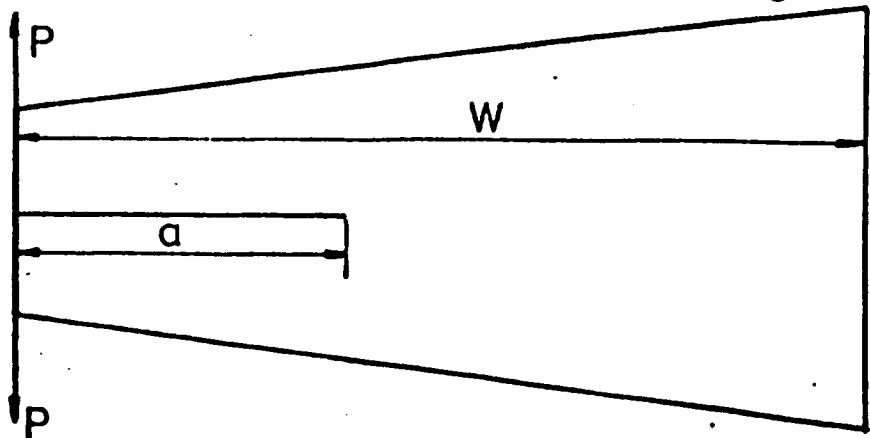
2.3c. Single-edge-notch

SEN
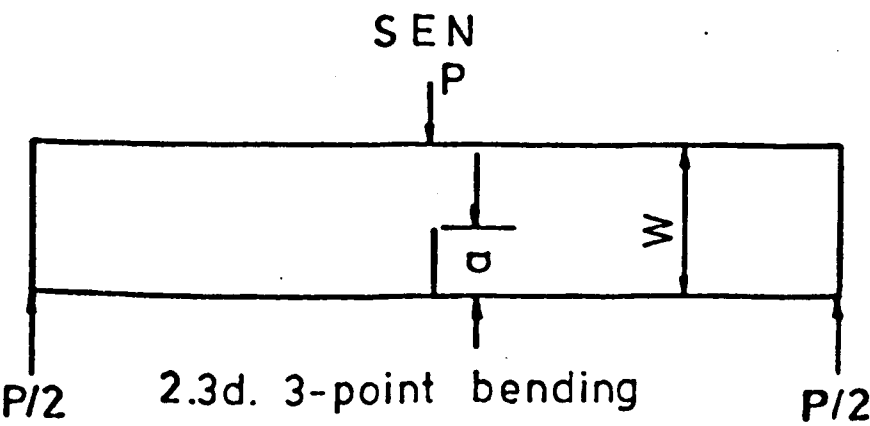
2.3d. 3-point bending

BEAM

All above specimens have thickness t

FIG.3.1 Tensile and compliance specimens

Dimensions in millimetres.

216

50·8

19

12·7

7·6R

N

a.

T1 type specimen

End piece

End piece

45 min.

140 ± 5

45 min.

End piece

End piece

25 ± 0·5

230 minimum

b.

T2 type specimen

1

θ P

h

2
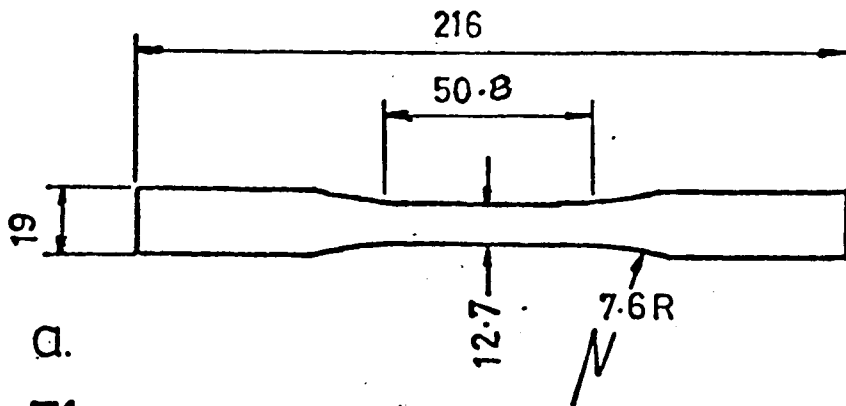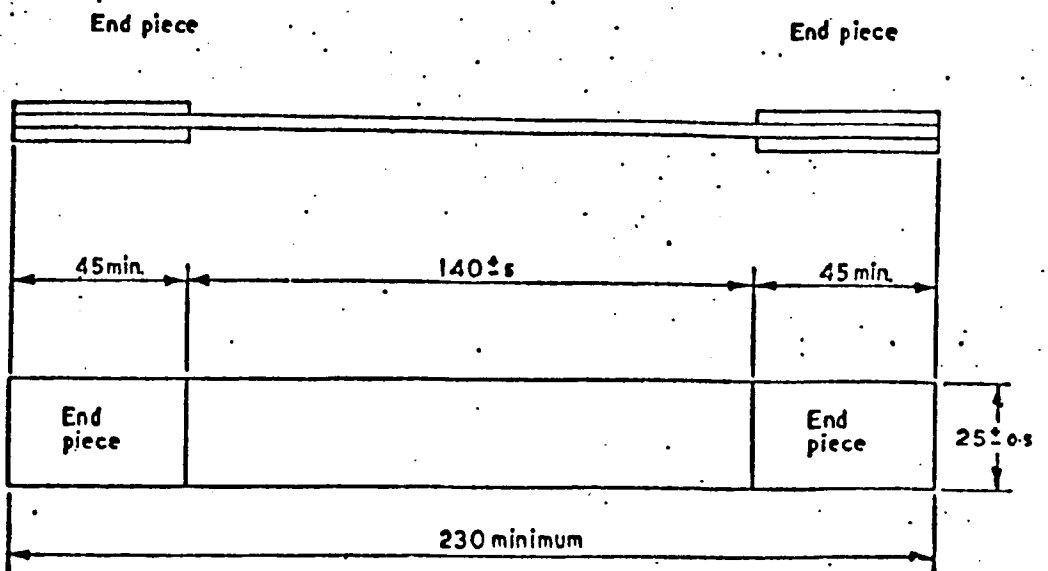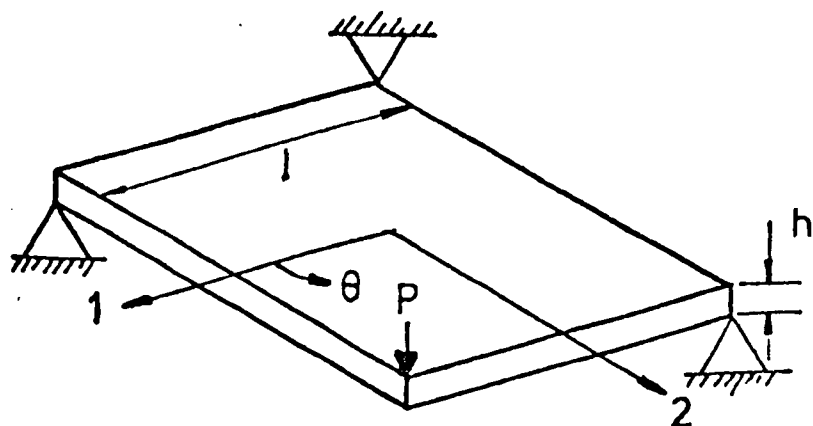
c.

Plate twist specimen

FIG.3.2 UTS, Resin cracking stress, S_{11}, S_{22} vs. Glass content

Type T1 specimens of CSM/PR, 3-layer laminates, RC1, RC2.

    +   UTS 90°   × Resin cracking stress 90°   △ S_{11}

    ⊕ UTS 0°   ⊗ Resin cracking stress 0°   ⬠ S_{2}
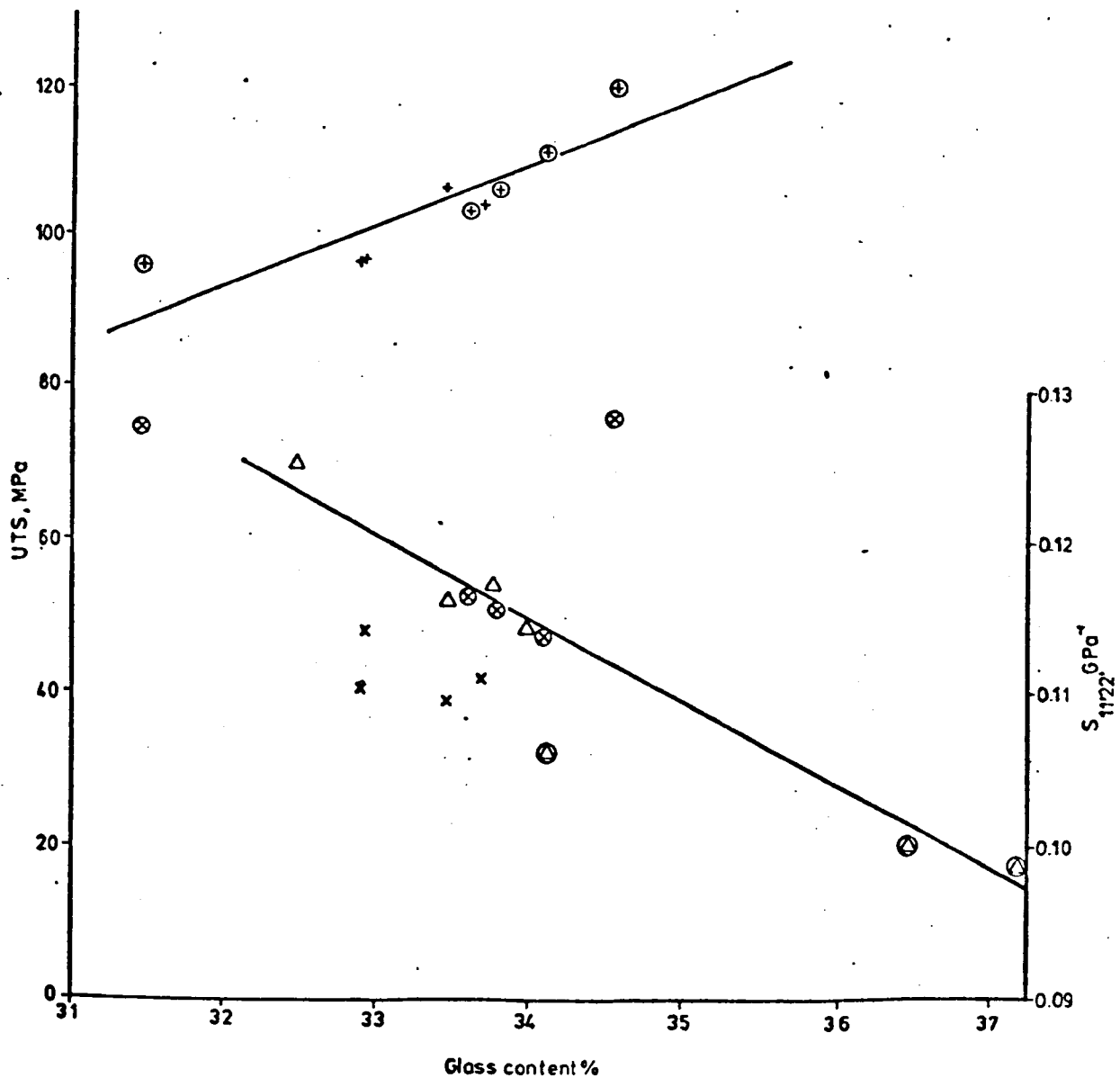
FIG.3.3 UTS, S_{11}, S_{22} vs. Glass content

Type T1 and T2 specimens of CSM/PR, 3,6,9-layer laminates

6 and 9 layer results numbered

UTS, MPa

$S_{11,22}$ GPa^{-1}

Glass content %

⊕ UTS T1 0°
+ UTS T1 90°
⊗ UTS T2 0°
✕ UTS T2 90°
⊘ S_{11} T1
△ S_{22} T1
⊛ S_{11} T2
▲ S_{22} T2
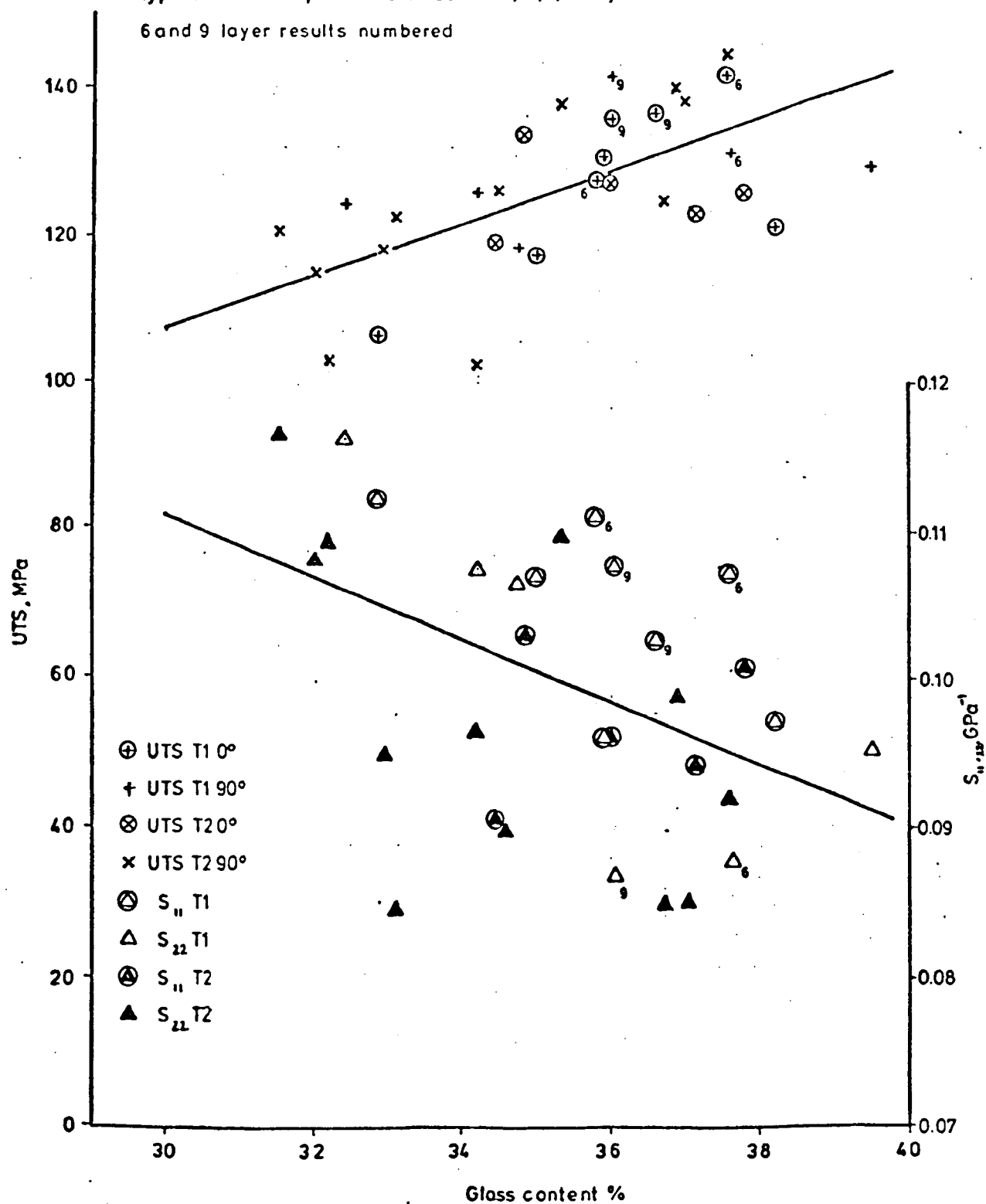
FIG.3.4

Distribution of
glass content in
915mm square

laminate, CSM/PR

←O→ TOP LAYER WARP DIRECTION

34,21┤ 33/3┤ 36,76┤ 31,53┤

36,03┤ 37,82┤

37,62┤ 37,06┤ 36,92┤ 35,39┤

34,88┤ 37,20┤ 34,49┤

34,54┤ 32,9┤ 32,04┤ 32,21┤
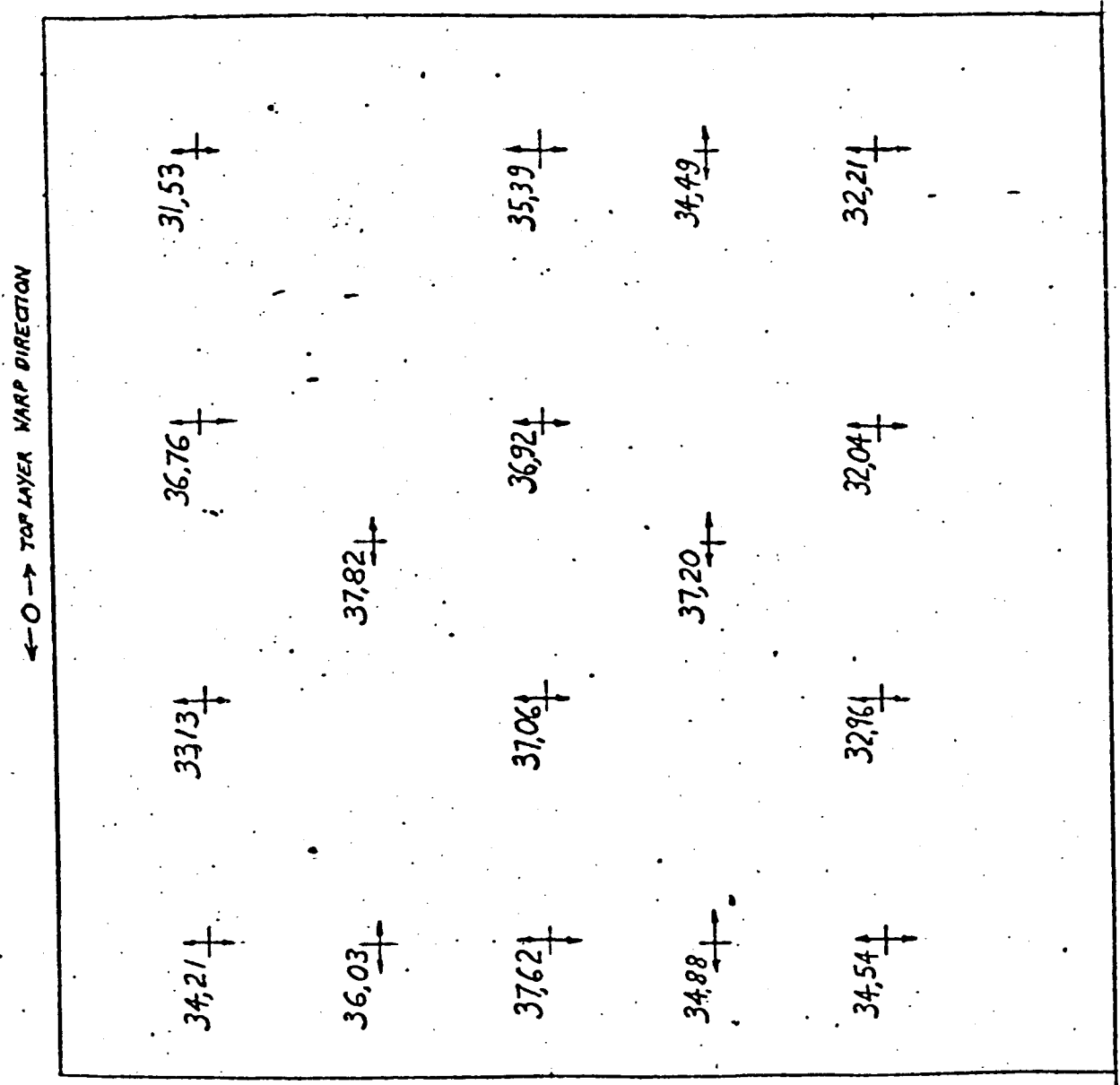
arrows show
direction in which
specimens were cut

FIG. 3.5

UTS. S_{11} and S_{22} vs. Glass Content by Weight

Type T2 Specimens of WRF/PR 3.6, and 9 layer.

(6 and 9 layer results numbered)
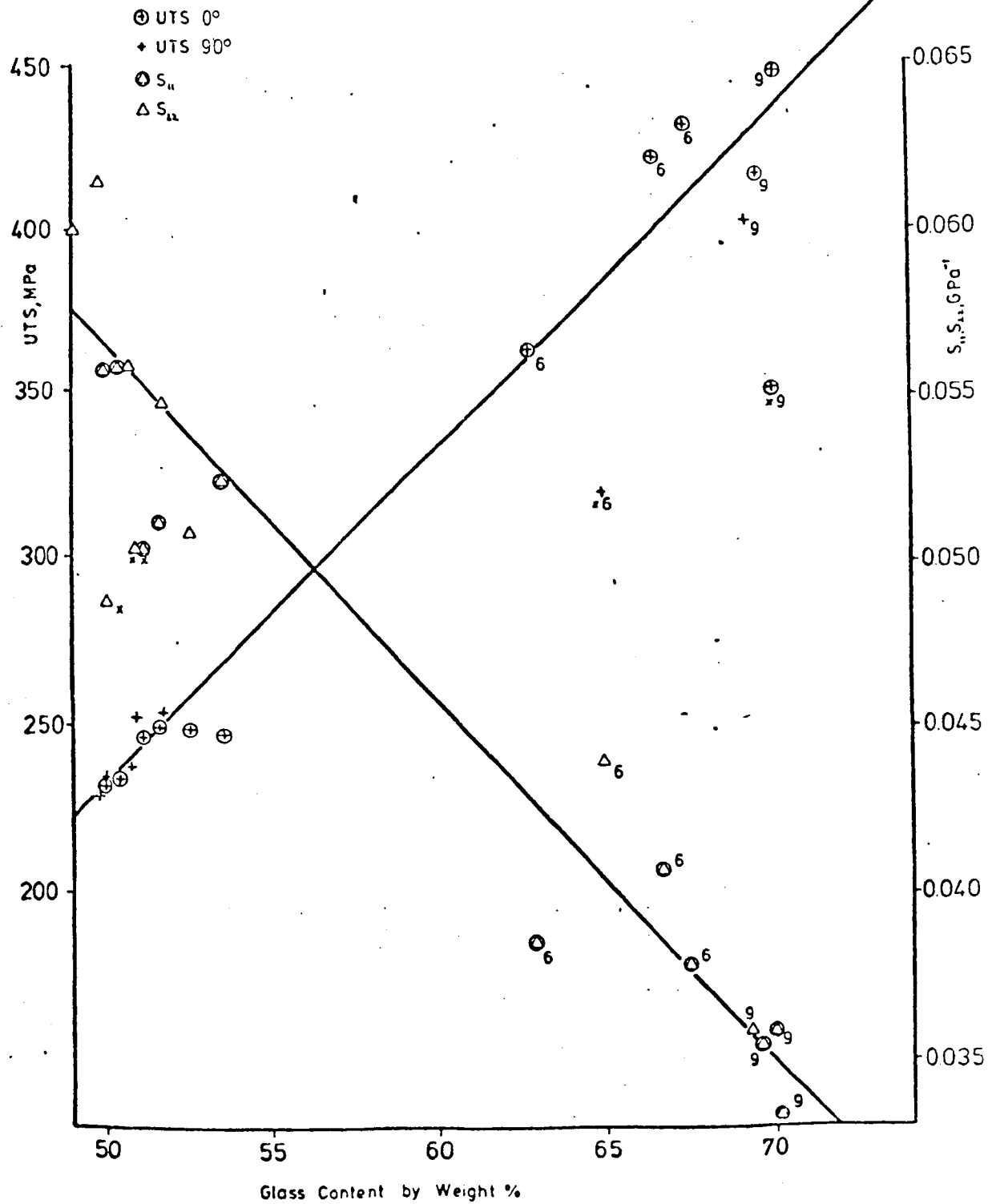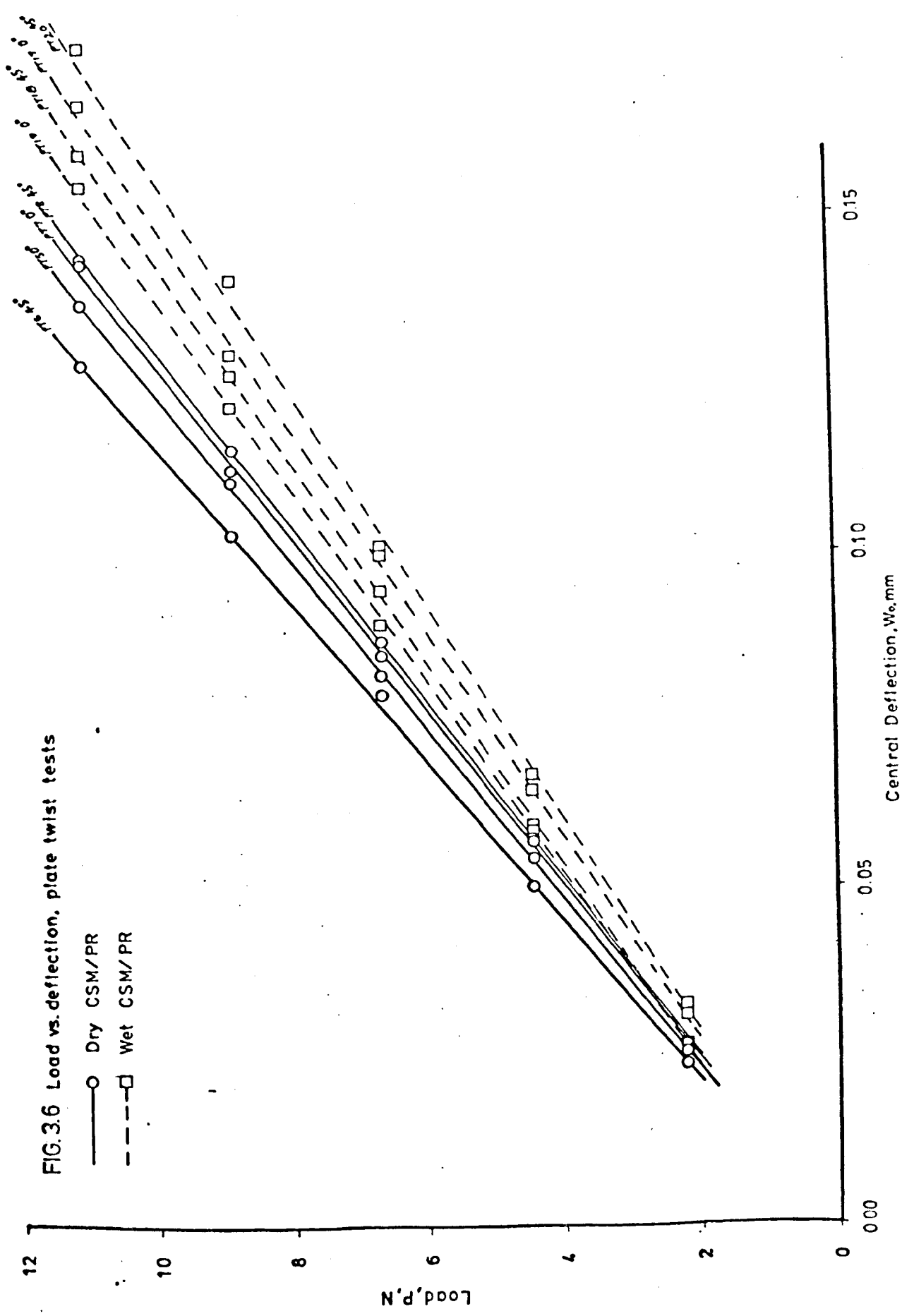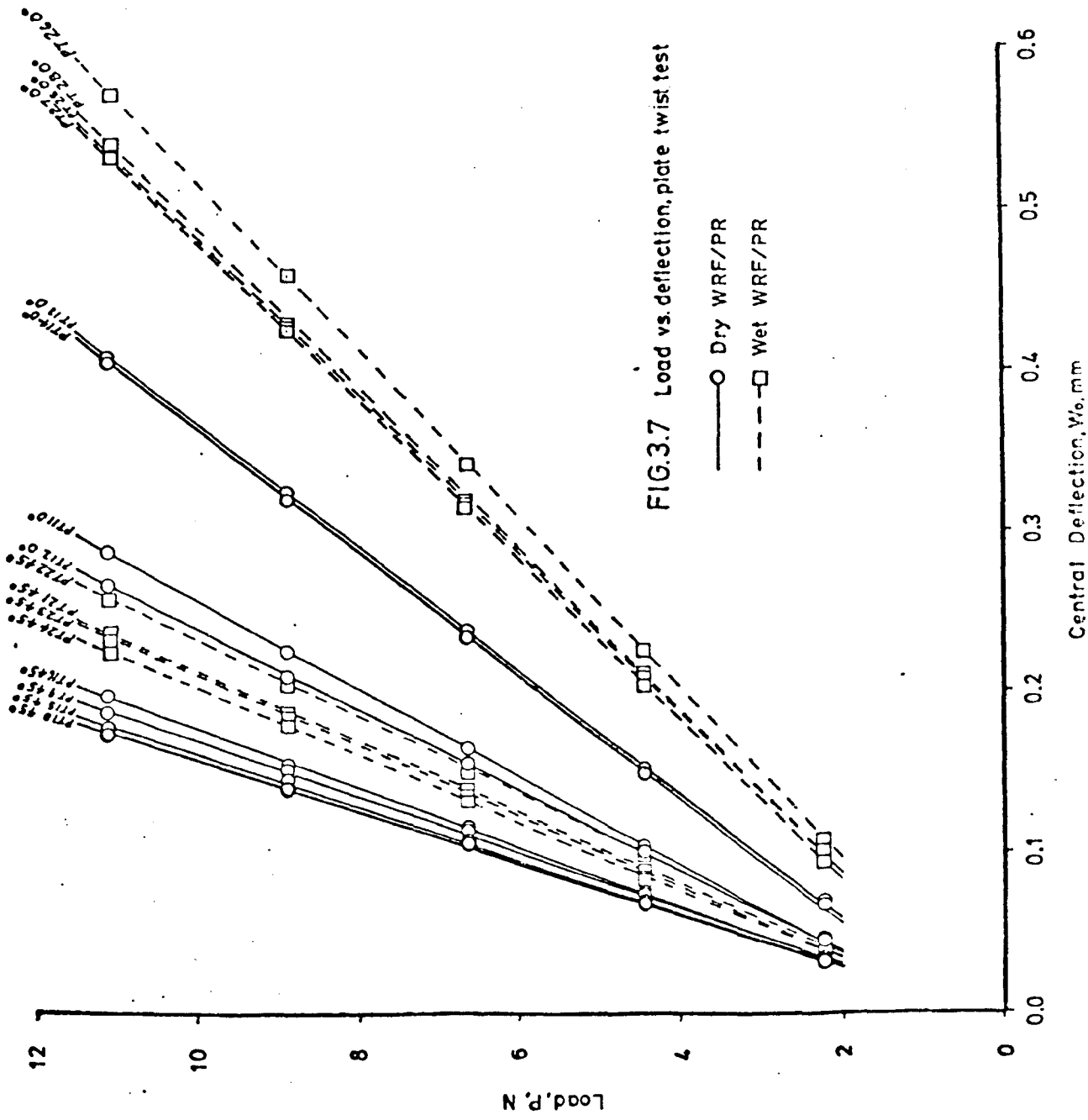
⊕ UTS 0°

✦ UTS 90°

◐ S_{11}

△ S_{22}

Glass Content by Weight %

FIG.3.6 Load vs. deflection, plate twist tests

Dry CSM/PR

Wet CSM/PR

Load,P,N

Central Deflection,Wo,mm

FIG.3.7 Load vs. deflection, plate twist test

○——○ Dry WRF/PR

□----□ Wet WRF/PR

Central Deflection, Wo, mm

Load, P, N

FIG.3.8 S_6 vs. glass content, dry WRF/PR

● 0°   ○ 45°

S_6, GPa^{-1}

Glass content %

FIG.3.9 S_6 vs. glass content, dry WRF/PR
⊙ 0° ○ 45°

S_6, GPa^{-1}
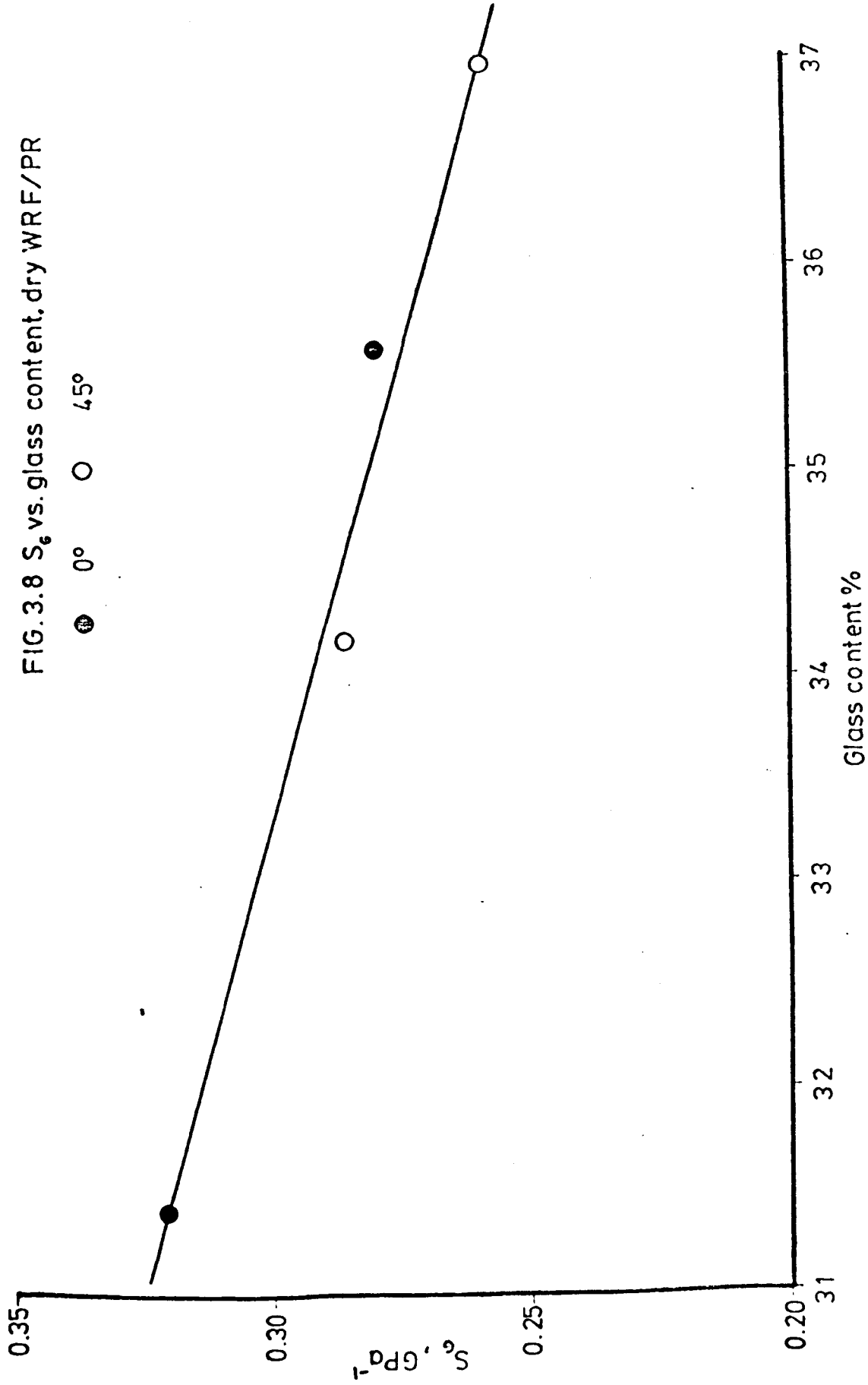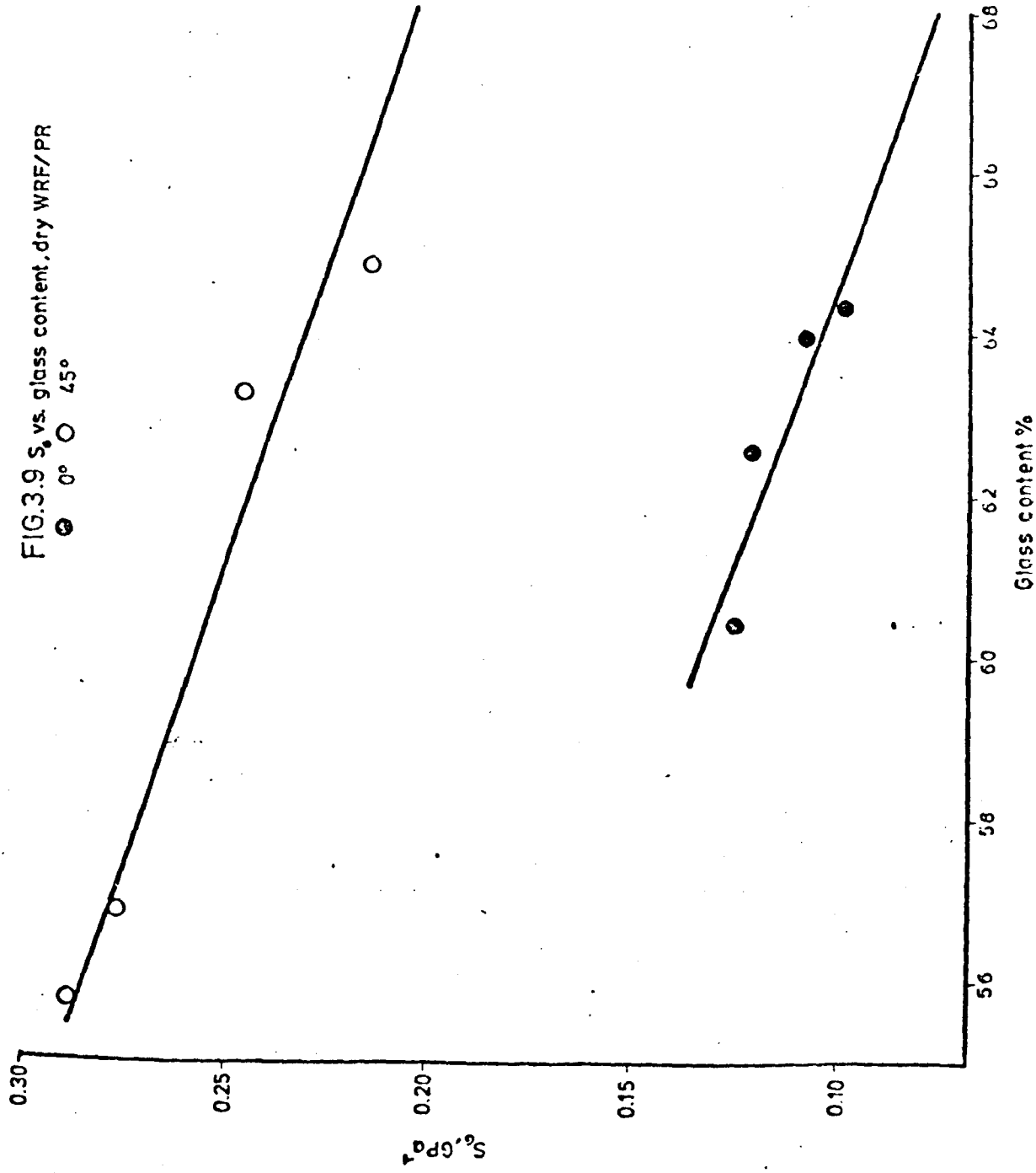
Glass content %

FIG.4.1 Finite element model
of CN specimen
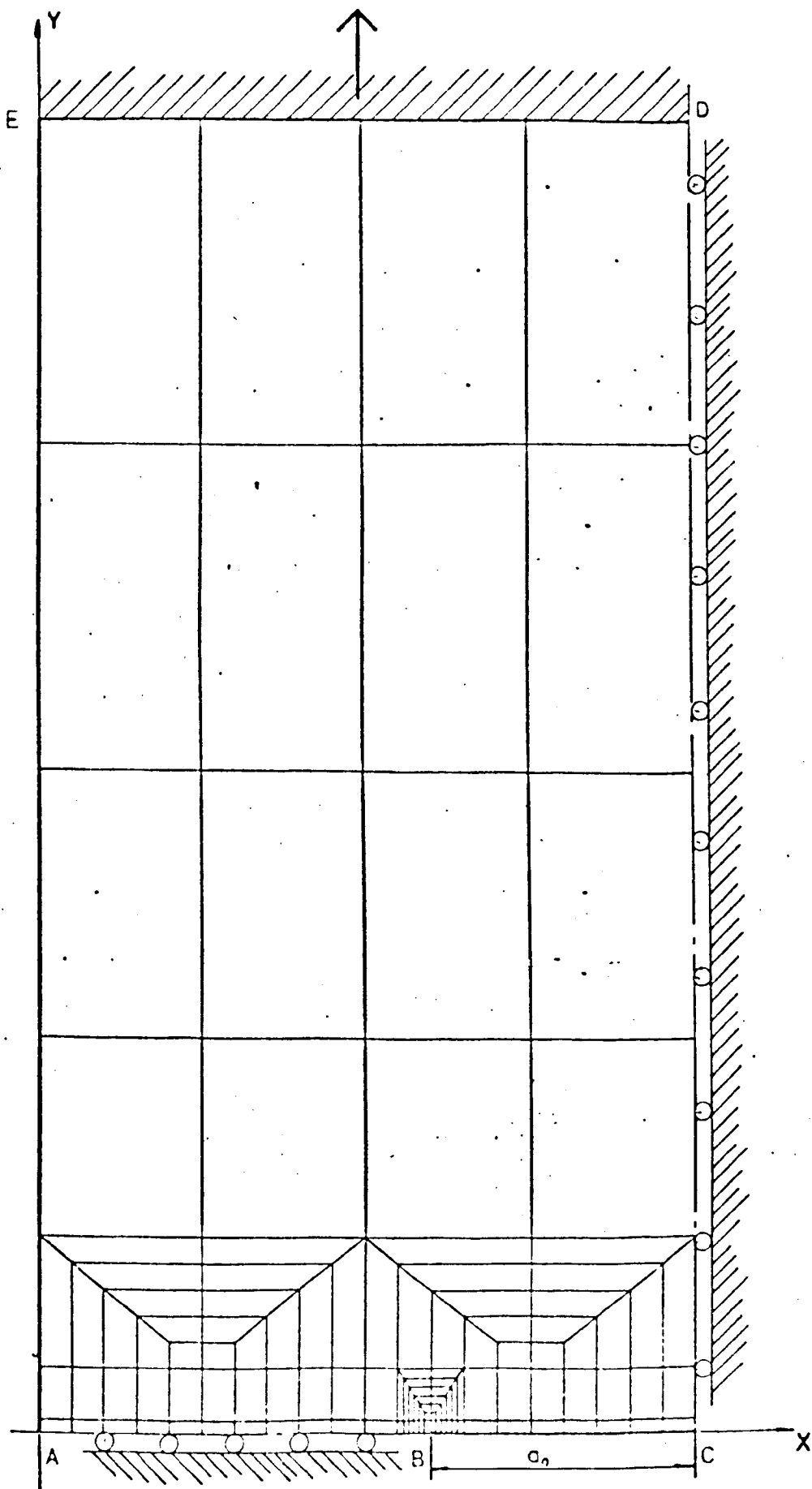
FIG.4.2 K*/K vs. r/W, a/W = 0.05
for key see table 4.1
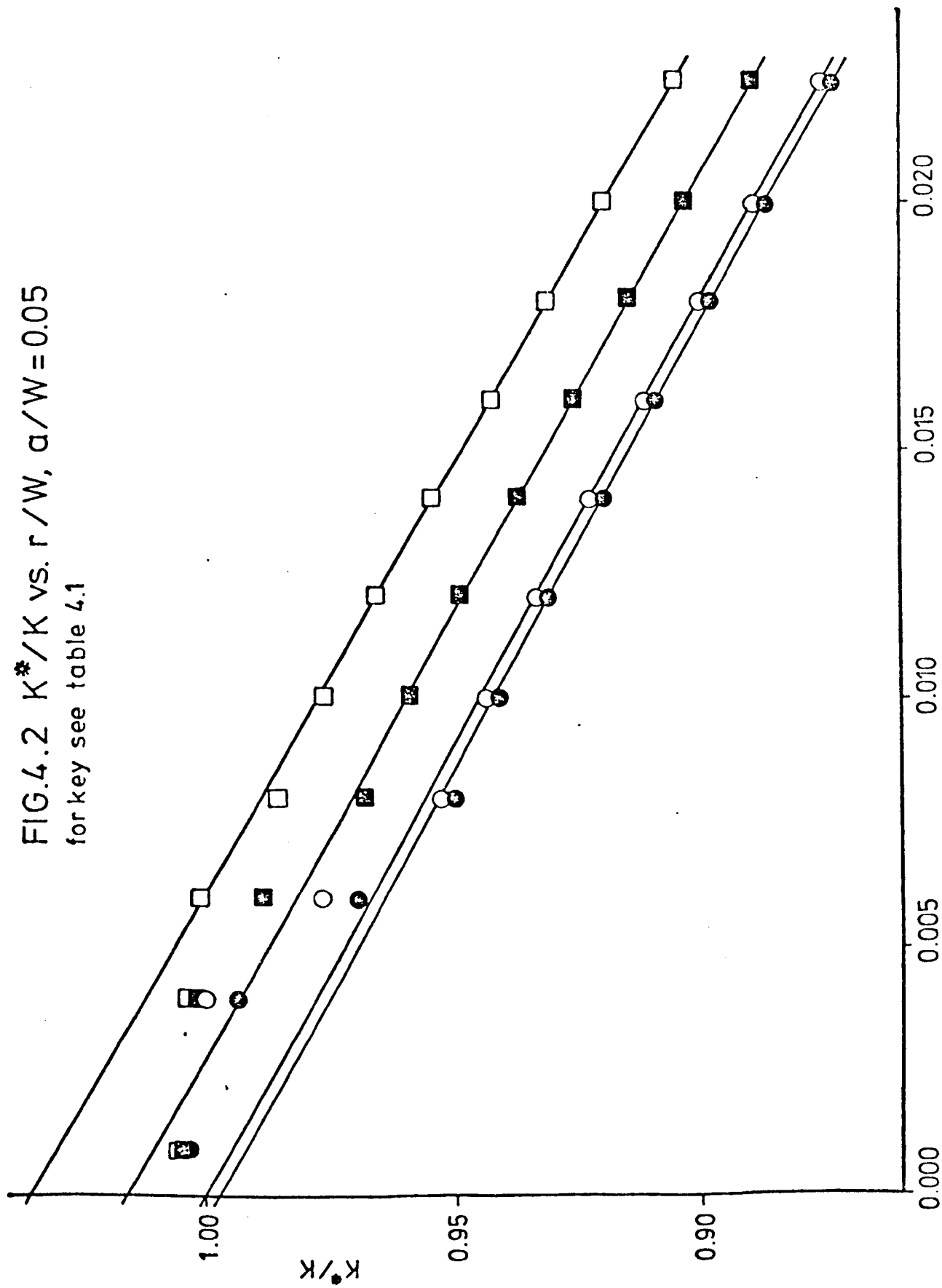
FIG.4.3 K*/K vs. r/W, a/W=0.30
for key see table 4.1

FIG. 4.4 C_D vs. a/W

KEY:

○   100mm CSM/PR

□   100mm WRF/PR

△   915mm CSM/PR

▽   915mm WRF/PR

— — — Eqation 4.4.1 with y=0.04

Black symbols are experimental
points corresponding to white
finite element points.

C_D

$[a/W]$

FIG.5.1

Static and Fatigue
Testing Frame
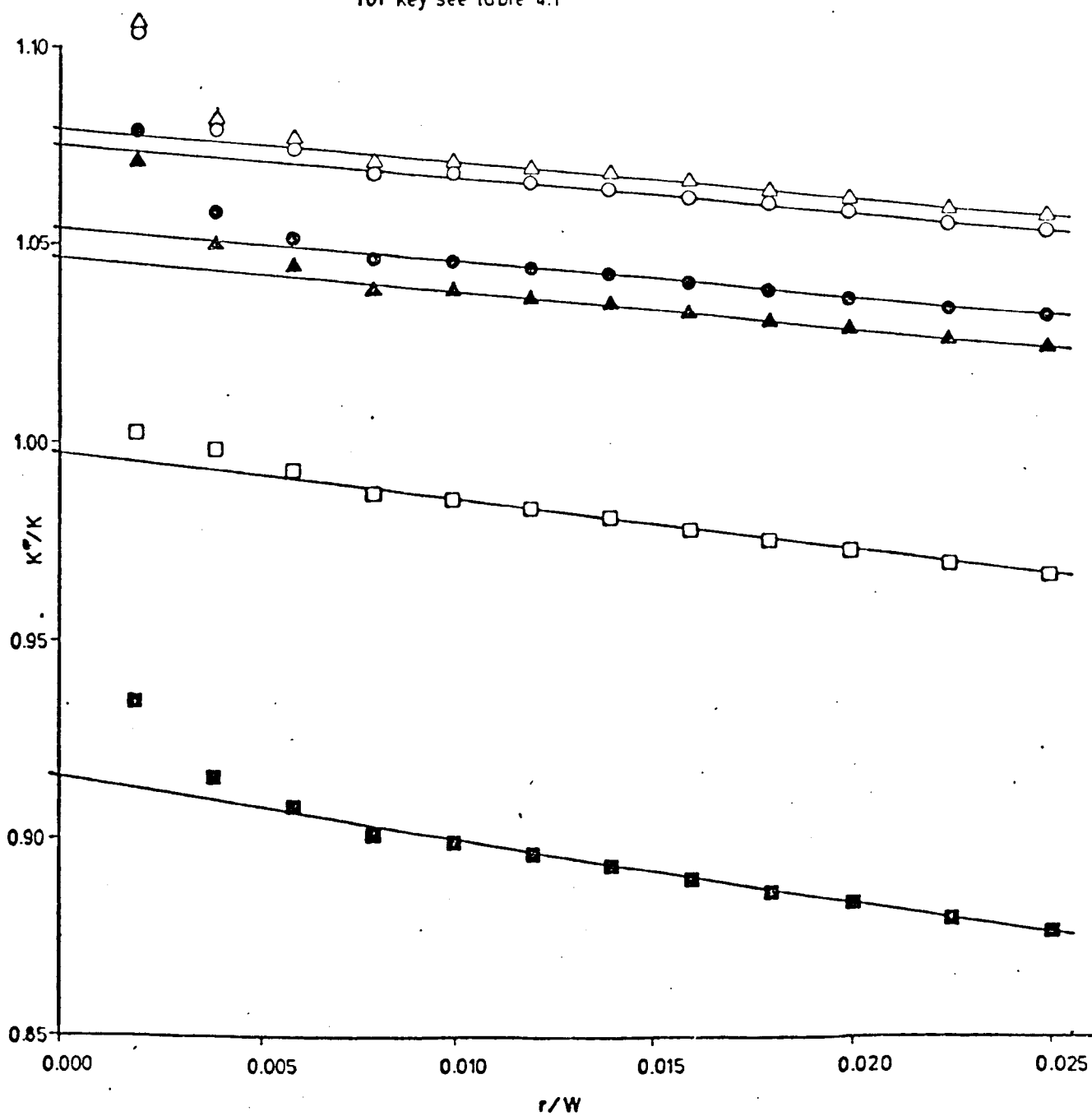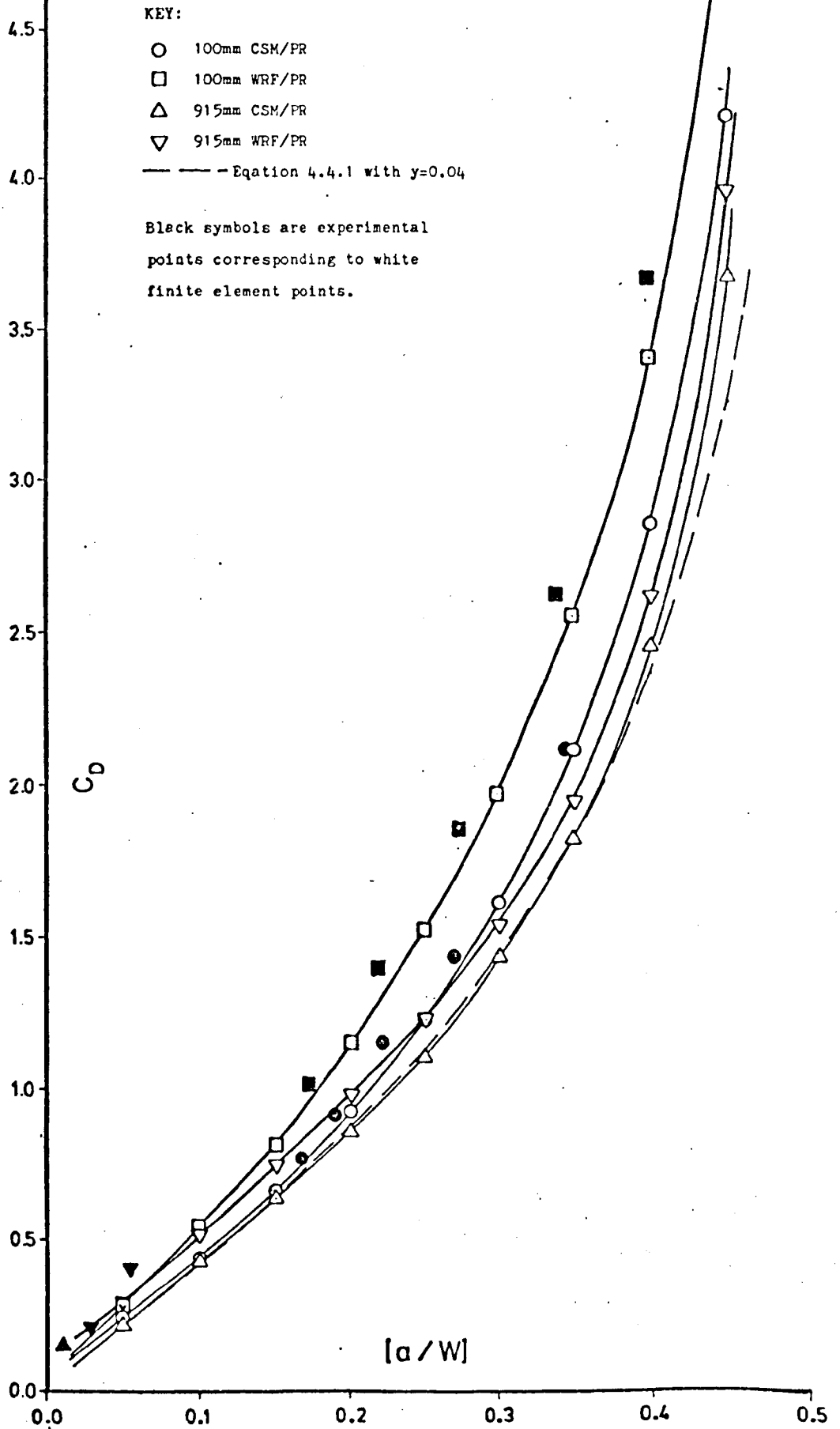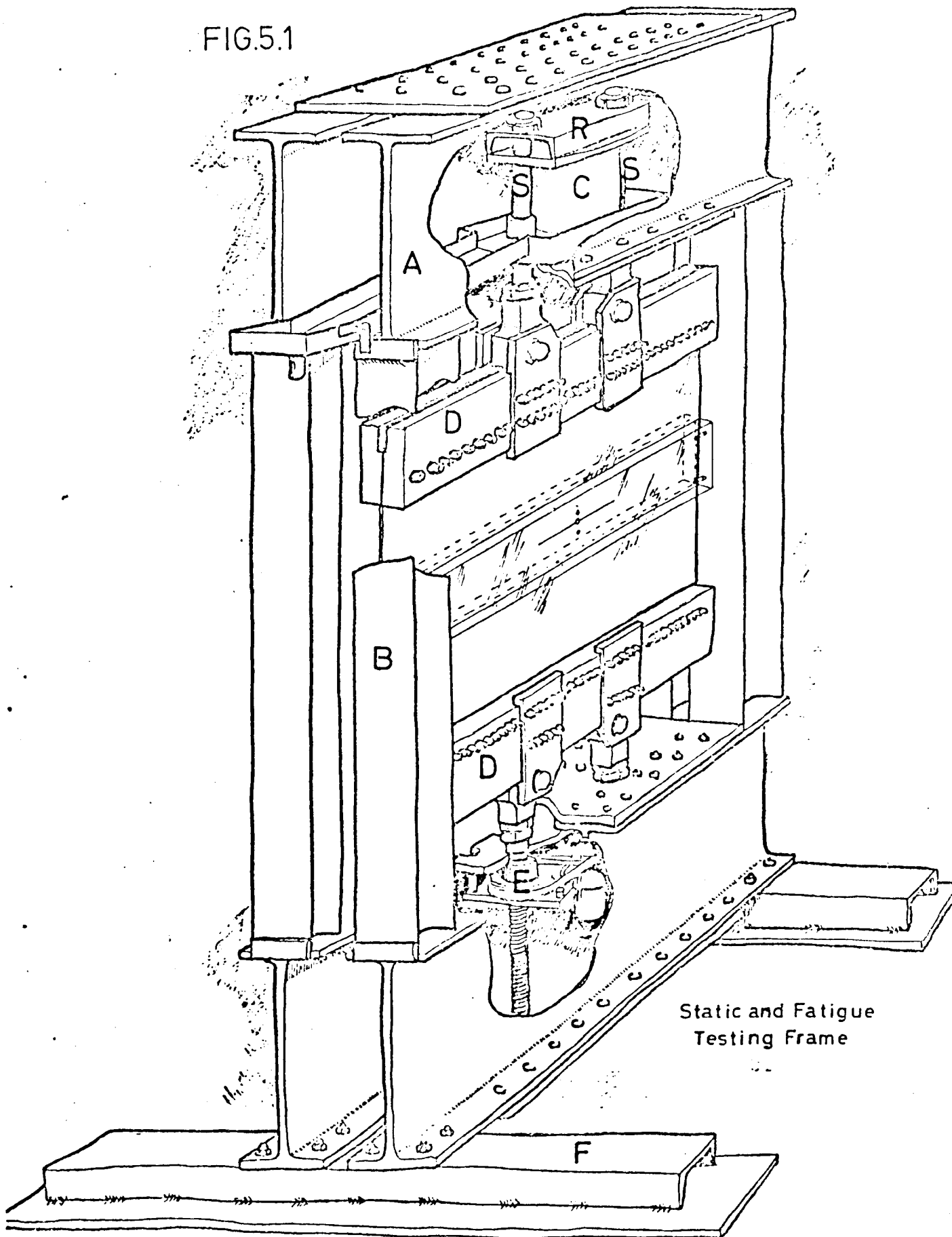
FIG.5.2
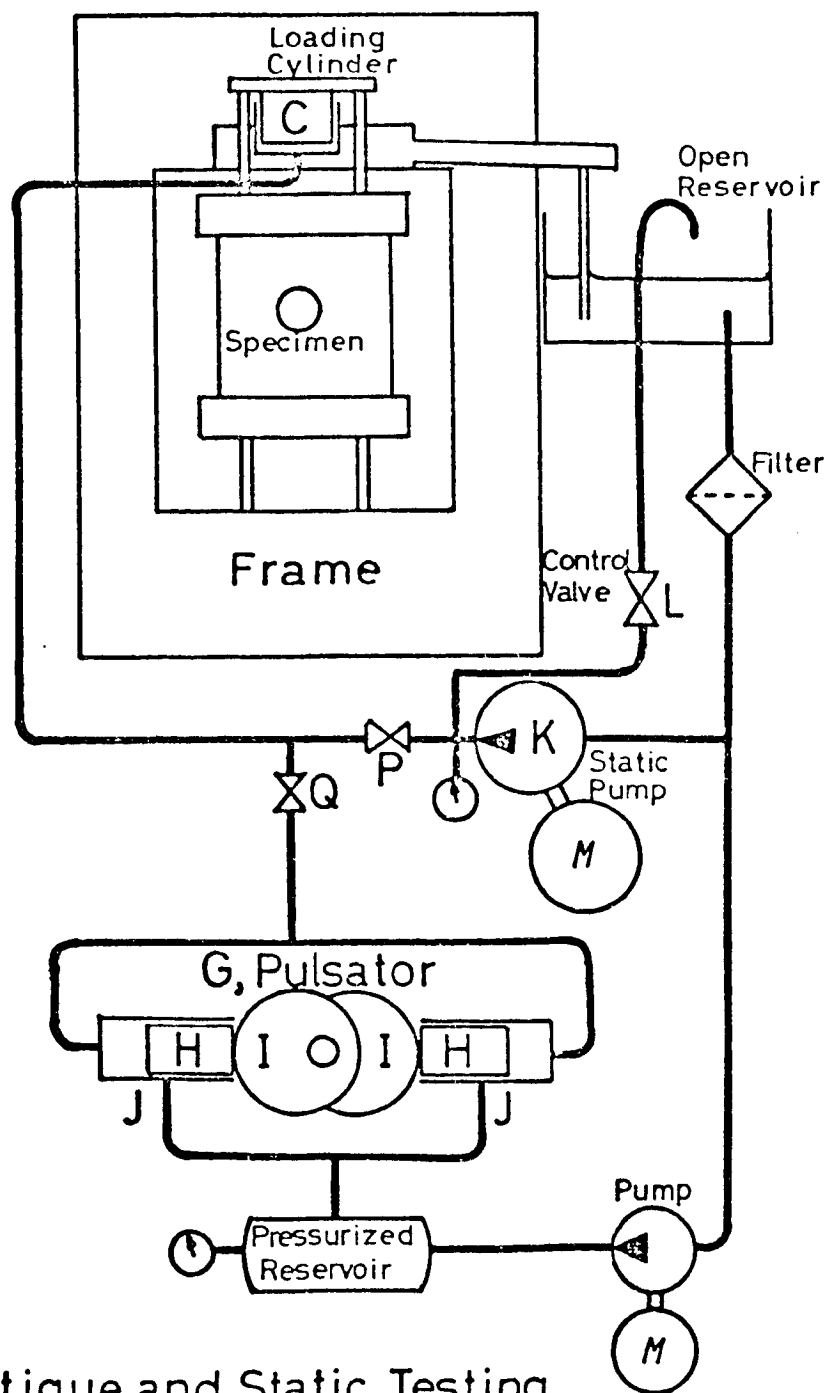
Fatigue and Static Testing
Machine, Hydraulic Circuit.

FIG.5.3 K vs. glass content 3 layer dry CSM/PR

○ W=50mm + W=100mm △ W=150mm

DEN specimens

FIG.5.4 K_c vs. glass content, 3,6,9 layer dry CSM/PR

O W=50mm + W=100mm △ W=150mm
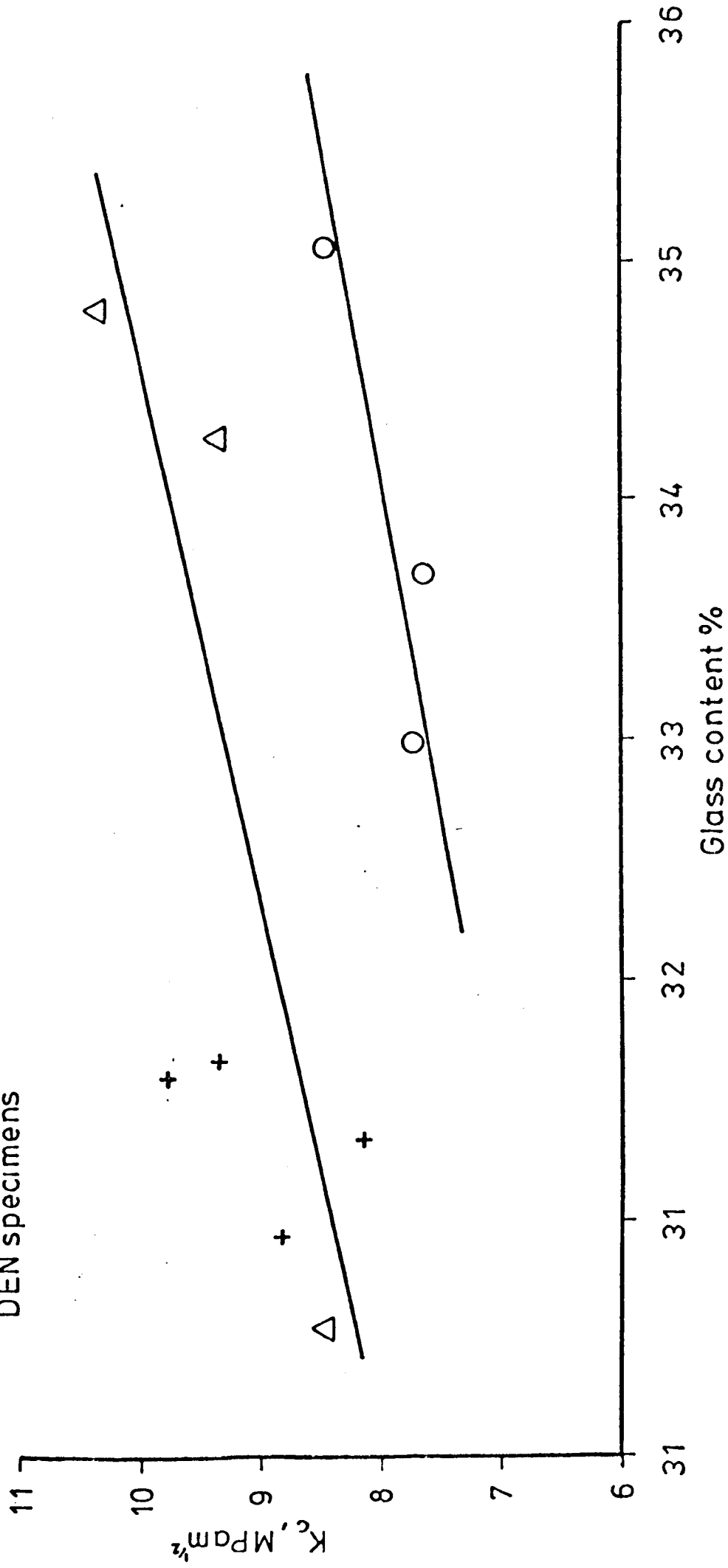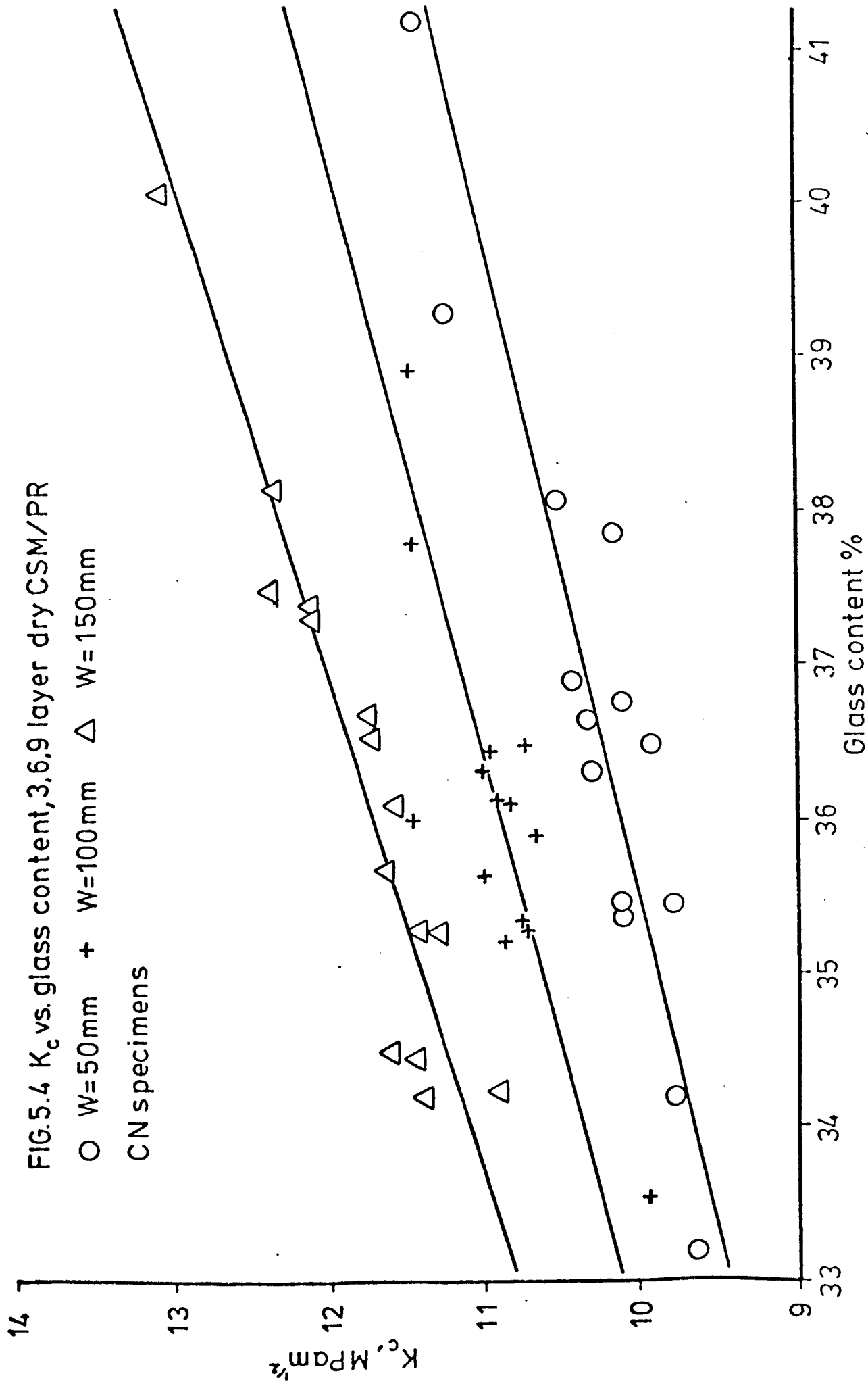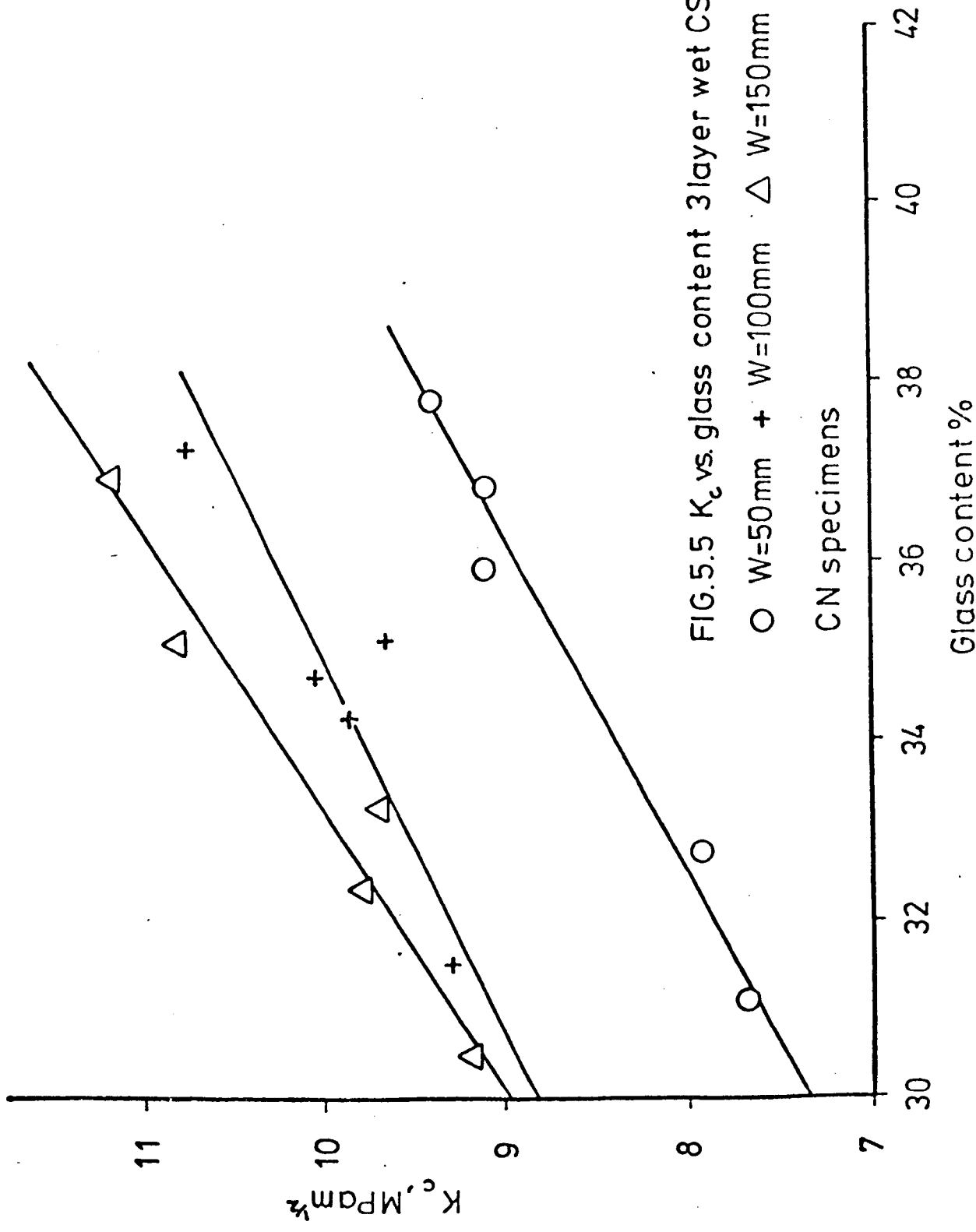
CN specimens

FIG.5.5 K_c vs. glass content 3 layer wet CSM/PR

○ W=50mm + W=100mm △ W=150mm

CN specimens

Glass content %

K_c, MPam$^{1/2}$

K_c vs. Glass Content; 3,6, and 9 layer WRF/PR material. Widths 50($\odot$), 100(+), and 150($\triangle$)mm. $a_c/w=0.1667$. Numbers adjacent to points indicates no. of layers of reinforcement. CN specimens

FIG.5.6

Glass Content by Weight %

K_c, MPa.m$^{\frac{1}{2}}$
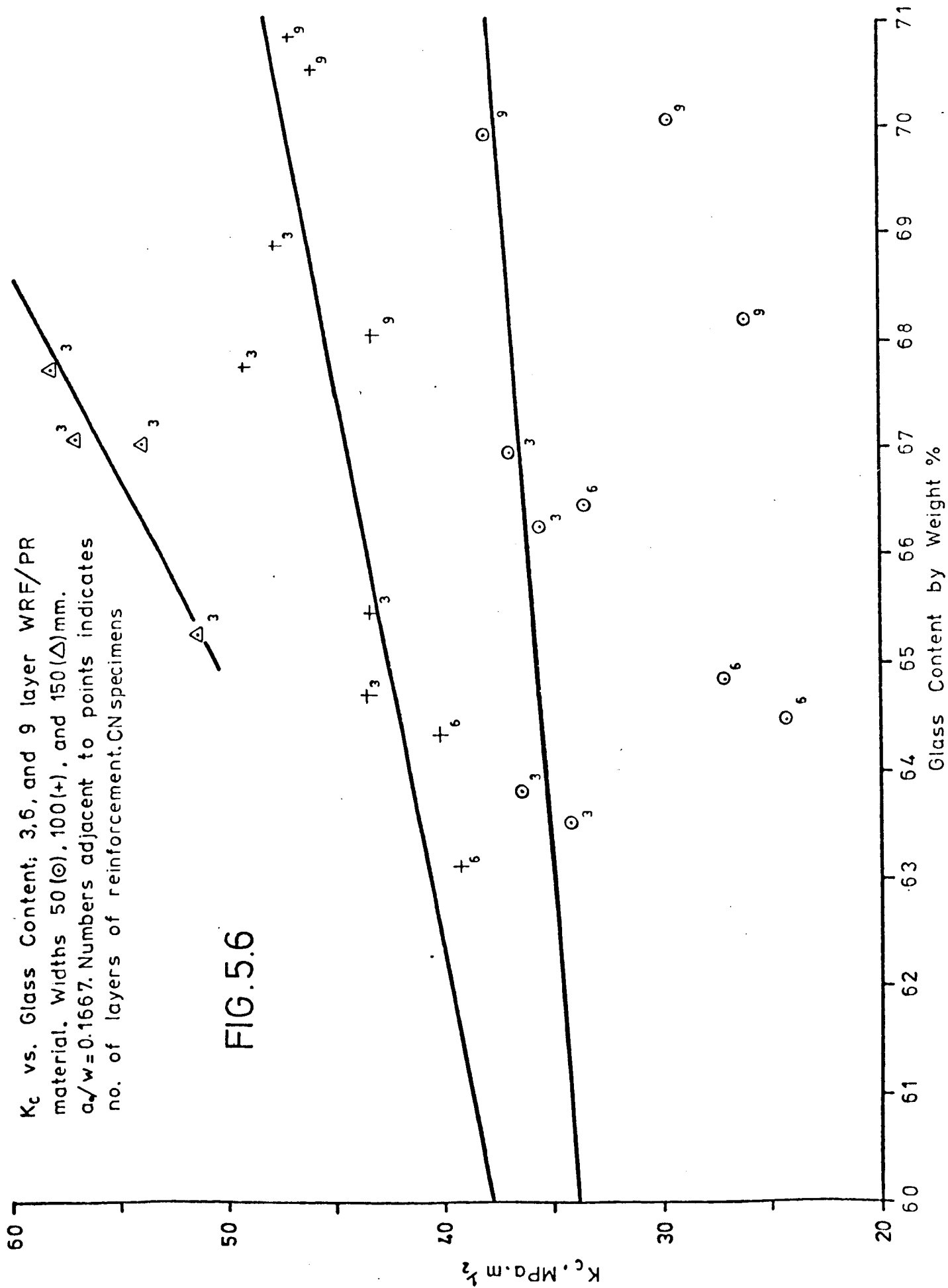
K_c vs. glass content for wet CN specimens of WRF/PR

FIG5.7

○ W = 50 mm
□ W = 100 mm
△ W = 150 mm

glass content %

K_c, MPa m$^{1/2}$
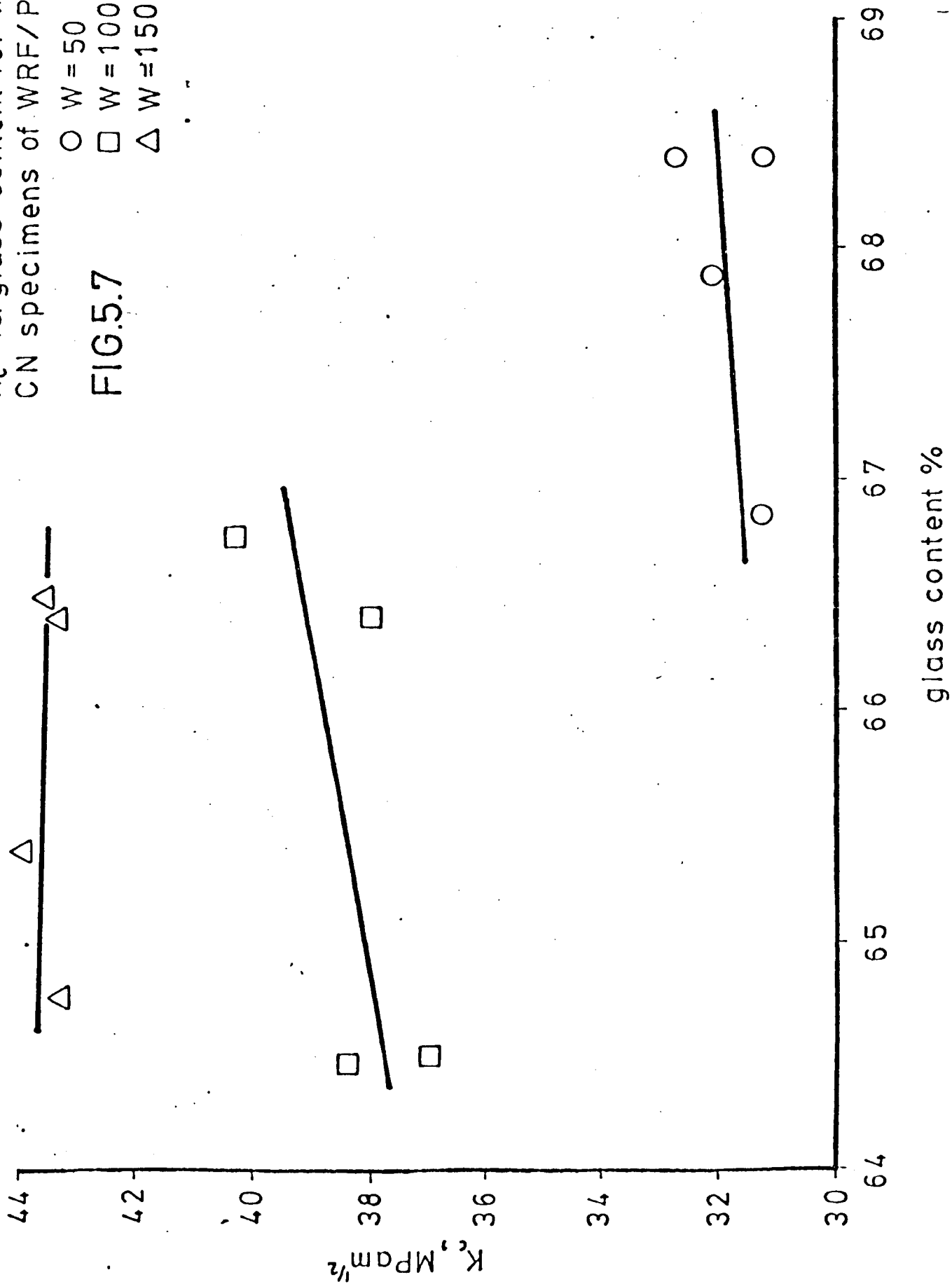
FIG.5.8

Comparison of K_c values for wet and dry CN specimens
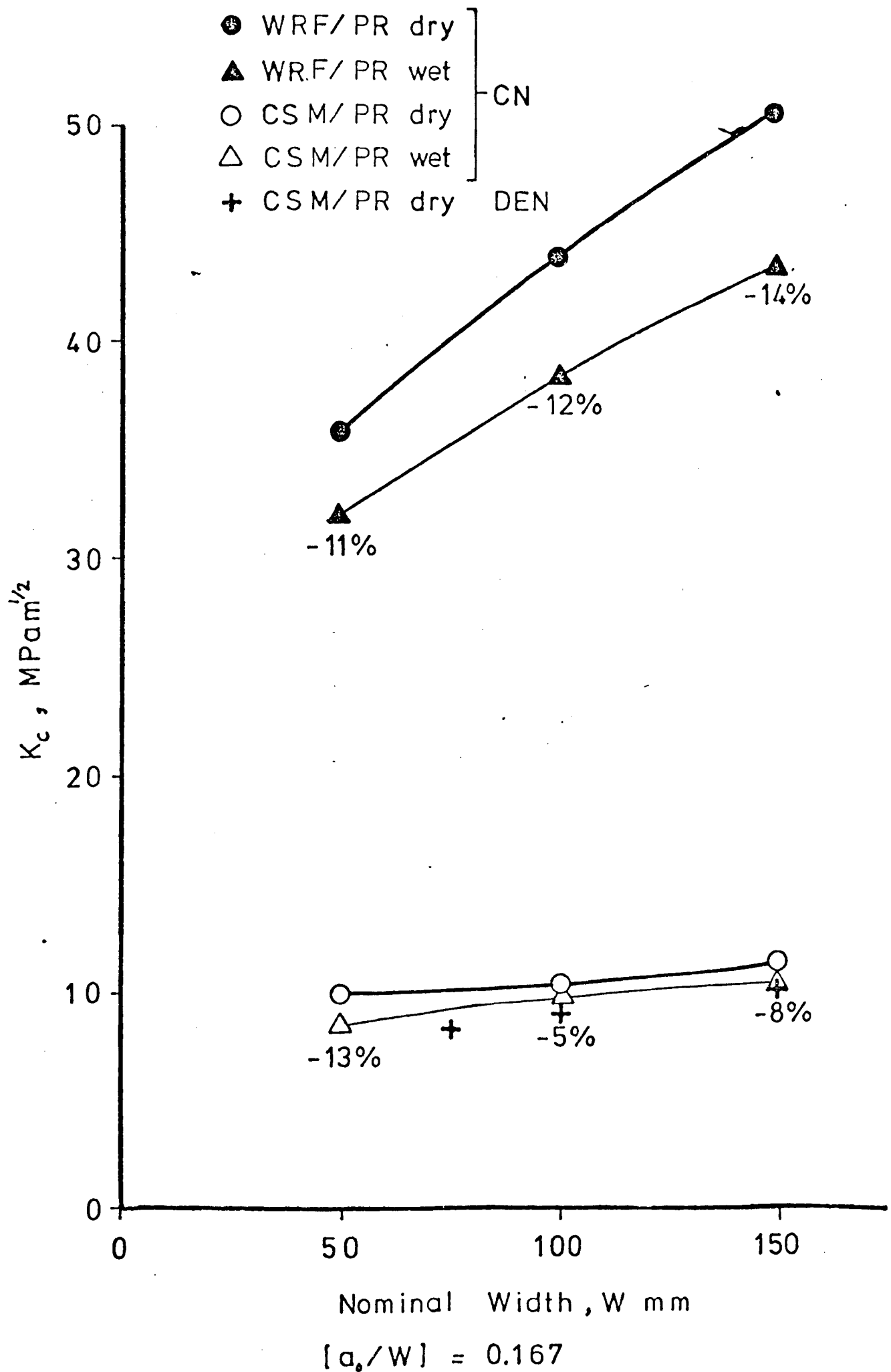
● WRF/PR dry
▲ WR.F/PR wet
○ CSM/PR dry   ⌉ CN
△ CSM/PR wet   ⌟
+ CSM/PR dry   DEN

K_c , $MPam^{1/2}$

-14%
-12%
-11%
-13%
-5%
-8%

Nominal Width , W mm

$[a_o/W] = 0.167$

FIG.5.9
Failure stresses and K_c vs.[a_o/W]
100mm wide CN specimens, CSM/PR

△ Gross Stress σ_{cG}
□ Net Stress σ_{cN}
● Stress Intensity Factor K_c

[a_o/W]

FIG.5.10

Dimensionless Stresses and Stress Intensity Factor vs. Half-crack length / Width Ratio 100mm. wide CN Specimens of CSM/ PR.

△ [σ_{ce}/σ_{uts}]

□ [q_{w}/σ_{n}]

● [$K_{c}/(\sigma_{nts}\sqrt{W})$]

$0.188 + 0.938[\frac{a}{W}] - 2.333[\frac{a}{W}]^2$
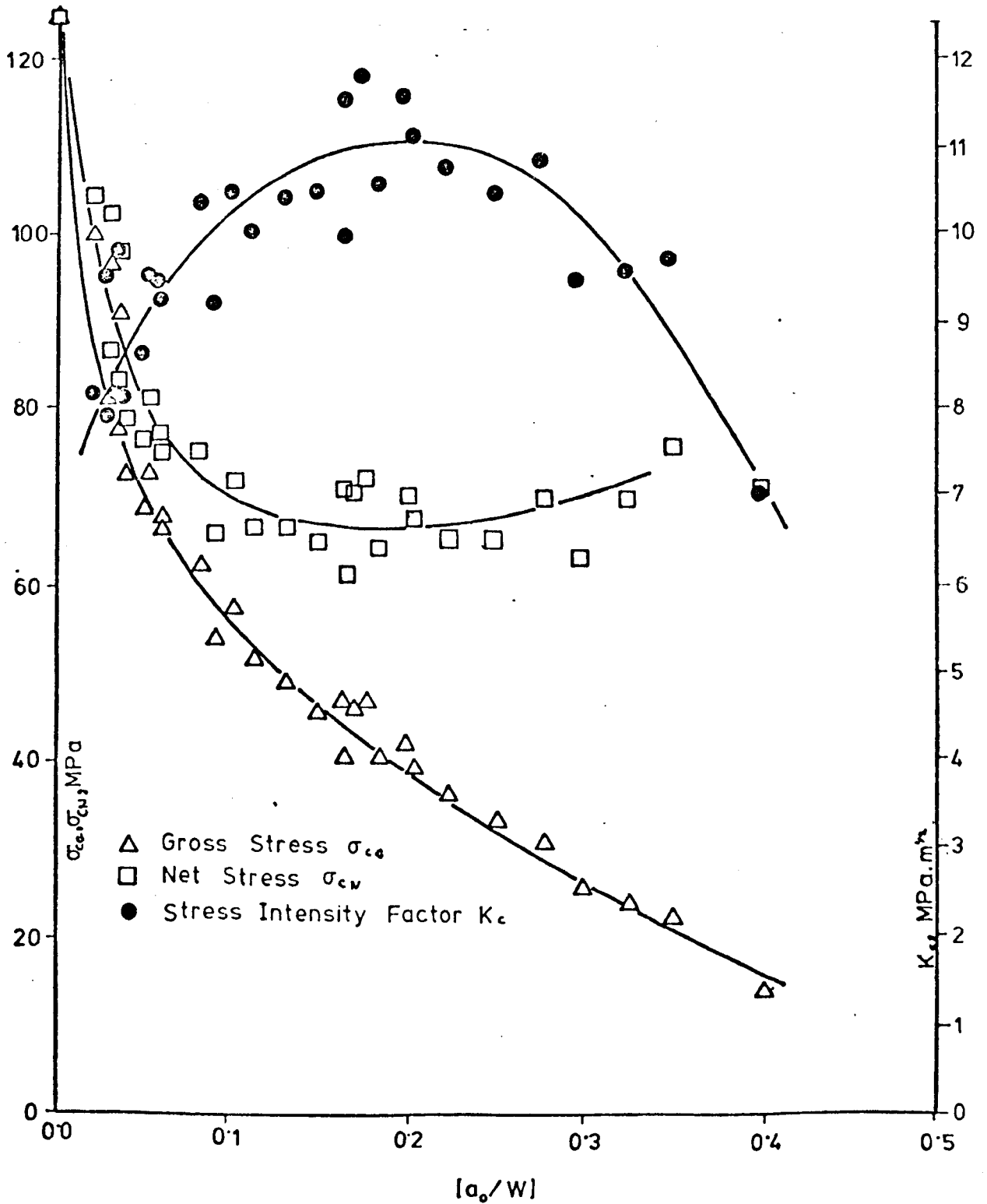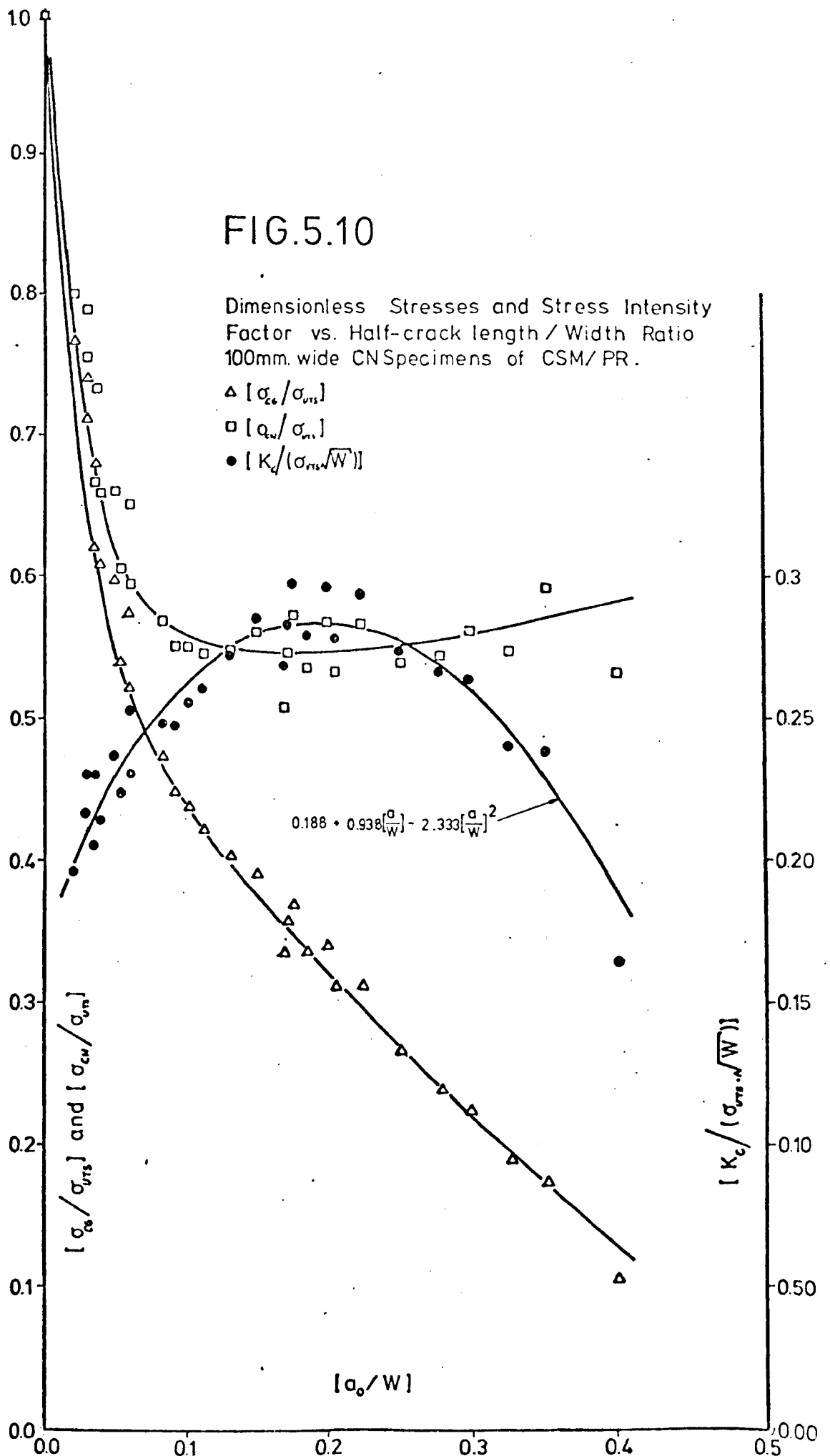
FIG.5.11

Failure stresses and K_c vs. $[a_o/W]$

100mm wide CN specimens of WRF/PR

- ● K_c
- △ σ_{cG}
- □ σ_{cN}
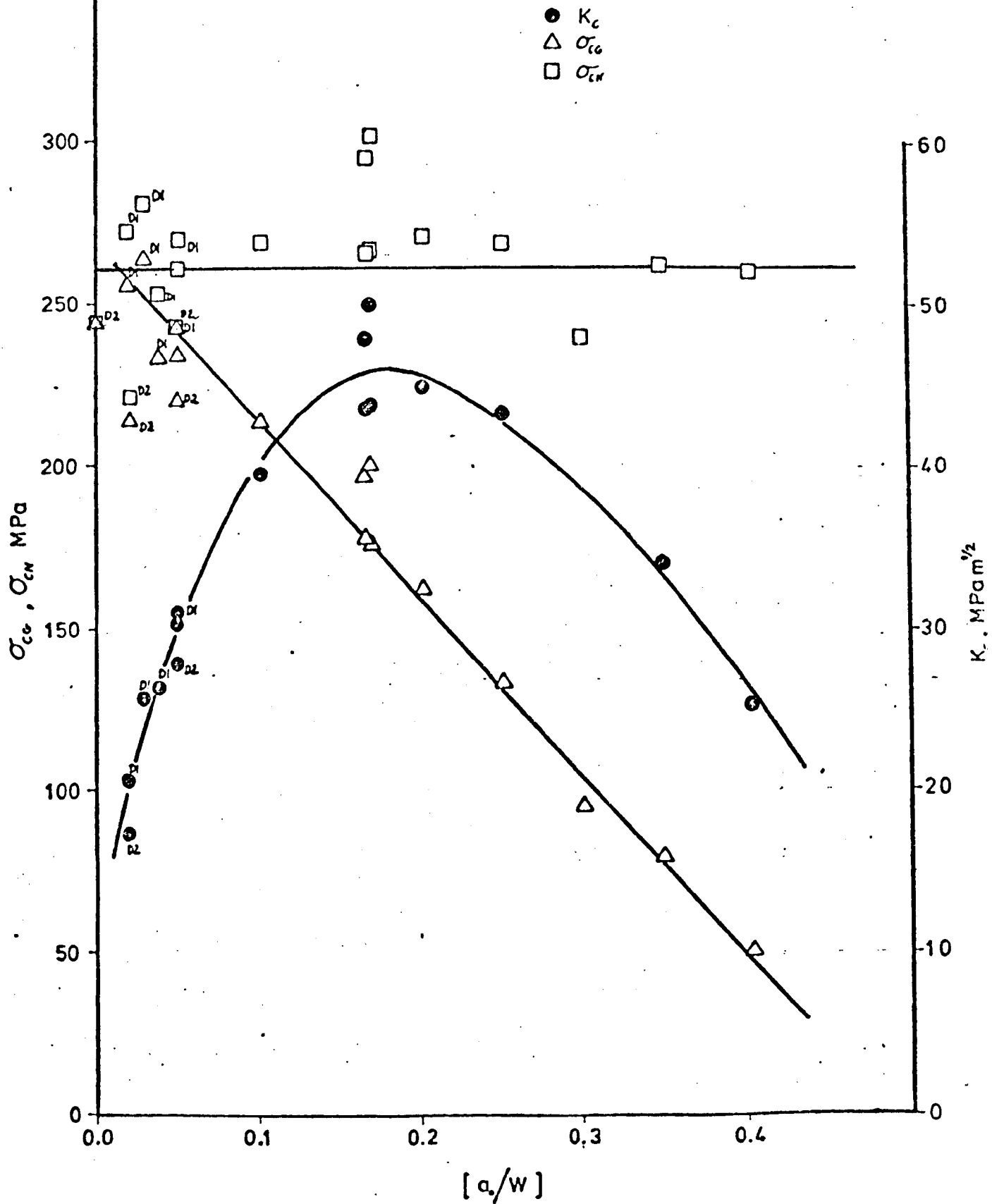
FIG.5.12

Dimensionless Stresses and Stress Intensity Factor vs. Half-crack length/ Width Ratio 100mm wide CN Specimens of WRF/PR
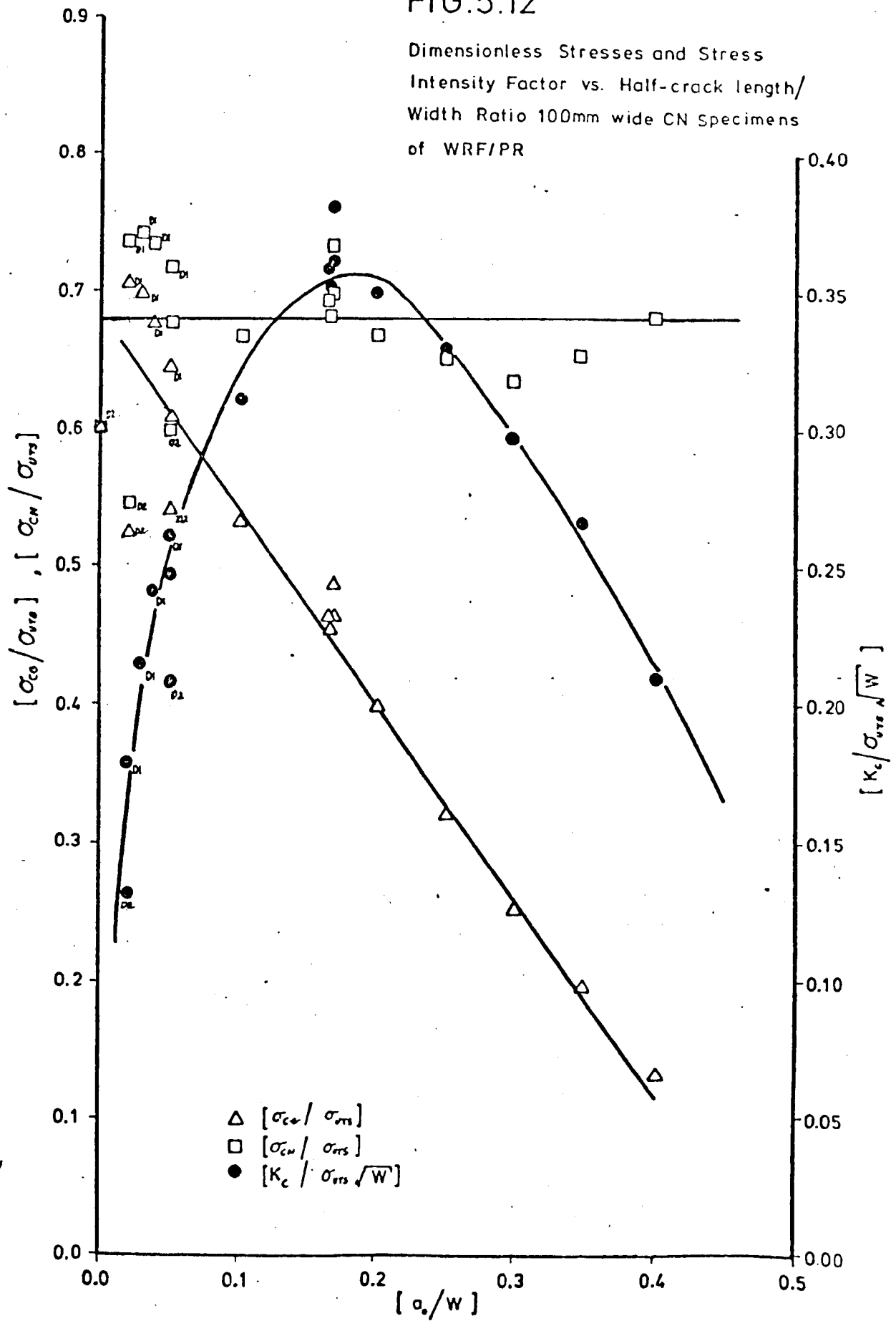
FIG.5.13

914mm wide CN specimens of CSM/PR
- ● K_c
- △ σ_{cc}
- □ σ_{cN}
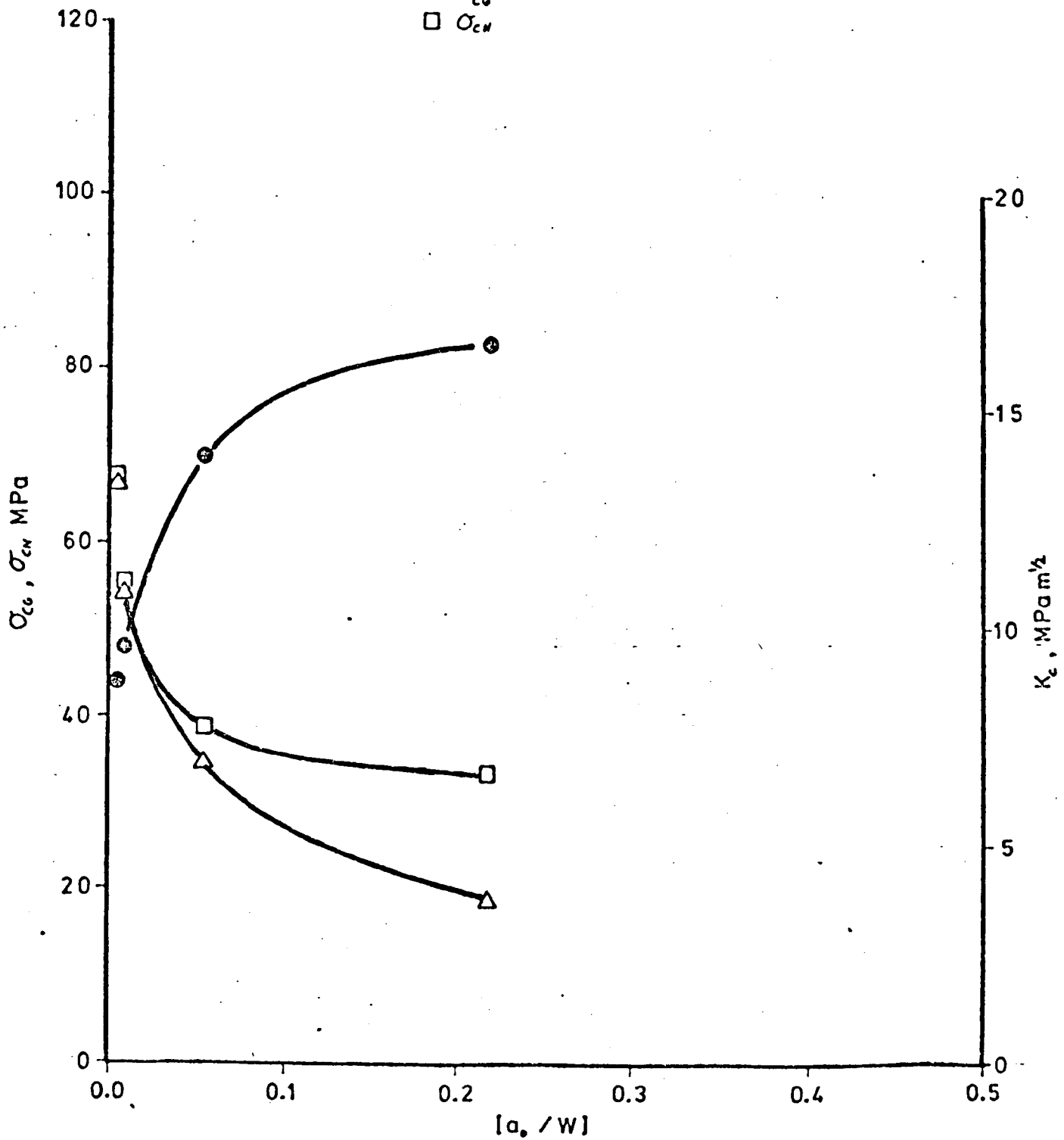
FIG.5.14

a. K_c vs. $\sqrt{W}$, notch sensitive materials

- ⬤ CSM/PR, CN specimens
- ☐ CSM/PR, Owen and Bishop (8), DEN specimens
- ▽ Y449/PR, Holdsworth (24), CN specimens
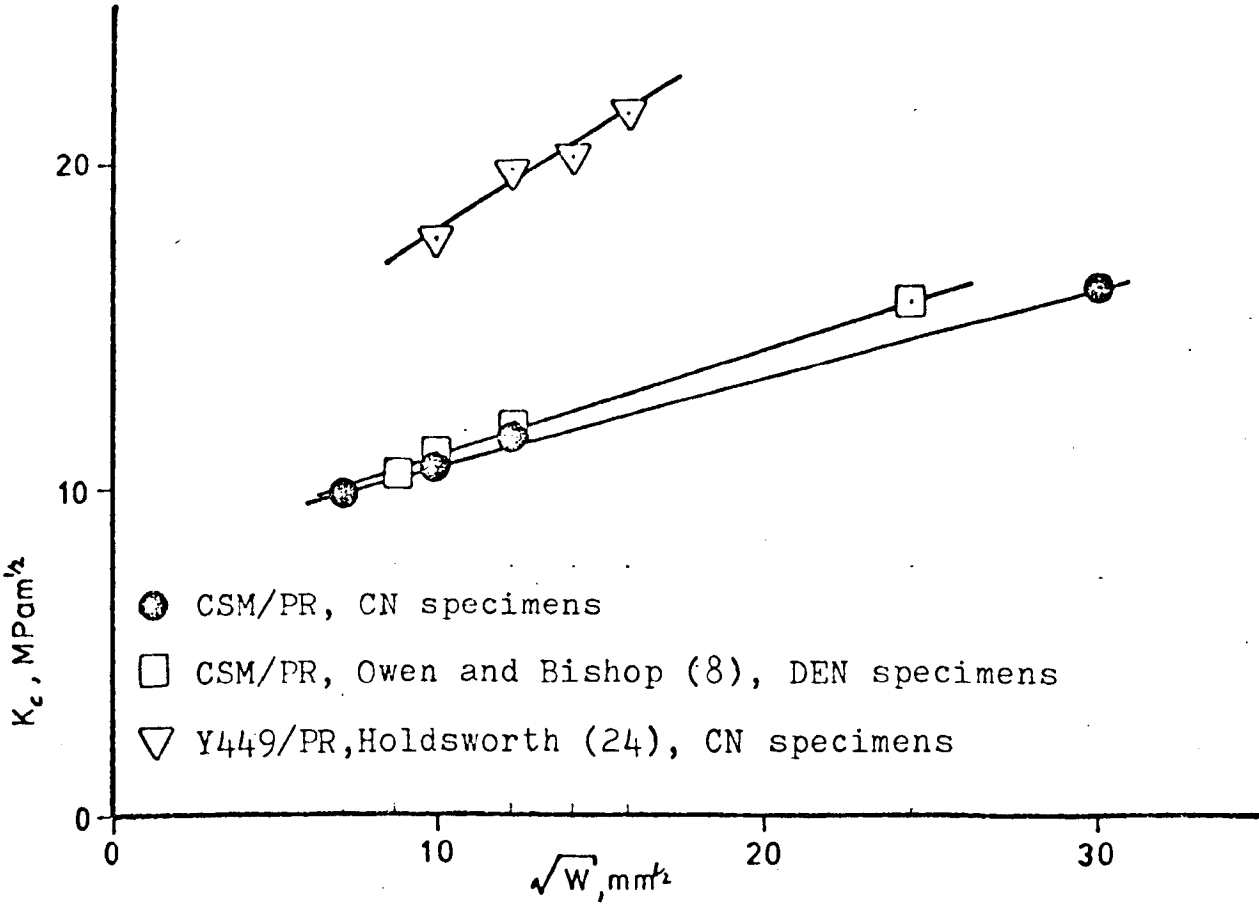
b. K_c vs. W, WRF/PR

FIG.6.1 Measurement of specimen compliance

Upper Grip

Mounting Bar

CN Specimen

Piston

Tooth

Tooth Retaining Bolt

Upper Probe (Fixed to Piston)

Crack

Lower Probe (Fixed to Body)

Transducer Mounting Body (Free to slide along Mounting Bar)

Clamping Screw

LVDT Transducer

Lower Grip
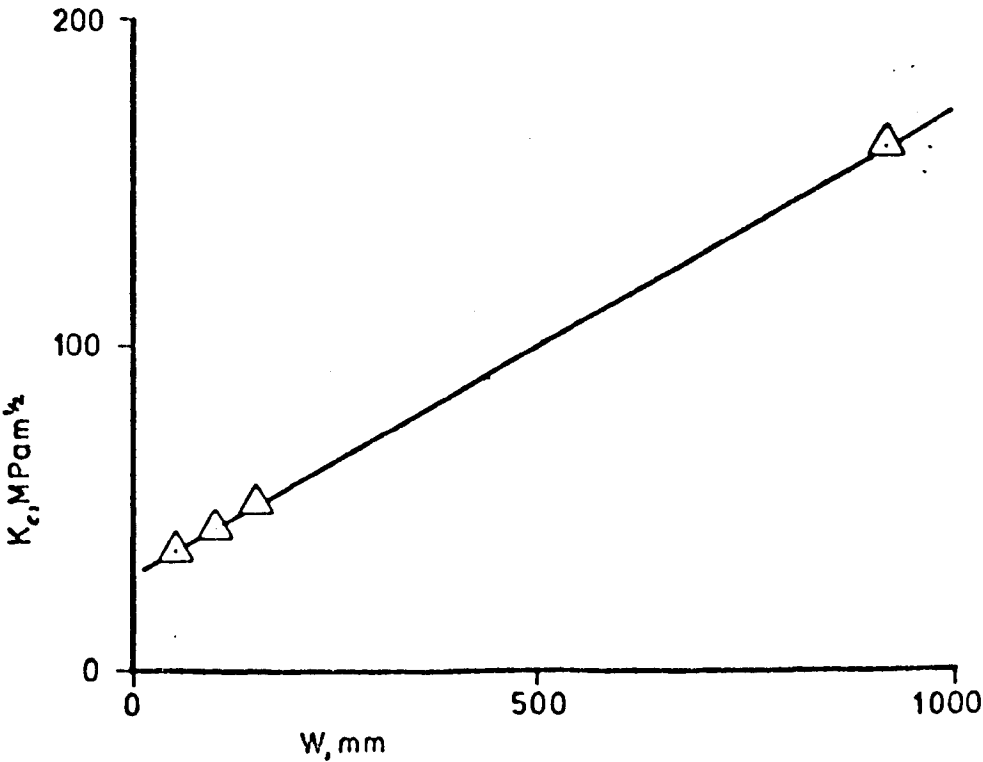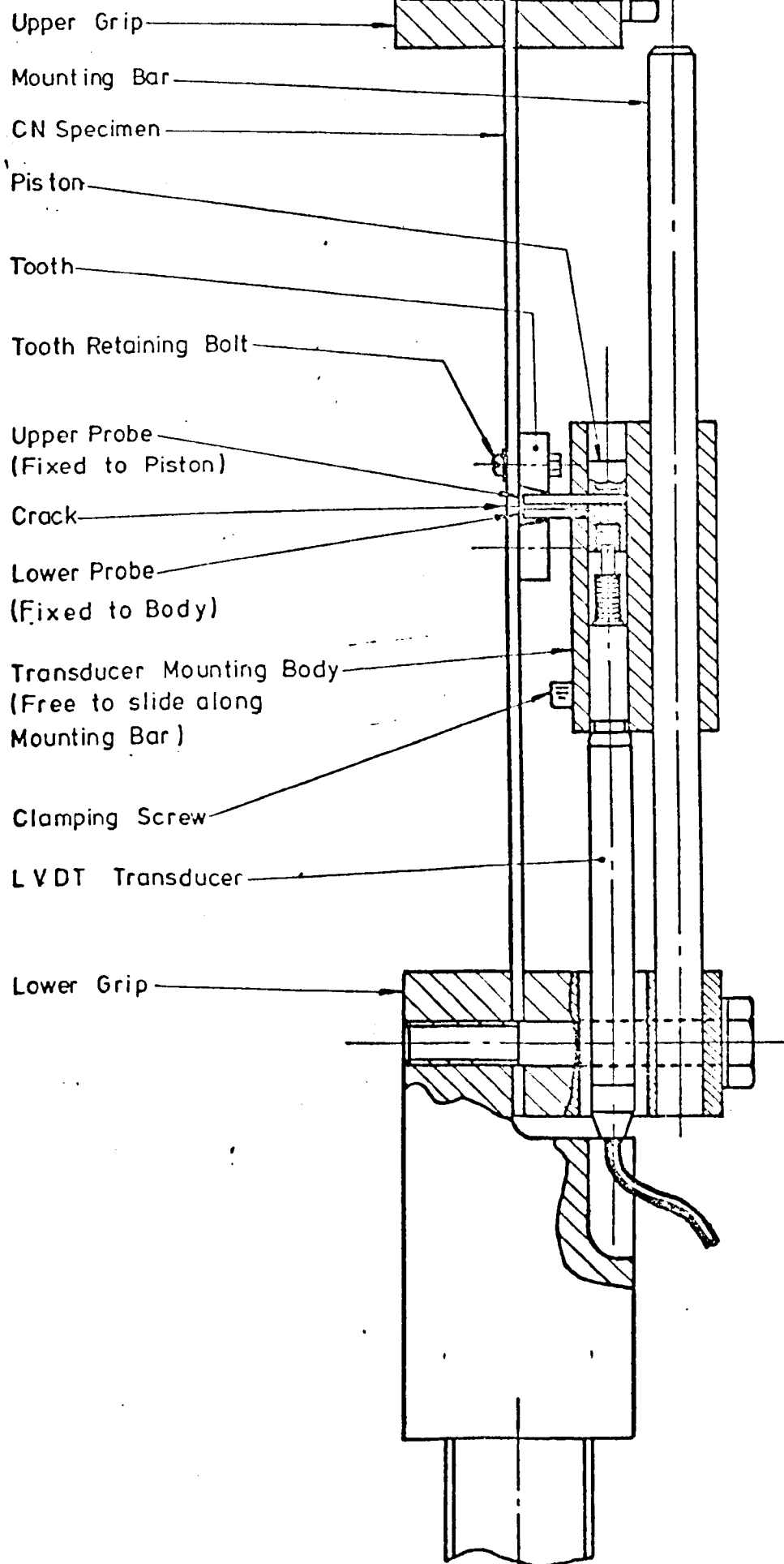
FIG. 6.2 Fatigue crack propagation in 100mm wide CN specimens of dry CSM/PR

Symbol	Glass Content %	ΔK	ΔK_b
●	39.48	7.75	0.174
□	34.93	7.50	0.190
▷	34.95	8.25	0.209
◀	34.92	9.00	0.228
○	32.09	8.00	0.221
▣	37.15	9.50	0.227
◁	31.21	8.50	0.241

— — — Paris law

———— Forman law

2373000 cycles →

Kilocycles

[C/W]

0.15 0.20 0.25 0.30 0.35 0.40

0 50 100 150 200 250 300 350 400

FIG.6.3 da_D/dN vs. $\triangle K_D$, dry CSM/PR

FIG.6.5
Fatigue crack propagation in 100mm wide
CN specimens of wet CSM/PR

Symbol	$\triangle$K.MPam$^{\frac{1}{2}}$
O	5.00
□	6.50
△	8.25

Kilocycles
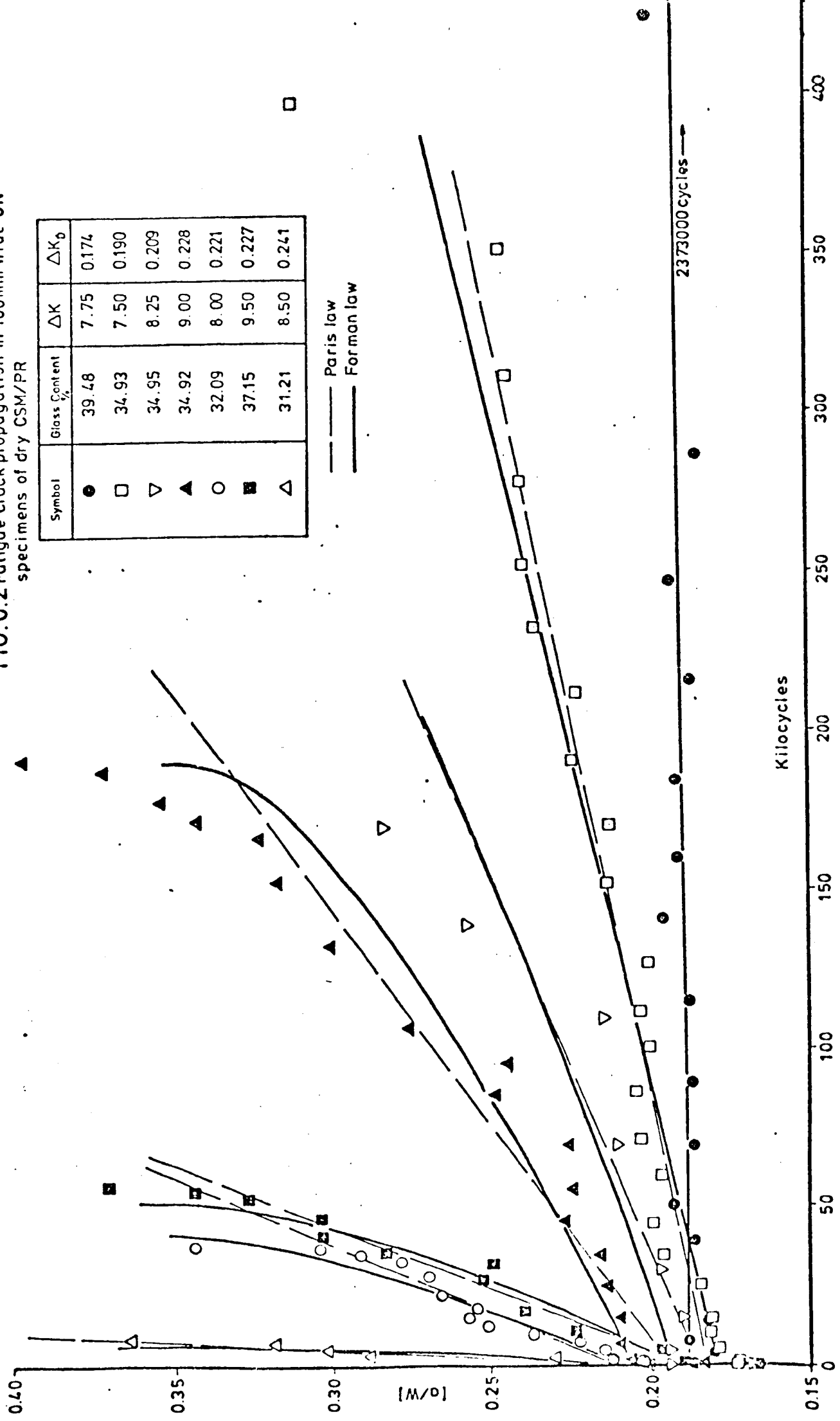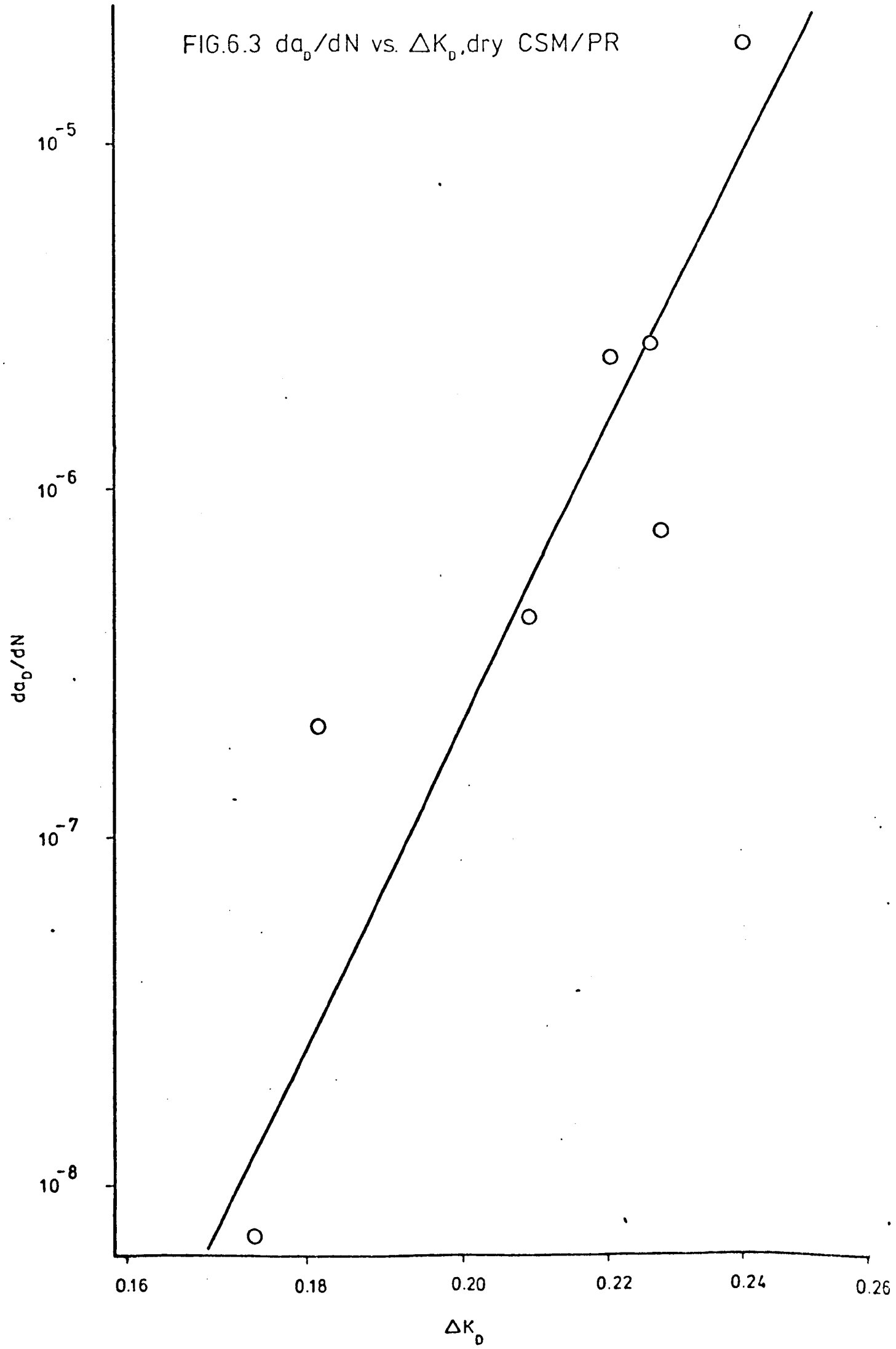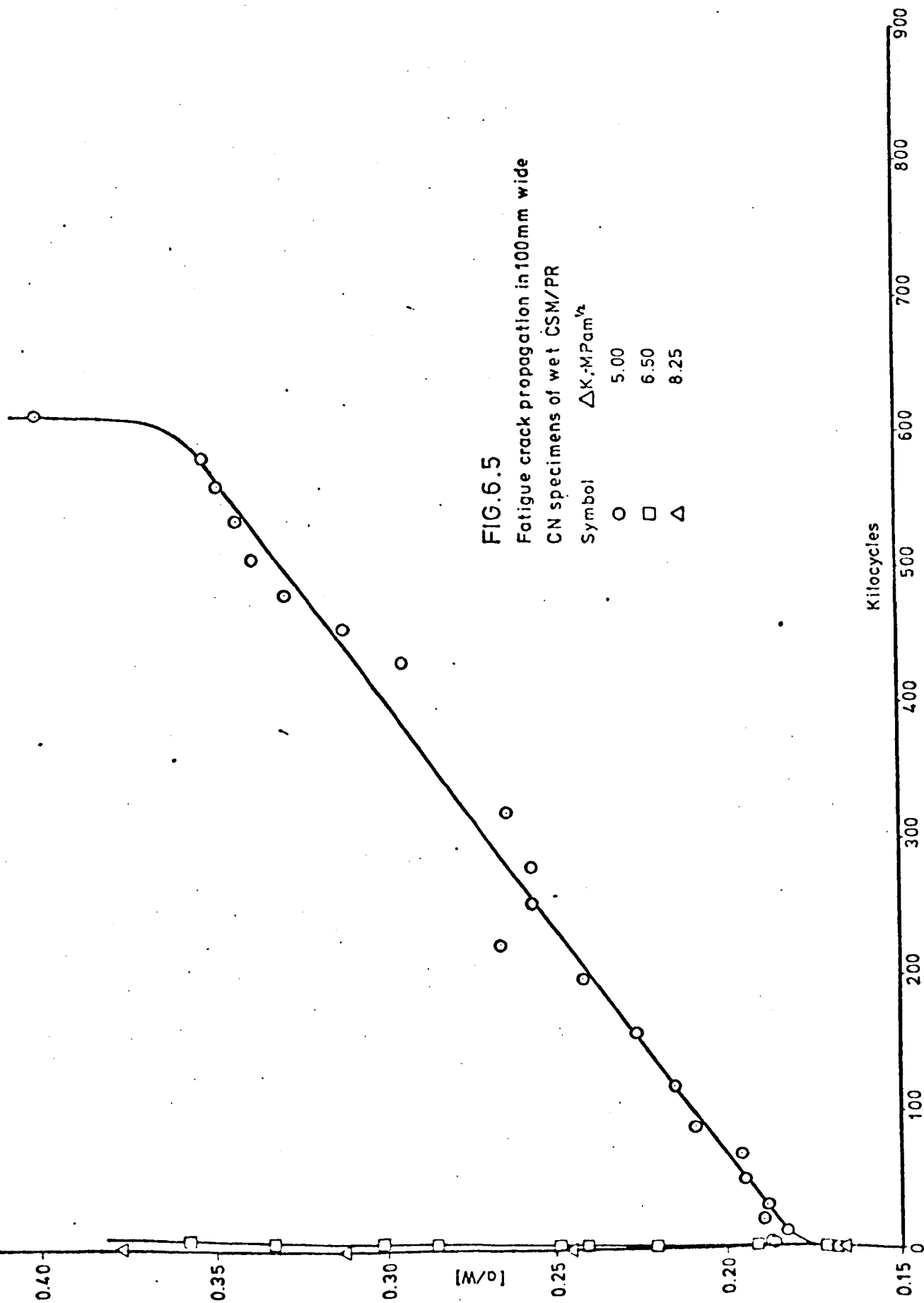
FIG.6.6 da_D/dN vs. $\triangle K_D$, wet CSM/PR
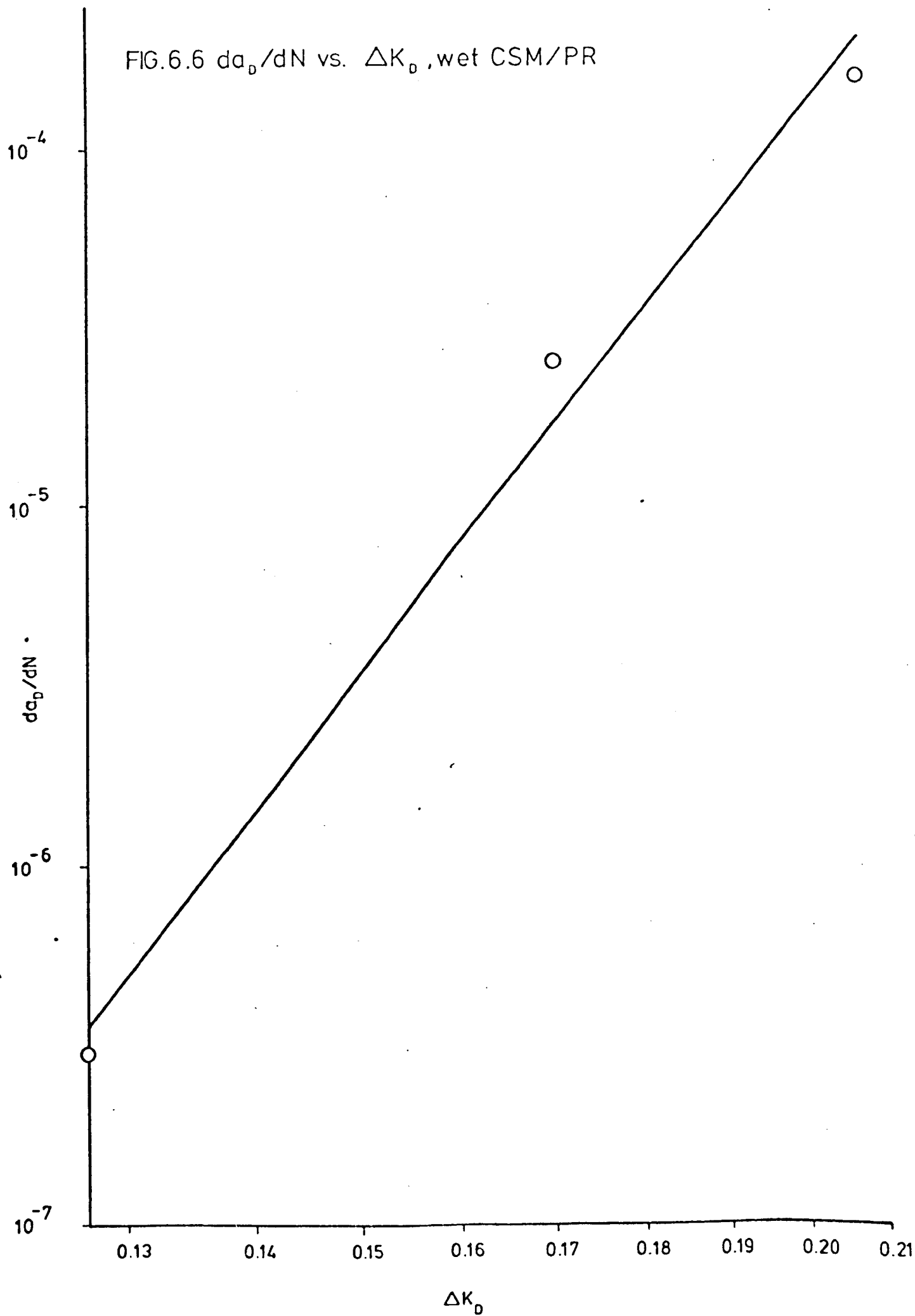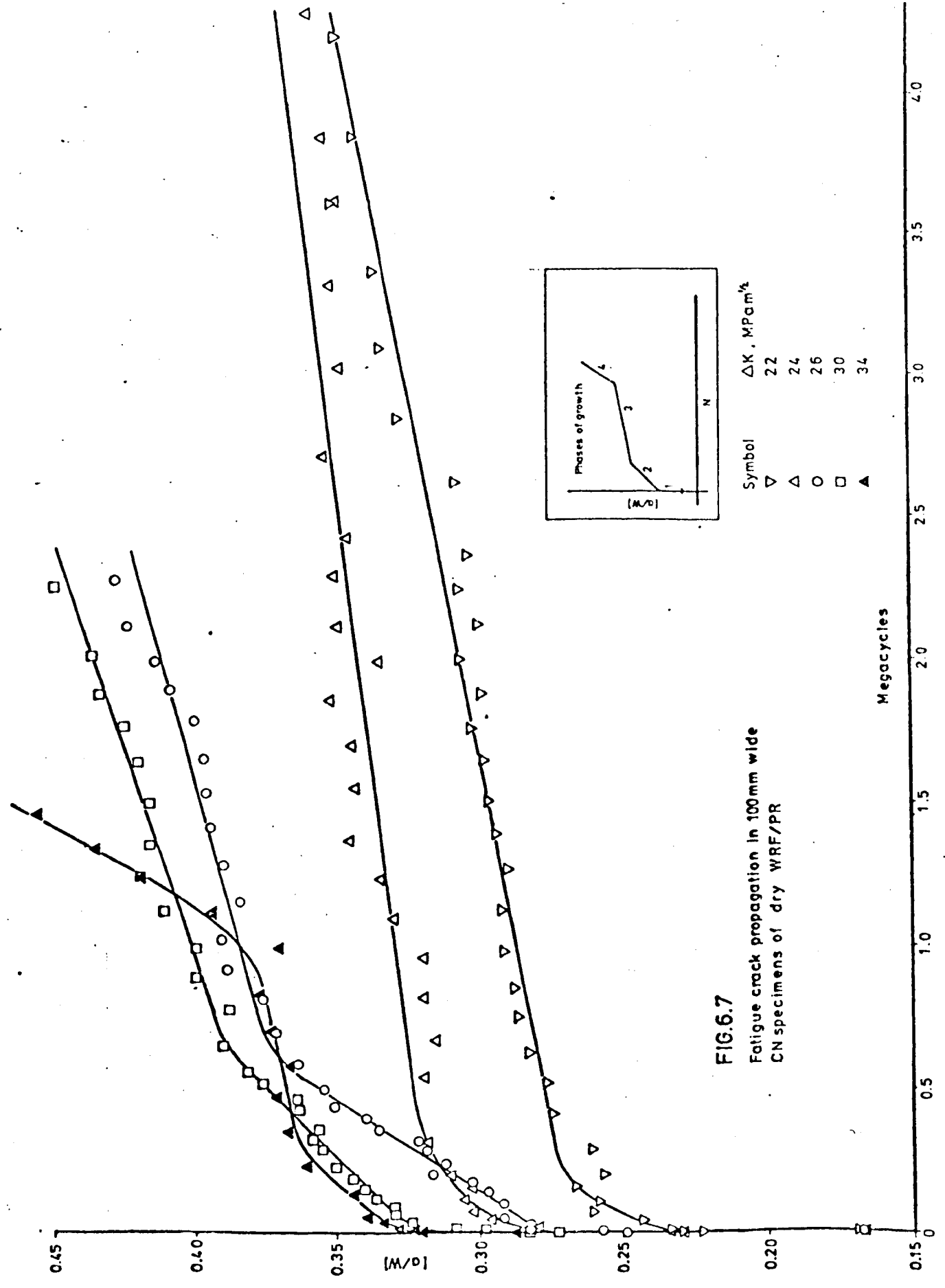
FIG.6.7

Fatigue crack propagation in 100mm wide
CN specimens of dry WRF/PR

Phase 2

vertical crack

rovings

initial crack

Phase 3

Final phase 4
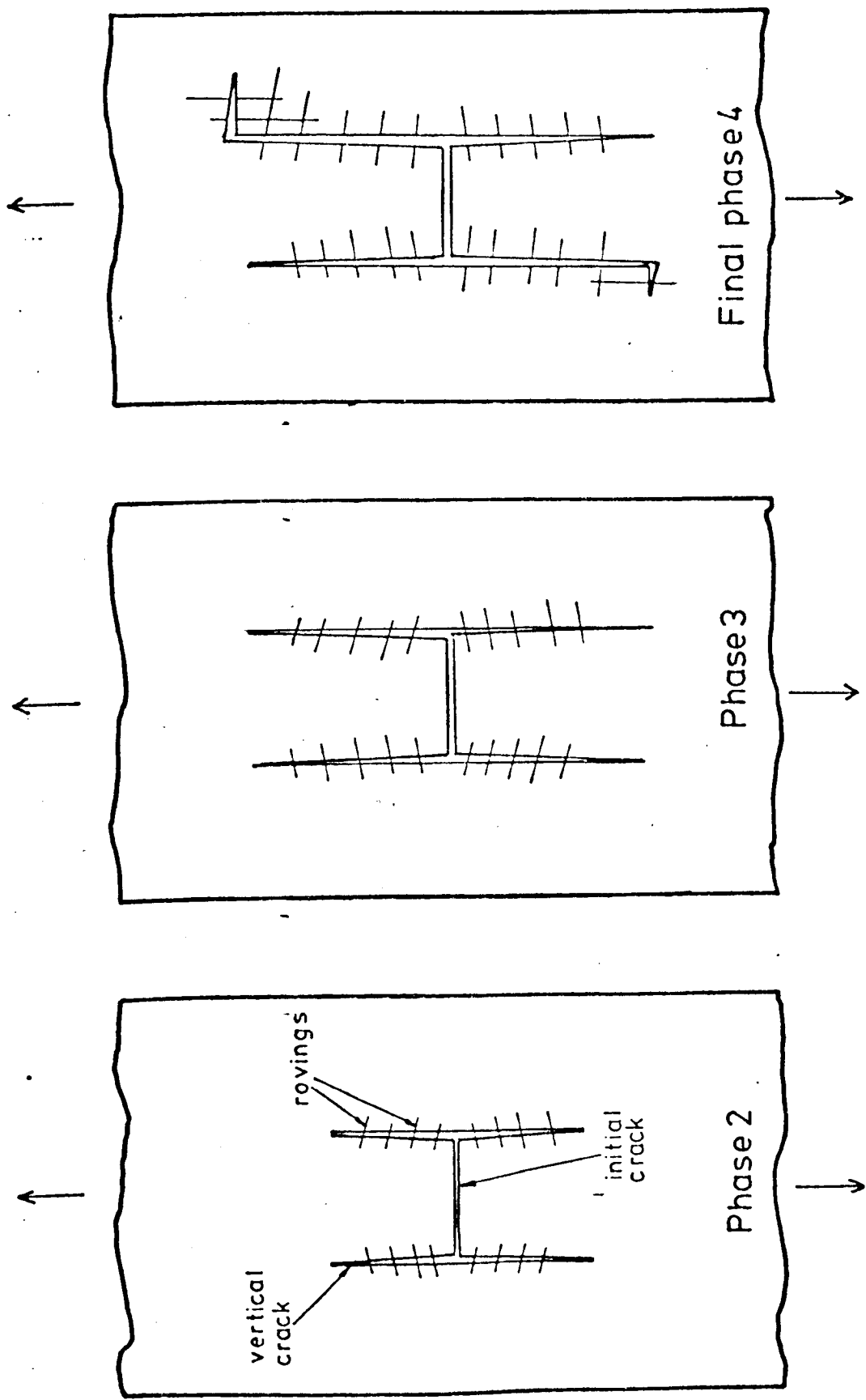
FIG.6.8 Stages of failure in a dry WRF/PR fatigue crack propagation specimen

FIG.6.9 [a/W] vs. cycles, 915mm wide CN specimen, WRF/PR
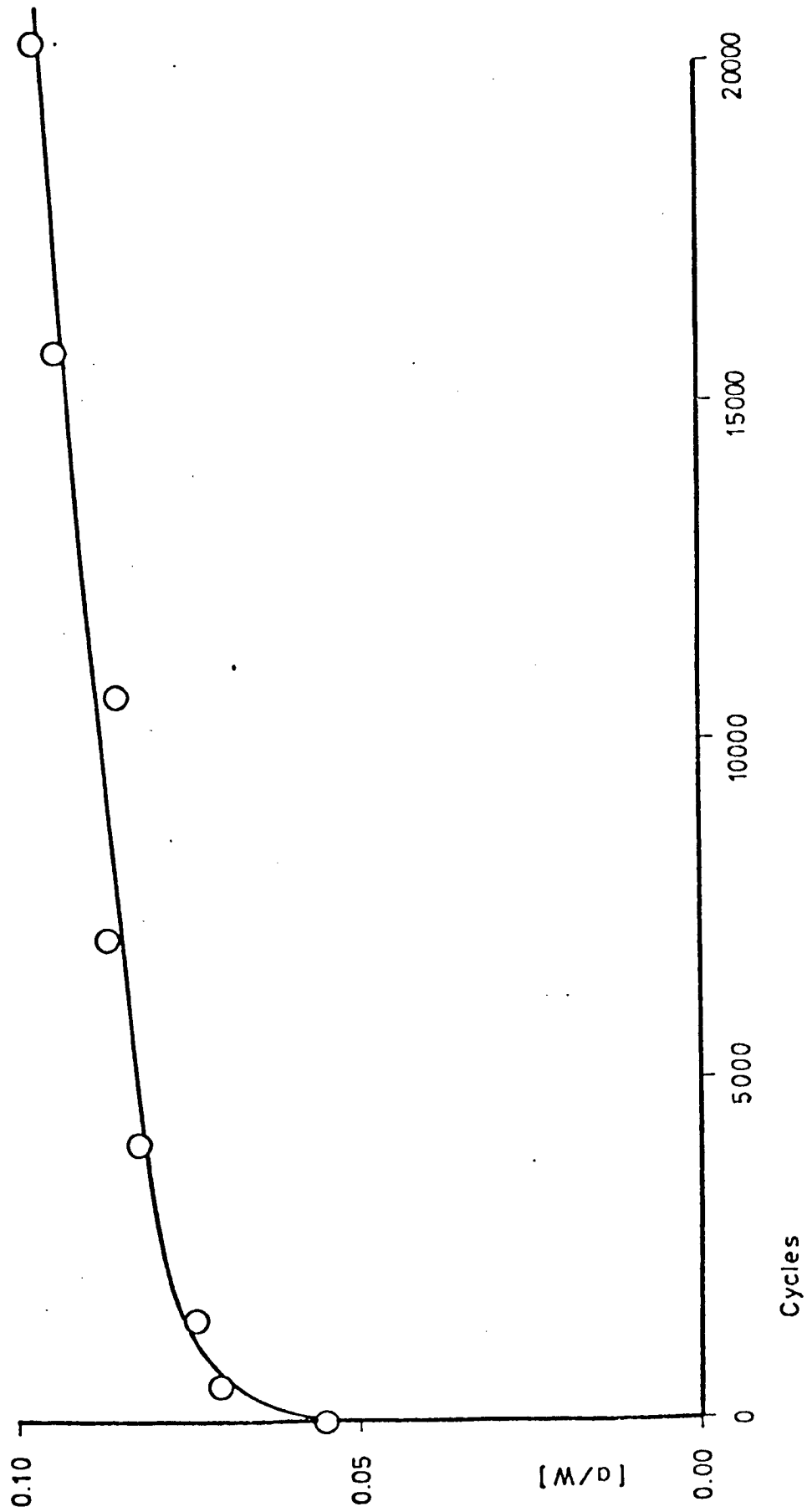
FIG.6.10 Fatigue crack propagation in 100mm wide
CN specimens of wet WRF/PR

Symbol	$\triangle K.MPam^{1/2}$
□	14
○	18
●	22

Kilocycles

[a/W]
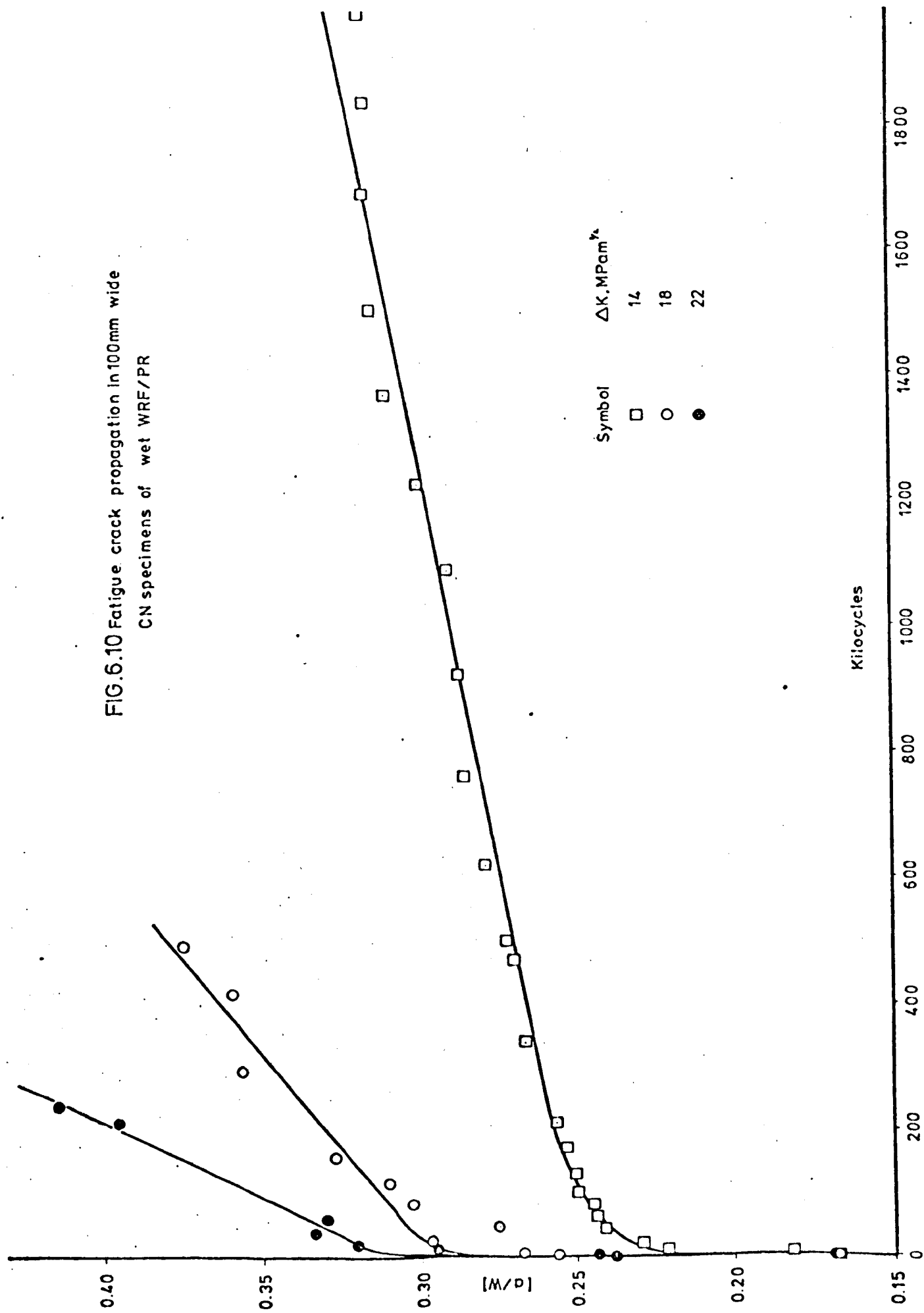
FIG.6.11 da_D/dN vs. $\triangle K_D$, wet WRF/PR
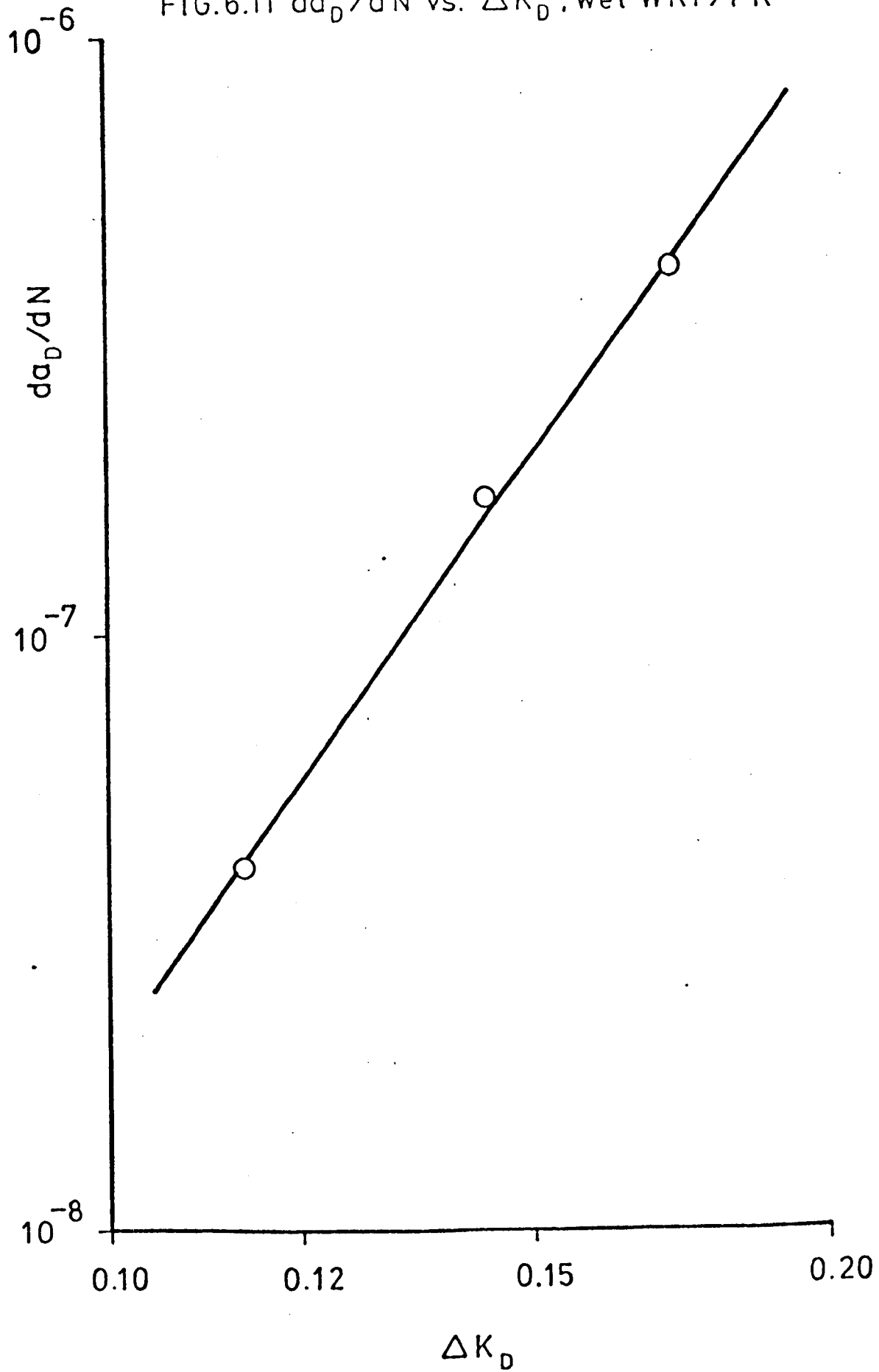
VOLUME CONTAINS CLEAR OVERLAYS

OVERLAYS HAVE
BEEN SCANNED
SEPERATELY
AND
THEN AGAIN OVER
THE RELEVANT PAGE

1) CSM/PR dry

2) WRF/PR dry

3) CSM/PR wet

4) WRF/PR wet

PLATE 1.

1) CSM/PR dry

2) WRF/PR dry

3) CSM/PR wet
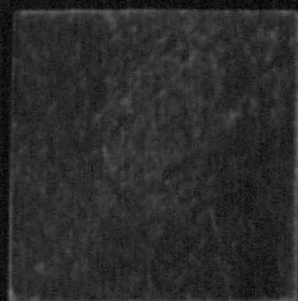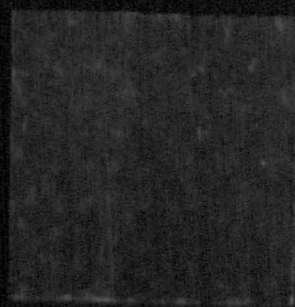
4) WRF/PR wet

1   2
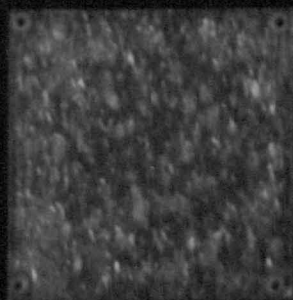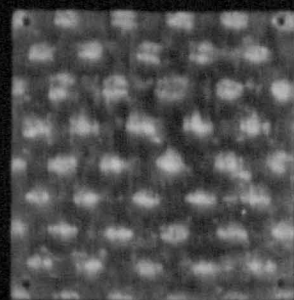
3   4
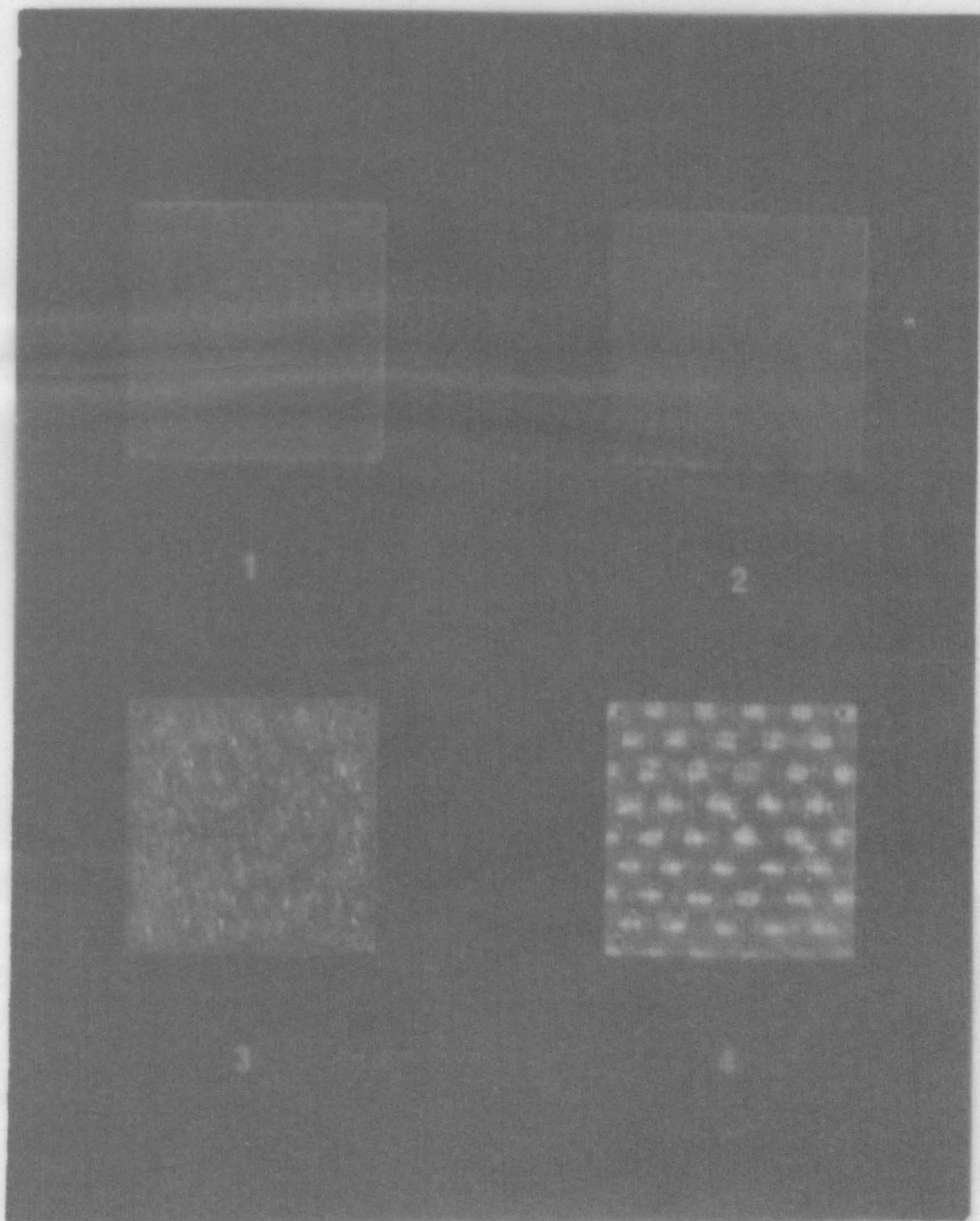
PLATE 1.

1) CSM/PR dry   2) WRF/PR dry

3) CSM/PR wet   4) WRF/PR wet

PLATE 2. 1000kN testing installation
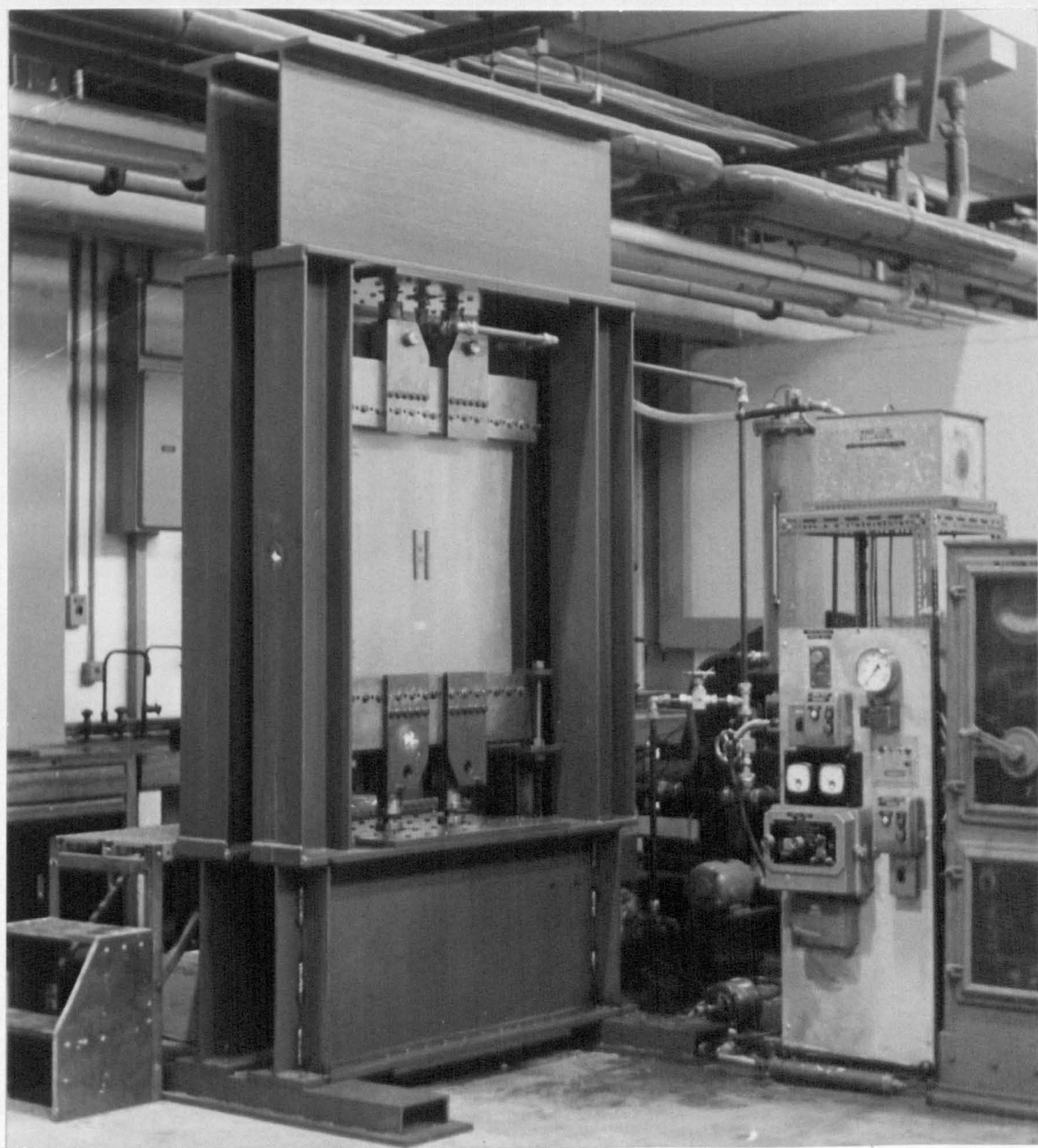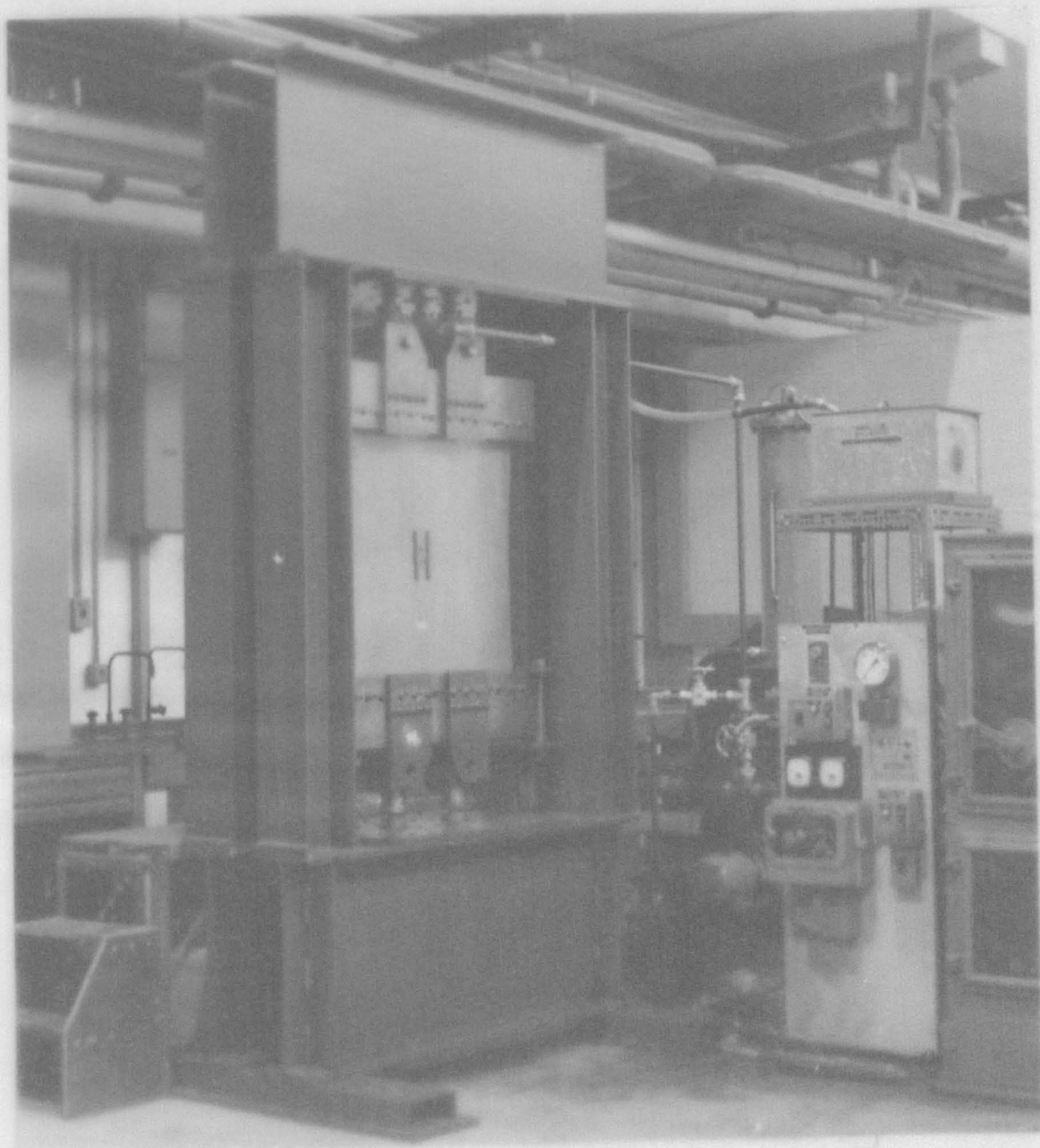
PLATE 2.   1000kN testing installation

3   6   9

PLATE 3.   50mm wide CN specimens of CSM/PR, thickness 3,6, and 9 plies

3   6   9

PLATE 4.   50mm wide CN specimens of WRF/PR, thickness 3,6, and 9 plies
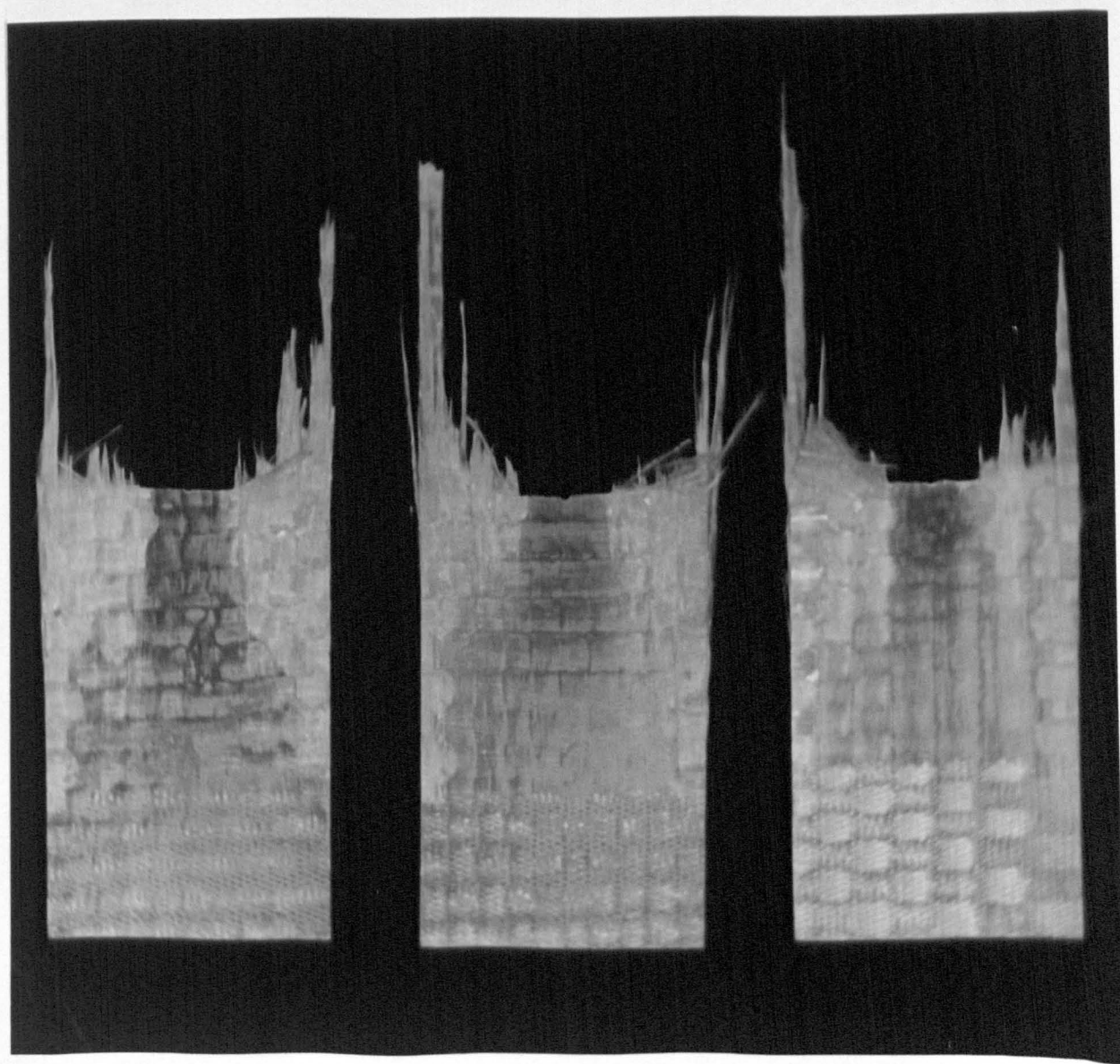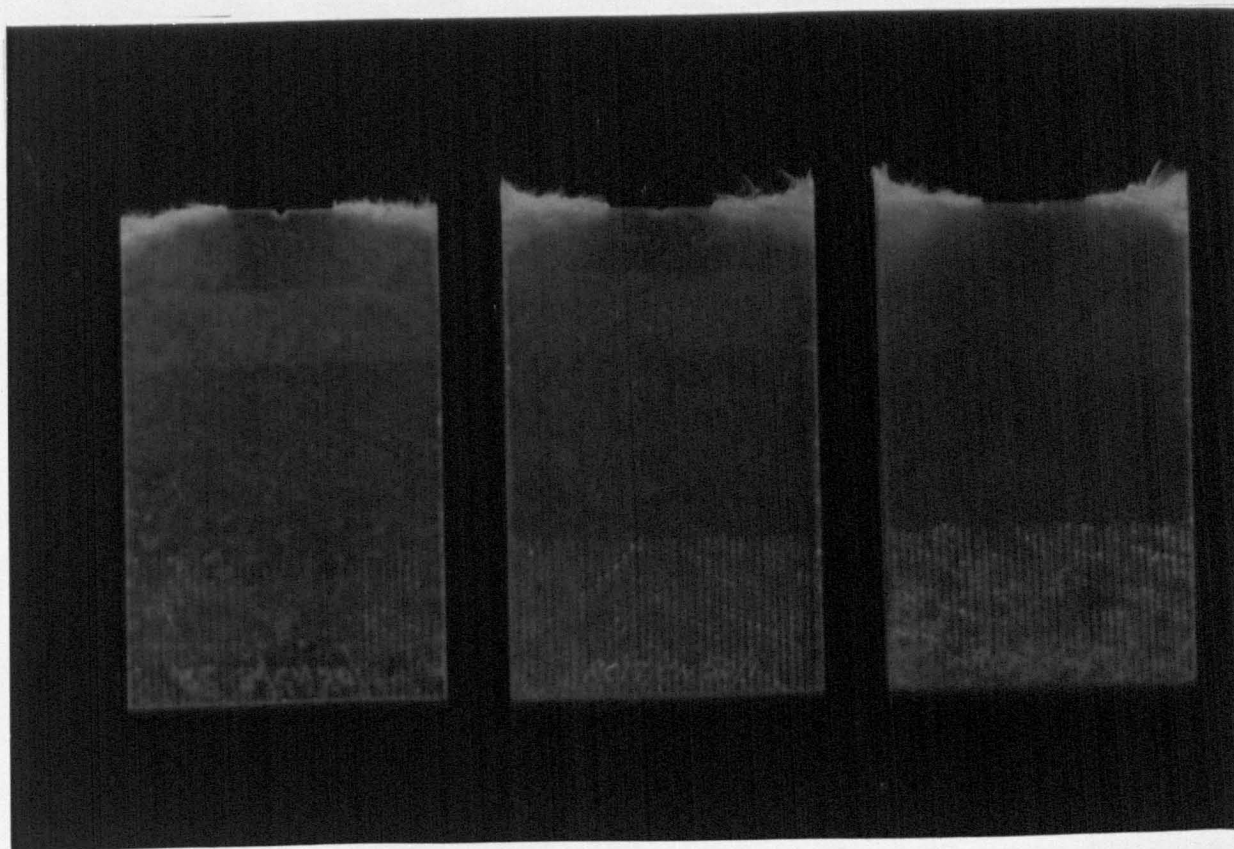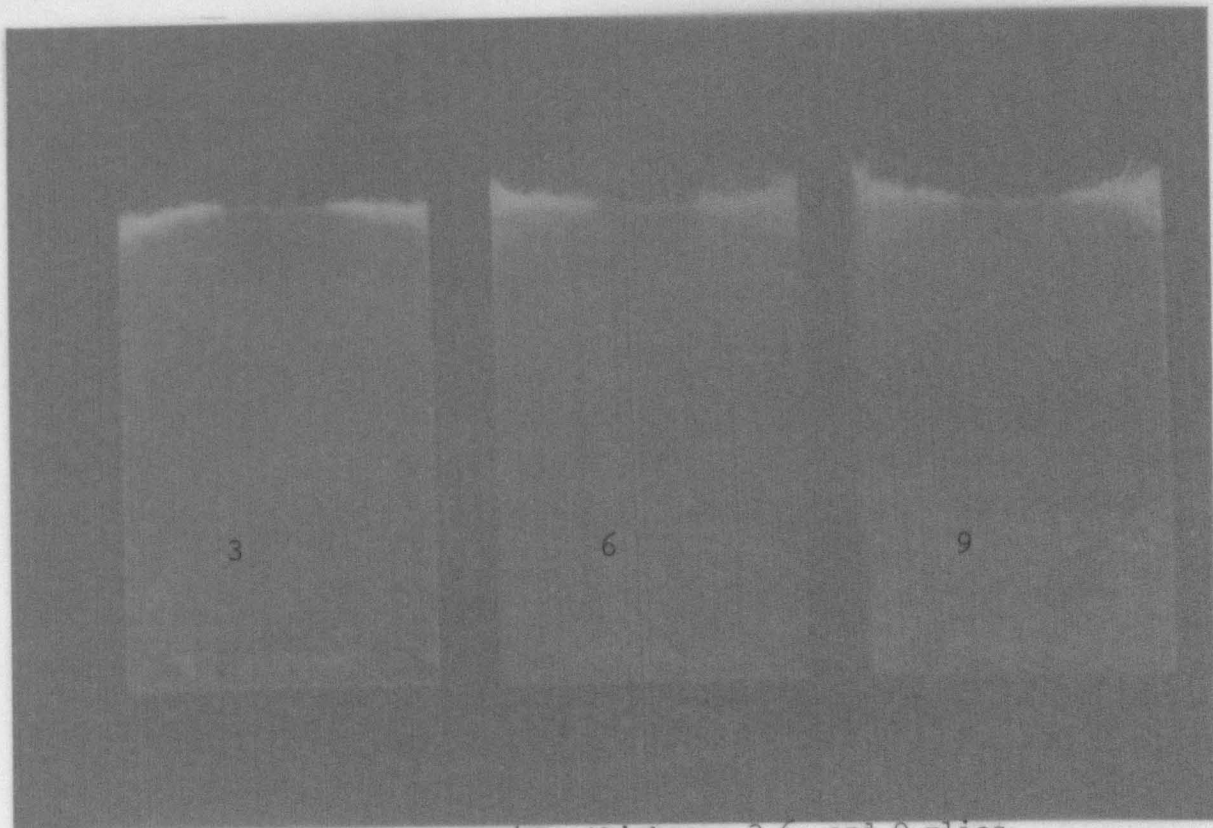
PLATE 3.   50mm wide CN specimens of CSM/PR, thickness 3,6, and 9 plies
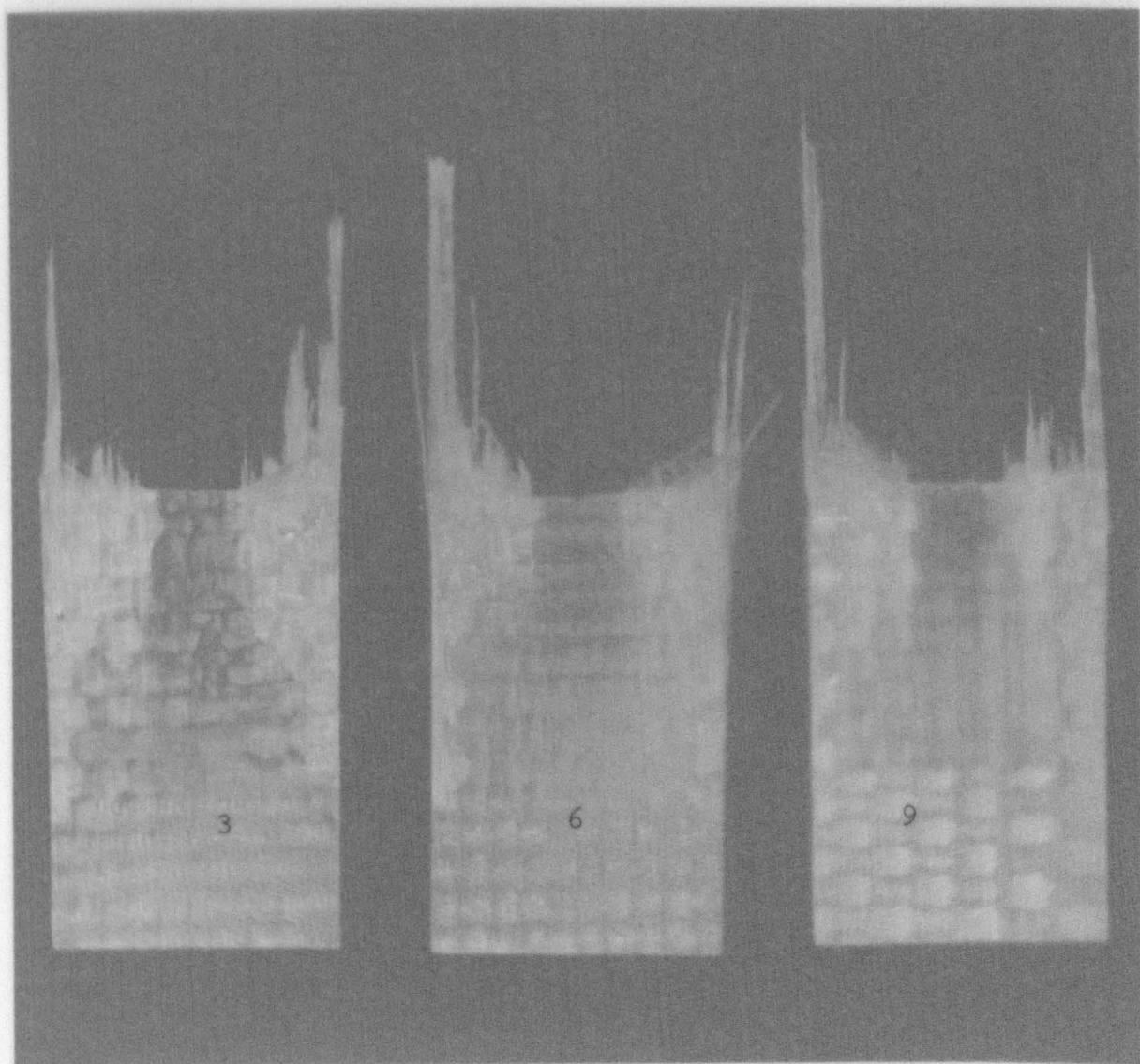
PLATE 4.   50mm wide CN specimens of WRF/PR, thickness 3,6, and 9 plies

PLATE 5. 150 mm wide CN specimens of CSM/PR and WRF/PR, 3 plies
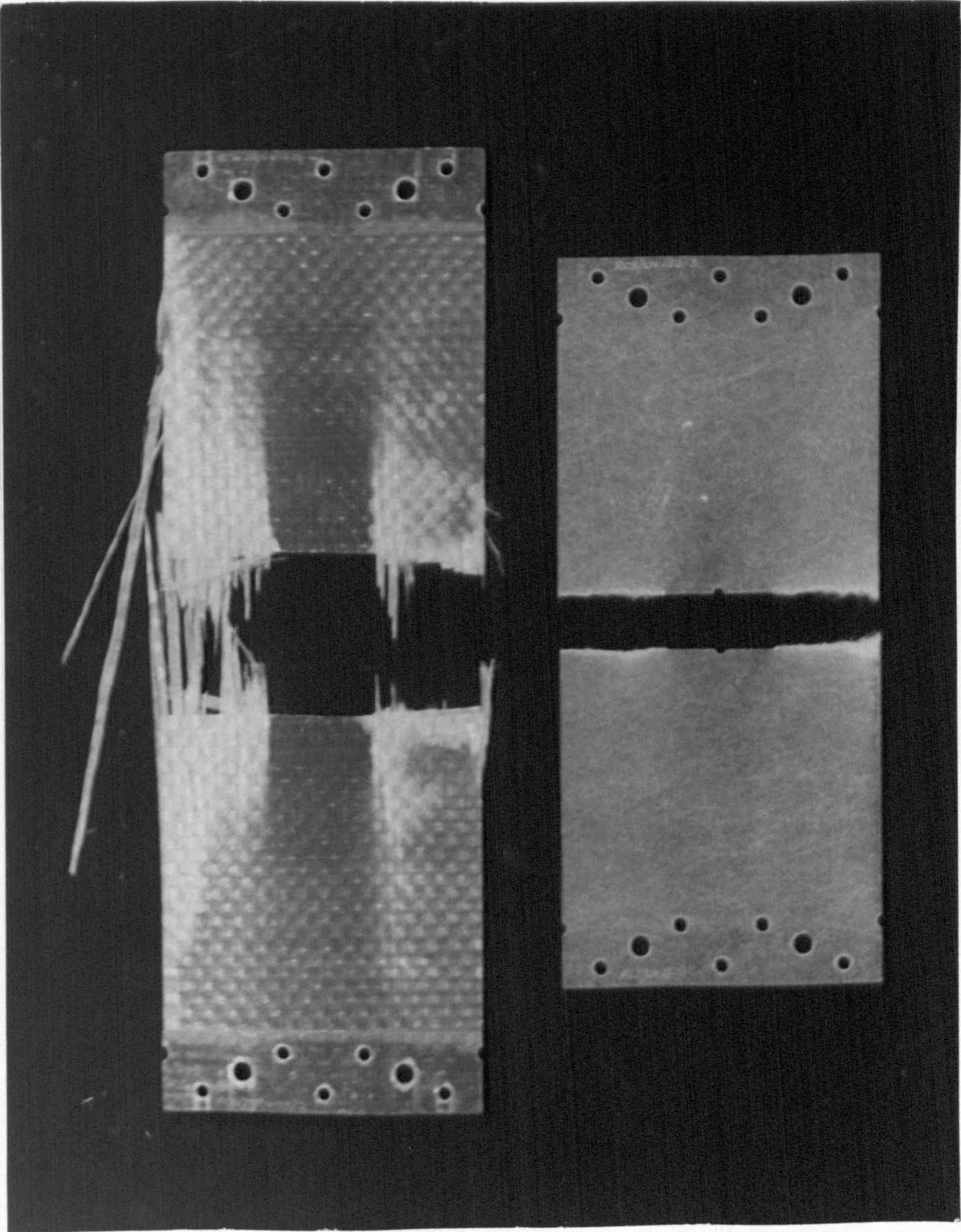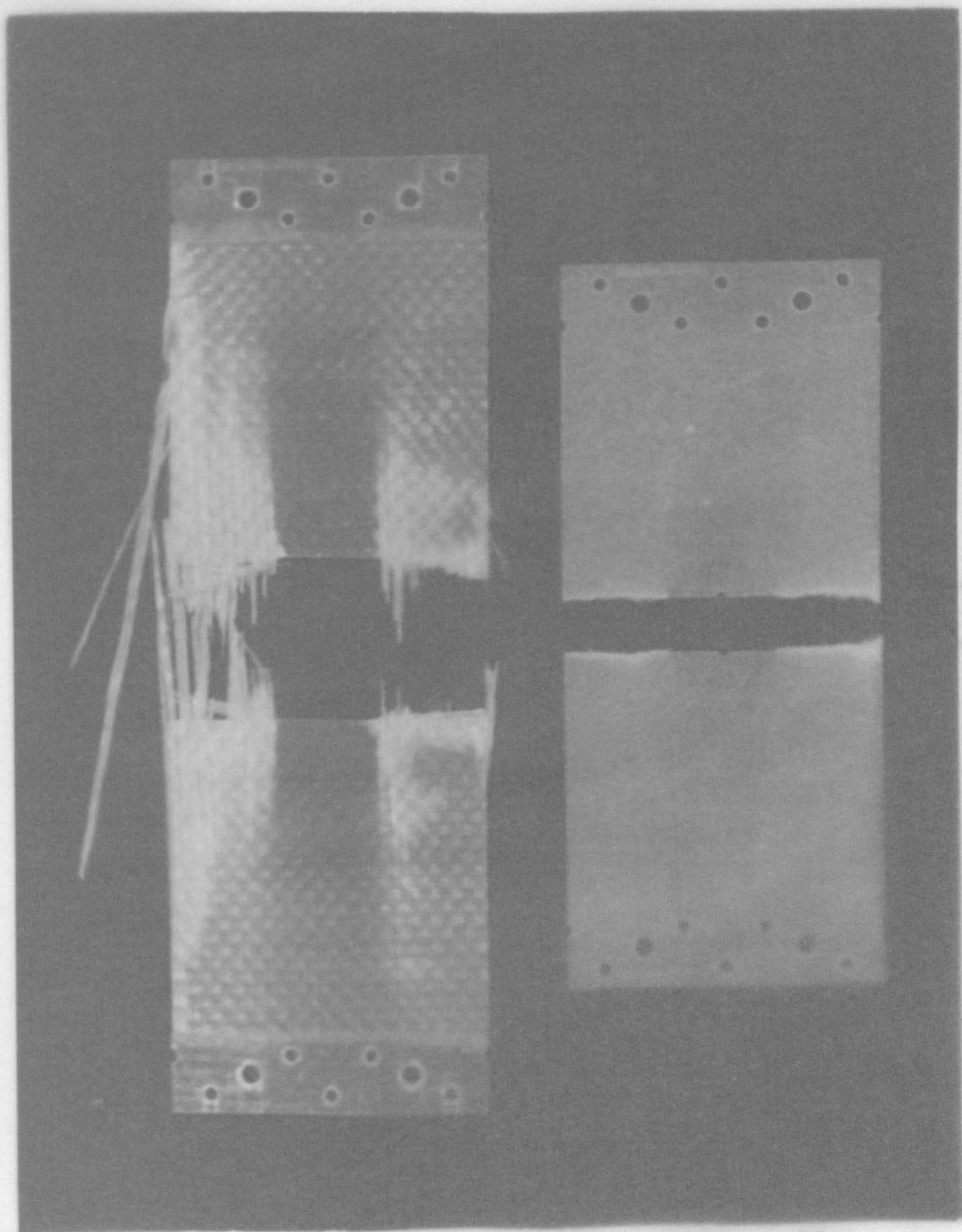
PLATE 5. 150 mm wide CN specimens of CSM/PR and WRF/PR, 3 plies

PLATE 6a.

PLATE 6b.

PLATE 6c.
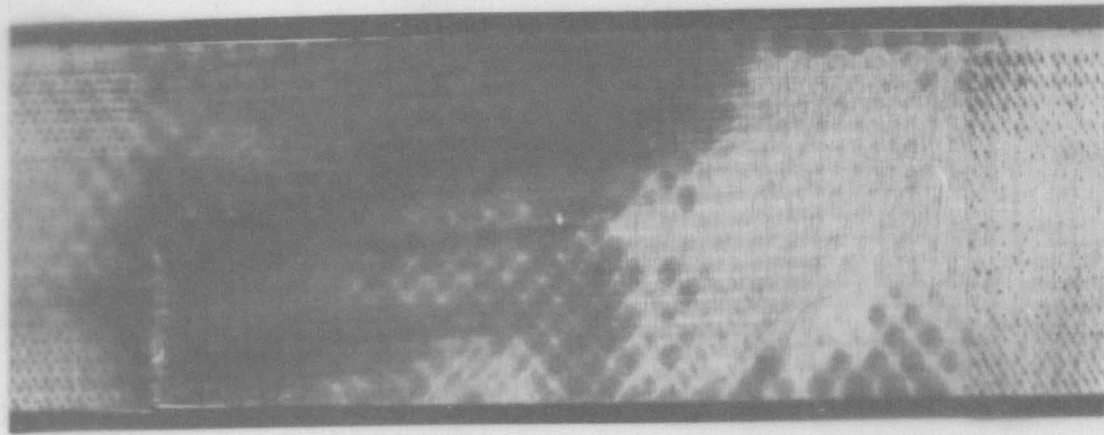
PLATE 6d.

PLATE 6d.

PLATE 6c.

PLATE 6b.

PLATE 6a.

PLATE 7c. 915mm wide CN specimen
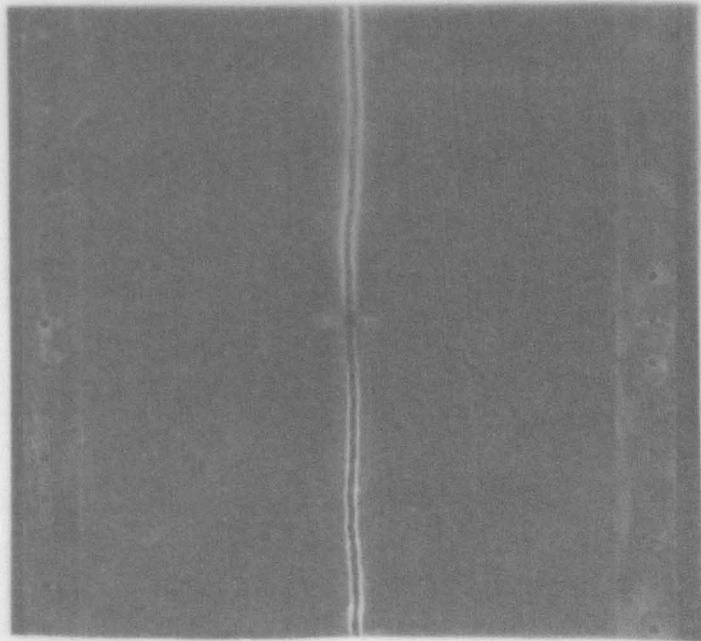
WRF/PR

PLATE 7b. 915mm wide CN specimen
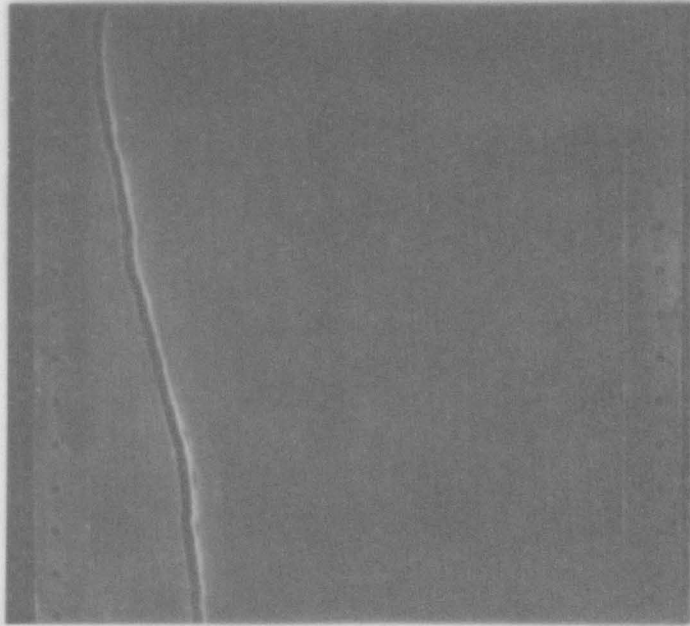
CSM/PR

PLATE 7a. 915mm wide CN specimen

CSM/PR

PLATE 7c. 915mm wide CN specimen.

WRF/PR

PLATE 7b. 915mm wide CN specimen
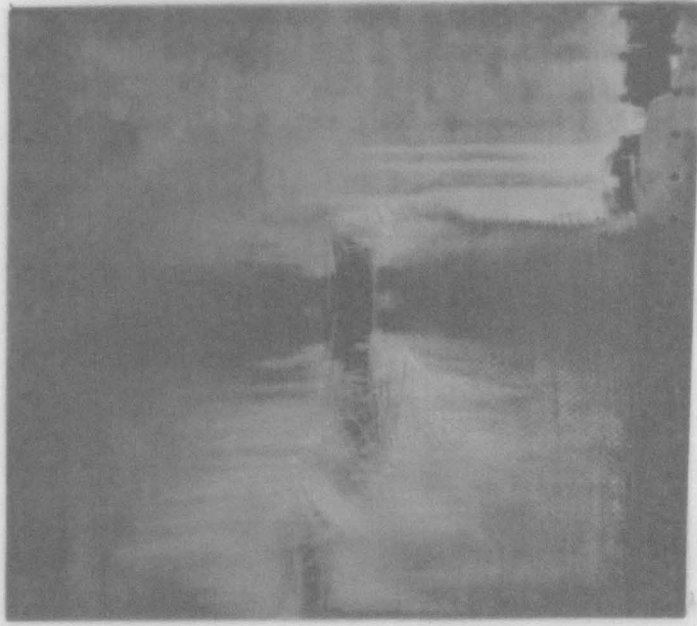
CSM/PR

PLATE 7a. 915mm wide CN specimen
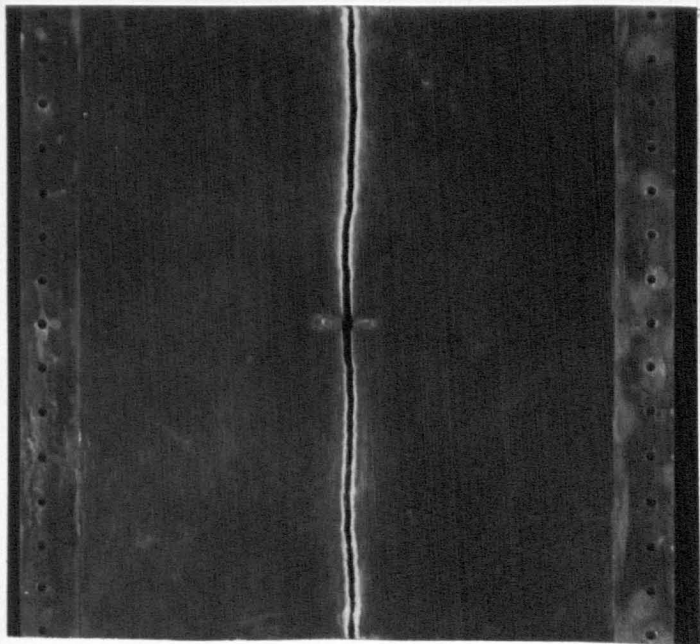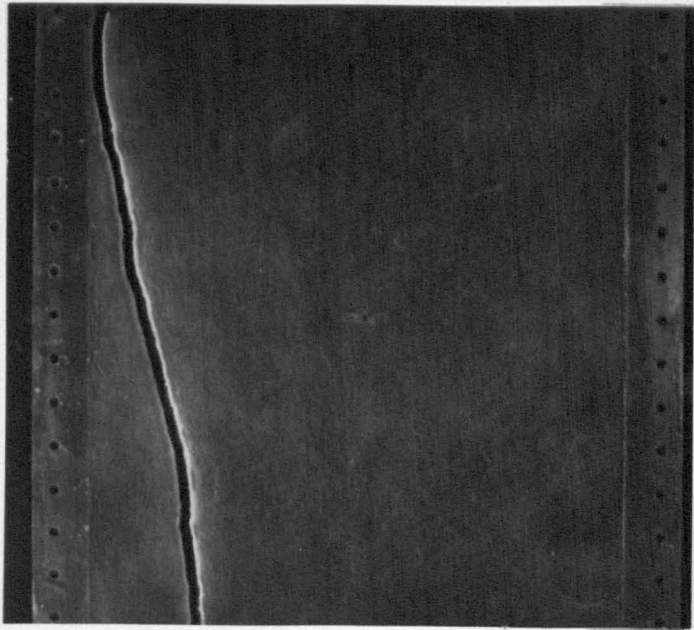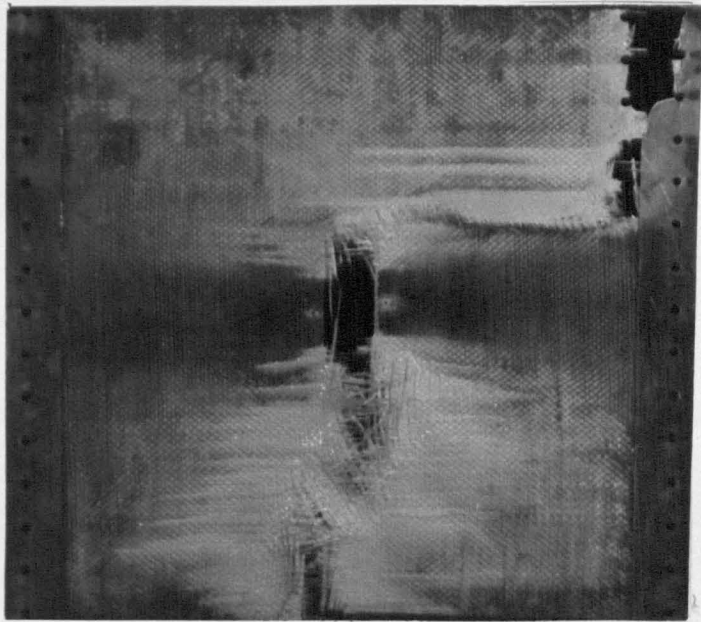
CSM/PR

Wet   Dry

PLATE 8.   Fatigue crack propagation in wet and dry CSM/PR specimens
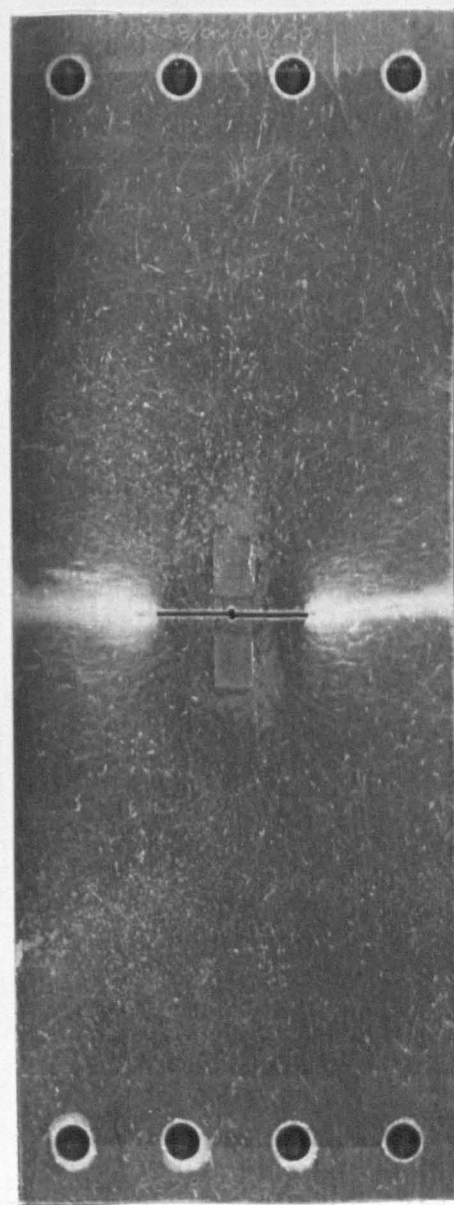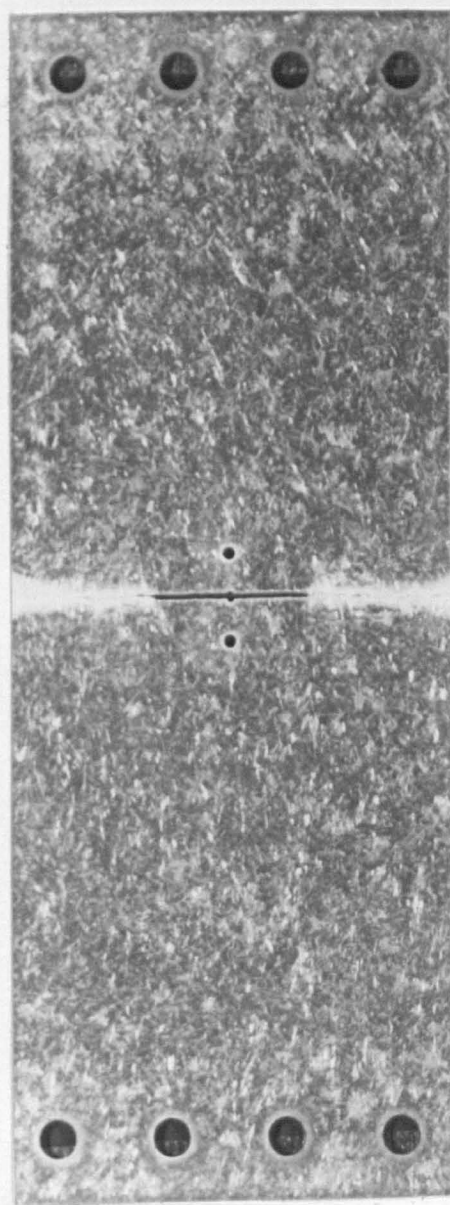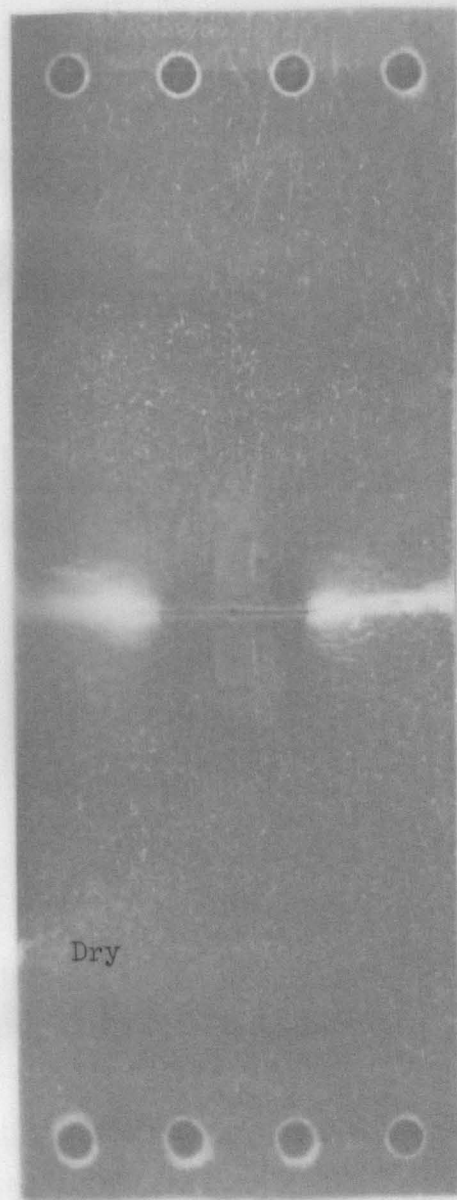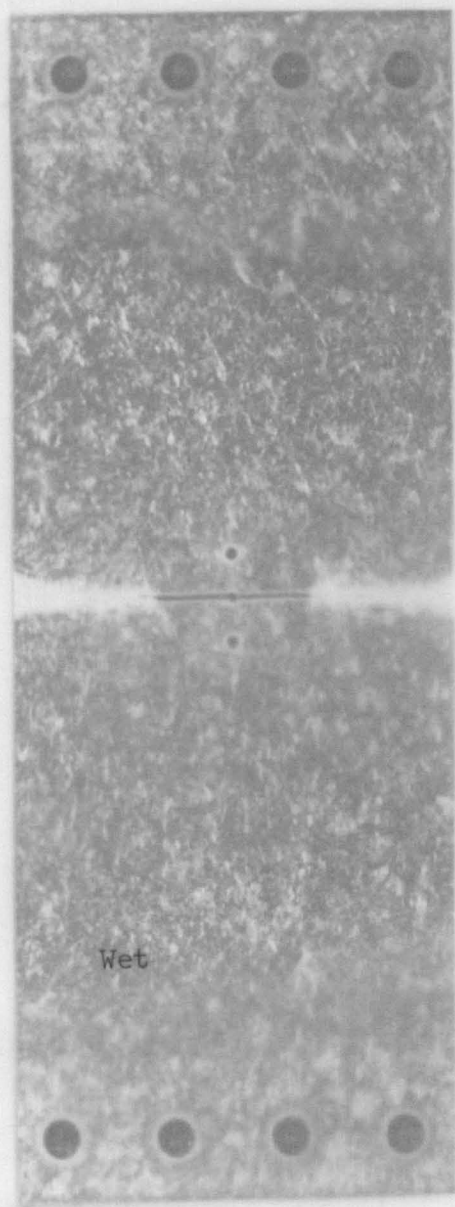
PLATE 8. Fatigue crack propagation in wet and dry CSM/PR specimens

PLATE 9a.

PLATE 9b.

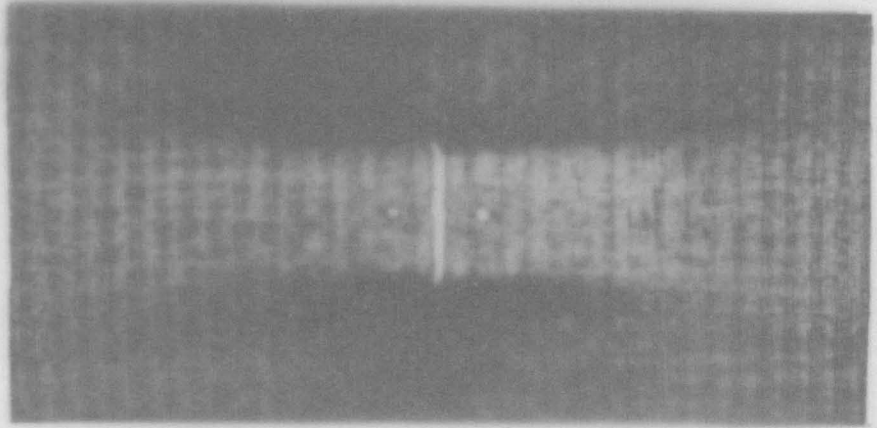PLATE 9c.
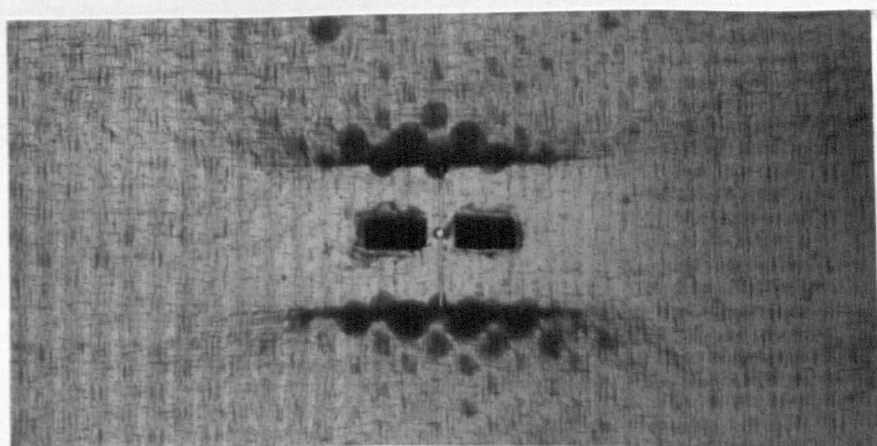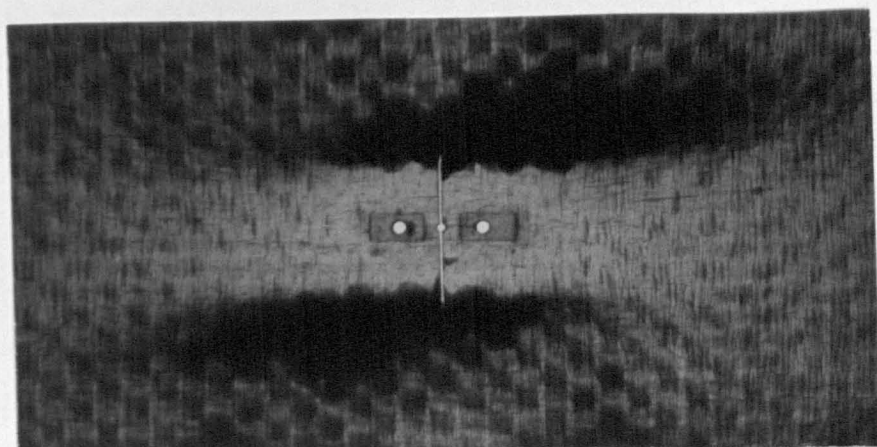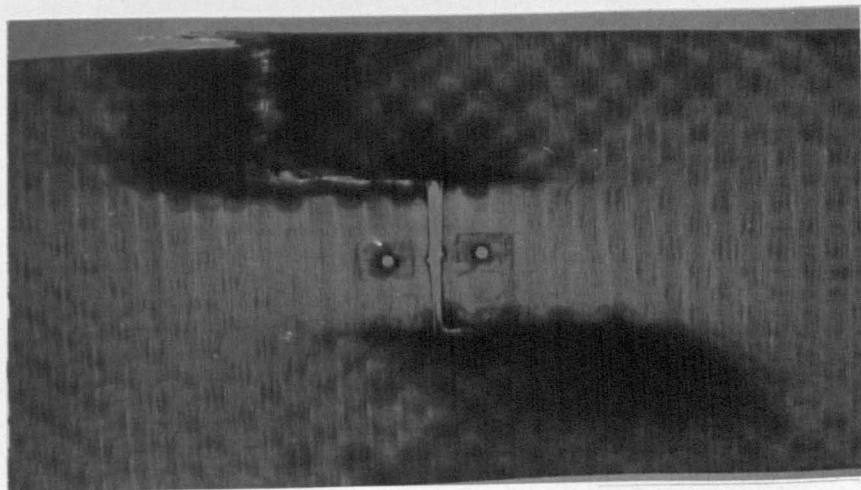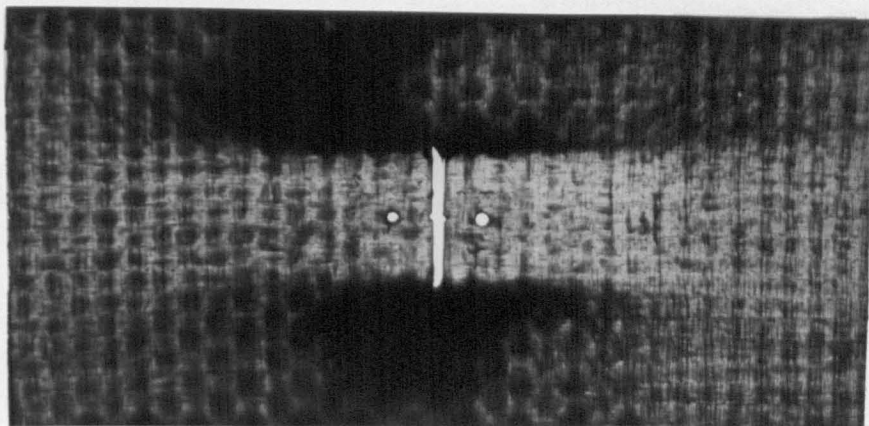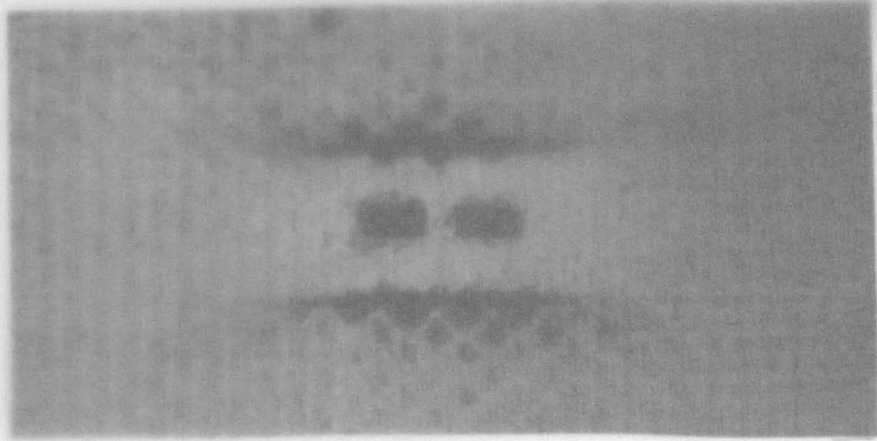
PLATE 9d. (wet)
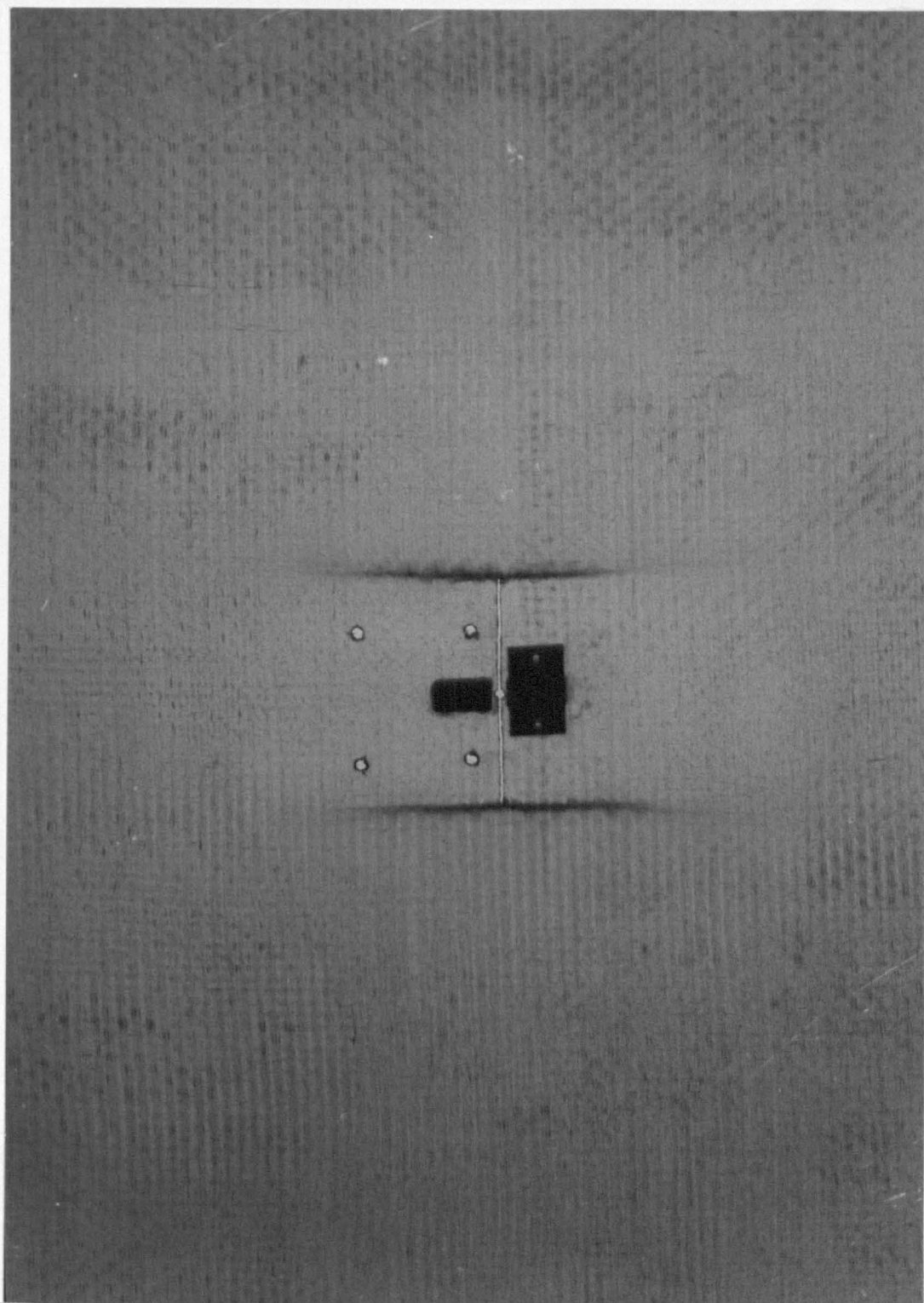
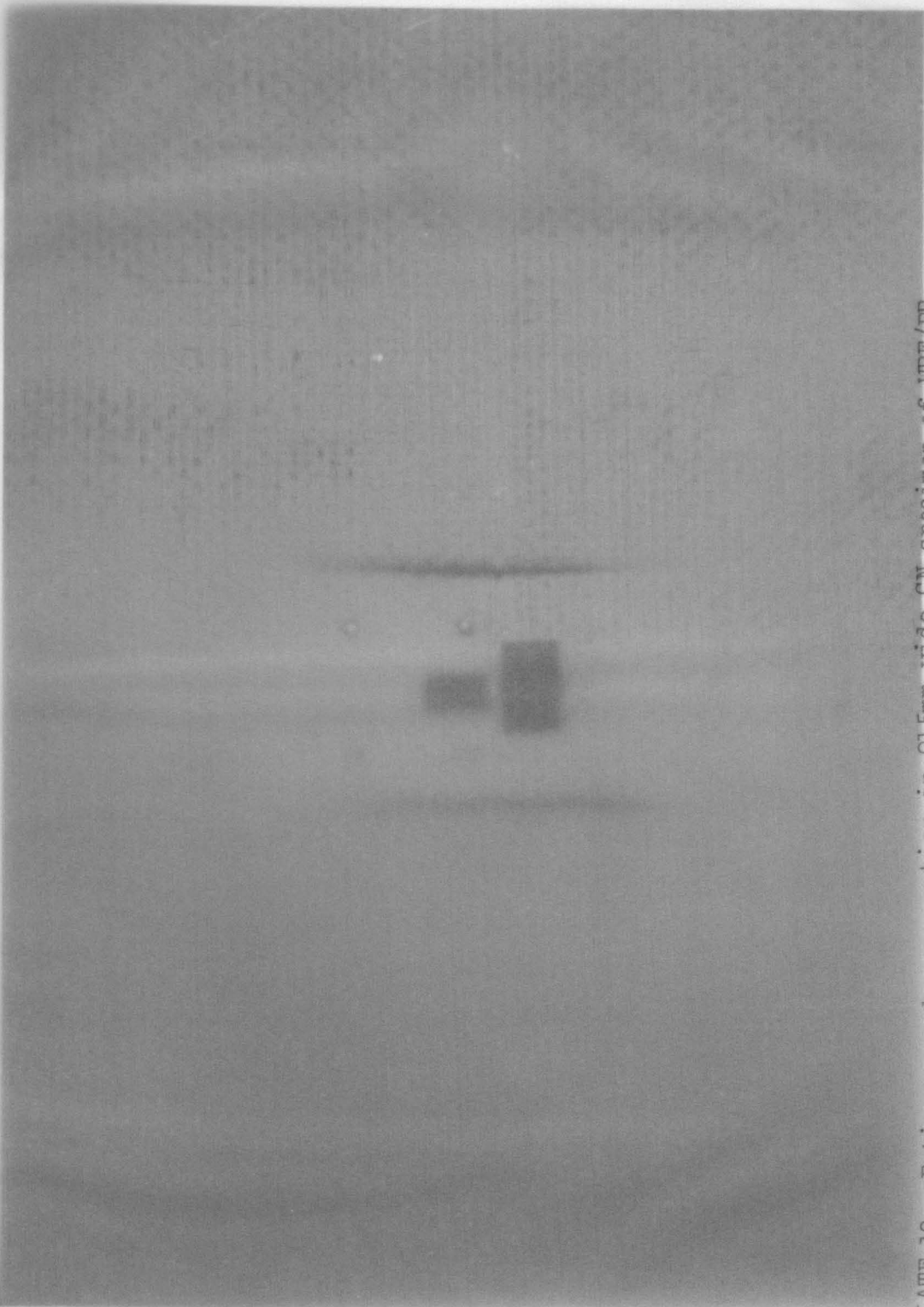PLATE 9a.

PLATE 9b.

PLATE 9c.

PLATE 9d. (wet)

PLATE 10.   Fatigue crack propagation in 915mm wide CN specimen of WRF/PR

PLATE 10. Fatigue crack propagation in 915mm wide CN specimen of WRF/PR